



**HAL**  
open science

## Kinetic study of ester biofuels in flames

Artëm Dmitriev

► **To cite this version:**

Artëm Dmitriev. Kinetic study of ester biofuels in flames. Chemical and Process Engineering. Université de Lorraine; Novossibirsk State University (Novossibirsk, Russie), 2020. English. NNT : 2020LORR0238 . tel-03264759

**HAL Id: tel-03264759**

**<https://hal.univ-lorraine.fr/tel-03264759>**

Submitted on 18 Jun 2021

**HAL** is a multi-disciplinary open access archive for the deposit and dissemination of scientific research documents, whether they are published or not. The documents may come from teaching and research institutions in France or abroad, or from public or private research centers.

L'archive ouverte pluridisciplinaire **HAL**, est destinée au dépôt et à la diffusion de documents scientifiques de niveau recherche, publiés ou non, émanant des établissements d'enseignement et de recherche français ou étrangers, des laboratoires publics ou privés.



## AVERTISSEMENT

Ce document est le fruit d'un long travail approuvé par le jury de soutenance et mis à disposition de l'ensemble de la communauté universitaire élargie.

Il est soumis à la propriété intellectuelle de l'auteur. Ceci implique une obligation de citation et de référencement lors de l'utilisation de ce document.

D'autre part, toute contrefaçon, plagiat, reproduction illicite encourt une poursuite pénale.

Contact : [ddoc-theses-contact@univ-lorraine.fr](mailto:ddoc-theses-contact@univ-lorraine.fr)

## LIENS

Code de la Propriété Intellectuelle. articles L 122. 4

Code de la Propriété Intellectuelle. articles L 335.2- L 335.10

[http://www.cfcopies.com/V2/leg/leg\\_droi.php](http://www.cfcopies.com/V2/leg/leg_droi.php)

<http://www.culture.gouv.fr/culture/infos-pratiques/droits/protection.htm>

**Ecole Doctorale SIMPPÉ**

**Thèse**

Présentée et soutenue publiquement pour l'obtention du titre de

**DOCTEUR DE L'UNIVERSITE DE LORRAINE**

**Mention : «Génie des Procédés et des Produits et des Molécules»**

par **Artëm DMITRIEV**

**KINETIC STUDY OF ESTER BIOFUELS IN FLAMES**

**18 décembre 2020**

**Membres du jury :**

**Rapporteurs :**

**M. Guillaume DAYMA**

**Professeur à l'Université d'Orléans, ICARE, Orléans**

**Mme Natalia TITOVA**

**D.R. à l'Institut Central des Moteurs d'Aviation, Moscou**

**Examineurs :**

**Mme Christine MOUNAÏM-ROUSSELLE**

**Professeur à l'Université d'Orléans, PRISME, Orléans**

**M. Pierre-Alexandre GLAUDE**

**D.R. au LRGP, CNRS, Nancy  
directeur de thèse**

**M. Denis KNYAZKOV**

**D.R. à l'Université de Novossibirsk, l'Institut de Cinétique  
Chimique et de Combustion, Novossibirsk  
co-directeur de thèse**

## **Acknowledgement**

*I want to express my deep gratitude to my supervisors, Pierre-Alexandre Glaude and Denis Anatolevich Knyazkov. Thanks to these people I got the opportunity to get in touch with a real scientific activity. They taught me how to perform an experiment or modeling, they taught me to formulate my ideas. My supervisors have introduced me to the scientific community and came up with the greatest adventure of my life, a joint French-Russian PhD program. At the same time I am very grateful to them for the fact that they have always provided freedom of my scientific thought.*

*I also want to say “merci beaucoup” to Valérie Warth, Juan Carlos Lizardo-Huerta, René Fournet, Frédérique Battin-Leclerc, Hervé LeGall and the entire KinCom team (now CiTherE) who welcomed me warmly in Nancy, shared their knowledge and helped me in my work.*

*I say “большое спасибо” to Andrey Gennadevich Shmakov, Tatyana Anatolevna Bolshova, Kseniya Nikolaevna Osipova, Ilya Evgenevich Gerasimov and the entire laboratory of Kinetics of Combustion Processes in Novosibirsk for their everyday help and support in the work on the thesis.*

*In conclusion, I want to thank all my family and friends for their patience and understanding. Special thanks to my grandfather, who gave me so much and who has always been an example of fortitude for me.*

# **Table of contents**

INTRODUCTION .....	6
1.1. FATTY ACID ESTERS AS A RENEWABLE BIOFUEL .....	7
1.2. SPECIFICS OF OXIDATION AND COMBUSTION OF FATTY ACID ESTERS .....	14
CHAPTER 1. LITERATURE REVIEW. EXPERIMENTAL AND NUMERICAL STUDY OF THE OXIDATION KINETICS .....	17
1.1. EXPERIMENTAL STUDY AND NUMERICAL SIMULATION OF OXIDATION OF FATTY ACID ETHYL ESTERS .....	18
1.1.1. Chemical-kinetic studies of small FAEs as model components of biodiesel .....	18
1.2.2 Kinetic investigations of oxidation and combustion of heavy FAEs and real biodiesel components .....	26
1.2. THE MAIN OBJECTIVES OF THE WORK .....	28
CHAPTER 2. METHODICS .....	30
2.1. EXPERIMENTAL DETAILS .....	31
2.1.1. Physical properties of the esters studied.....	31
2.1.2. Molecular-beam mass-spectrometric setup for studying the chemical flame structure at atmospheric pressure .....	32
2.1.3. Online sampling gas chromatographic setup for studying the chemical flame structure at low pressure .....	41
2.1.4. Flame temperature measurements .....	48
2.2. NUMERICAL SIMULATIONS.....	54
2.2.1. Theoretical problem description.....	54
2.2.2. Detailed kinetic mechanisms of oxidation and combustion .....	57
2.2.3. Mechanism analysis methods .....	61
CHAPTER 3. RESULTS. EXPERIMENTAL STUDY AND NUMERICAL SIMULATION OF THE FLAMES OF FATTY ACID ETHYL ESTERS .....	63
3.1. EXPERIMENTAL MEASUREMENTS OF ETHYL ESTER FLAME STRUCTURES .....	64
3.1.1 Ethyl acetate .....	64
3.1.2 Ethyl butanoate.....	75
3.1.3 Ethyl pentanoate .....	83
3.2. ANALYSIS OF DETAILED COMBUSTION MECHANISMS USED .....	95
3.2.1. Analyses of the primary decomposition pathways of esters in flames .....	96

3.2.2. Calculation of the ethyl pentanoate laminar burning velocity .....	112
MAIN RESULTS AND CONCLUSIONS .....	118
APPENDIX 1 .....	121
APPENDIX 2 .....	123
APPENDIX 3 .....	124
LIST OF REFERENCES .....	125

# **INTRODUCTION**



## 1.1. FATTY ACID ESTERS AS A RENEWABLE BIOFUEL

The continuously growing consumption of energy resources and the struggle for the ecological safety of the energy sector are forcing researchers all over the world to develop new energy sources. One of the key topics is looking for renewable fuels as alternative to the fossil fuels. Special attention is paid to alternative fuels for the transportation sector, since such fuels must correspond to a variety of physical, chemical and economic factors straight away. At the same time liquid hydrocarbon fuels remain to be the best solution for long-distance transportation due to its high energy density [1]. In this regard, internal combustion engines (ICE) will remain the main driving force of the transportation for a long time despite the rapid development of electric vehicles. [2], [3]. In such circumstances searching for the environmental friendly alternative fuels for ICE is an urgent task which is being solved in developed countries all over the world.

Liquid biofuels based on fatty acid esters appeared to be one of the possible solutions to this problem. Such fuels are renewable, as they are produced from biomass, they have a fairly high energy density and ester biofuels almost do not form soot and polyaromatic hydrocarbons during combustion [4]. Also, bioderived fuels considered as carbon-neutral since carbon dioxide produced in combustion was previously captured in the biomass from the atmosphere. At the same time, such a fuel has physical characteristics close to conventional gasoline or diesel fuel which allows it to be used either in pure form or in a mixture with traditional fuel without significant modification of engines [5], [6]. Fatty acid esters could be roughly divided into light ( $C_2$ - $C_8$ ) and heavy ( $C_9$  and heavier). According to boiling points and viscosity, light fatty acid esters are considered as fuel additives to gasoline to reduce the consumption of conventional petroleum gasoline. At the same time, it is noted in several works that the addition of light esters increases the octane number of the fuel mixture [7]–[9]. Physical properties of heavier esters are close to those of the diesel oil fractions [10]–[13],

therefore mixtures of heavy fatty acid esters are called biodiesel. Biodiesel and ethanol are the most common alternative liquid fuels for internal combustion engines, which already exist on the fuel market and actively used in a number of countries [5], [14]. In particular, there are technological standards for the biodiesels and its mixtures with conventional fuels in the European Union (EN 14214) [15], USA (D6751-02, D7467 - 20a) [16], [17], Canada (CAN/CGSB-3.524) [18] etc. At the moment, the main problem of introducing such types of fuel remains the higher production costs compared to the traditional gasoline and diesel [4]. Nevertheless, in many countries there are government programs for the development of the biofuel industry which stimulates development of new cost-effective technologies for the biomass refinery and biofuel production from a variety of raw materials [19]–[22].

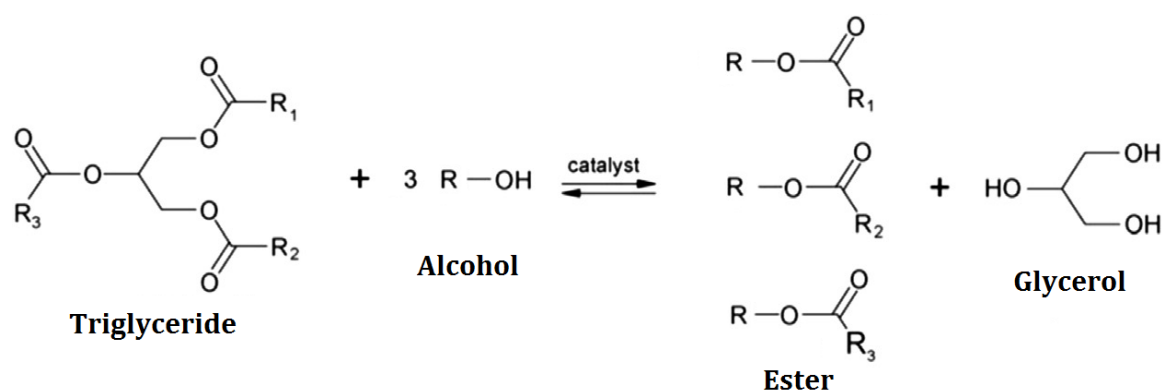


Figure 1.1. Transesterification reaction of triglyceride with alcohol. It is the main industrial method of fatty acid ester production.

By itself the biodiesel is a mixture of fatty acid esters which is most often produced during the transesterification reaction of fats (triglycerides) with light alcohols [19, 20]. As usual the cheapest and commercially available alcohols are used for these purposes, such as methanol (CH<sub>3</sub>OH) and ethanol (C<sub>2</sub>H<sub>5</sub>OH). In the case of transesterification with methanol fatty acid methyl esters (FAME) are formed, and in the case of the reaction with ethanol fatty acid ethyl esters (FAEE) are formed. The by-product of the transesterification is glycerin which is a useful product in itself. The general reaction scheme is shown in Figure 1.1.

The choice between methanol and ethanol is determined by a number of factors since both alcohols have their own advantages and disadvantages. Methanol has a higher reactivity in the transesterification process in comparison with ethanol. Also, methanol is easier to remove at the stage of the final product cleaning [23]. In industry methanol is mainly obtained from the synthesis gas which makes methanol quite cheap. The last factor is decisive in the choice of alcohol for the industrial production of biodiesel at the moment. However, such fuel is not fully renewable, since methanol for its production is obtained from the non-renewable sources (natural gas and coal). Also, high toxicity and corrosive effects on metals are the significant disadvantages of methanol. Unlike methanol, ethanol is significantly less toxic making production much safer. Moreover, production of ethanol from the renewable sources is already well established and is constantly evolving towards lower prices. [24]–[26]. The use of bioethanol makes biodiesel a completely renewable energy source. The advantages of ethanol also include a higher reaction yield in terms of the mass ratio of FAEE/triglyceride and better solubility of fats in ethanol [27]–[29]. In addition, many studies have noted that biodiesel based on FAEE has better fuel characteristics than those of FAME-mixtures [30]–[32]. This is also an argument in favor of using ethanol for the transesterification. The main disadvantage of ethanol is its higher cost compared to methanol. It should be noted that using methanol and ethanol simultaneously is also considered as an effective approach in biodiesel production [23], [33].

Almost any kind of biomass with a high fat content can be used as a feedstock. The main requirements for are low price and high production volumes of the feedstock. In the last decade a huge number of possible raw materials have been proposed for the production of biodiesel. On the one hand, a lot of possible resources have expanded the possibilities of biofuel production, but on the other hand, such diversity has complicated the technical verification and standardization of the fuels. At the moment, various kinds of oilseeds are the main sources from which vegetable oil can be extracted for the further

transesterification [11], [34]. More than 350 types of crops have been proposed as potential raw materials for biodiesel production [10]. However biodiesel production technologies from other types of raw materials have been actively developed in recent years. Let's consider in more detail the classification and types of the raw materials for the biodiesel production.

It is customary to classify biodiesels in literature by generations depending on the feedstock. However, the number of generations in different sources varies from three [35] to four [36] or five [37]. It seems most logical to consider four generations of biodiesel fuels according to the classification from the work [36].

First of all biodiesels are distinguished as the fuel from edible or inedible plant materials, the so-called first and the second generation of biodiesels. Edible crops such as soybeans, sunflowers, rapeseed, peanuts and others contain a lot of vegetable oil and are grown in large quantities in many countries. Agrarian production of these plants is well established. Therefore edible oilseeds were the first one feedstock proposed for the biodiesel production. However, the use of edible plants for the fuel production poses a number of serious problems. First of all it is a lack of arable lands, high production costs and conflicts with the food industry. Moreover, the use of edible crops is unsustainable in the long term, since the increasing fuel demands will not be covered by the production of edible crops [38], [39]. In view of the problems discussed the attention of researchers and producers has turned to inedible oilseeds such as oil palm, jatropha, karanja and many others [40]. As a rule industrial oilseeds are less demanding on agricultural technologies and soil quality, therefore they can be grown in more difficult conditions and at a lower cost. The use of inedible crops allows biomass production to be adapted to the geographic characteristics of the region that significantly increases the availability and economic attractiveness of the biodiesels. Another major advantage of these raw materials is the lower content of sulfur and aromatic substances that significantly improves the quality of the resulting fuel. The main disadvantages are the need to collect raw materials from

large territories and the insufficient development of technologies for processing various types of crops [40].

Aside from the plant crops, food by-products such as beef, lard, used frying oil, fish or poultry oil can be also used as raw materials for the biodiesel production [41], [42]. This group of biofuel feedstock is considered as the third generation of biodiesels, but sometimes it is also referred to the second generation. Such fats are produced in large quantities all over the year, they do not require special production and agricultural territories. Besides, the use of waste oils as the raw materials helps to solve the problem of waste disposal. Since 70-80% of the biodiesel production costs is determined by the price of the raw materials [43] the use of waste oils can significantly reduce the total cost of the final product. It is noted that processing fatty waste is more profitable than growing special crops for some countries with arid climates [37]. The use of fatty food waste is considered as the most profitable strategy for the production of biofuels at the moment by a number of experts. [44], [45]. The key disadvantages of these raw materials are the food impurities and high water content which reduce the useful product yield during transesterification. In this regard the raw materials from wastes require serious preliminary treatment that consequently complicates production and ultimately affects the biofuel price [10], [45], [46].

According to many scientists the most promising raw material for the biodiesel production are microalgae. The microalgae biofuels are often called the fourth generation of biodiesels [47]–[50]. Microalgae number tens of thousands of naturally and artificially bred cultures. During the photosynthesis process they absorb carbon dioxide and sunlight increasing their biomass, and the efficiency of this process is much higher than that of terrestrial plants. Dry microalgae can be used as a fuel directly or can be converted into the feedstock for a variety of biofuels, including triglycerides [51]. Some types of microalgae can produce and store fat in their cells up to 70% of their dry weight. For comparison, in ordinary plants this value is about 5% [52]. During mechanical or chemical processing triglycerides can be extracted from the microalgae [53]. The large yield per unit

mass, rapid growth and relatively small production areas make microalgae potentially the most efficient and sustainable feedstock for the biofuel industry in the long term. Despite the already existing startups of microalgae biofuel production, the large-scale production does not seem to be profitable yet due to a number of serious technological difficulties. [54]. The key problems are the lack of sunlight and carbon dioxide when algae are grown in large vessels. Because of this, the yield of a useful product drops significantly. Also, microalgae require phosphorus, nitrogen and other inorganic additives for active growth. Together with the energy consumption for the full cycle of the fuel production that makes this approach quite expensive on a large scale [55]. Nevertheless, the development of bioengineering technologies and new approaches to the industrial production organization leave microalgae in the list of the most promising bioenergy resources for the near future [56].

The feedstock and its availability mostly determine the cost of the final biofuel, so the search for new sources of feedstock does not stop. As the new raw materials appeared, parallelly new technologies for their processing and production of the final product are developing. Particular attention is paid to the search for catalysts and optimization of conditions for the processing of different types of feedstock [57]–[59]. It is worth to know that the classification of biodiesel by generation does not mean that the third generation biodiesel will be more profitable than the second generation biodiesel. Moreover, the combined production of biodiesel of different generations can be an effective strategy in future. [60].

Regardless the types of feedstock and alcohol for the transesterification, basing on the literature review the general advantages and disadvantages of biodiesels can be identified.

#### **Benefits of ester biofuels:**

- Mixture of fatty acid esters is a renewable, non-toxic, environmentally friendly fuel
- It could be easily used as a single fuel or in blends with traditional fossil fuels

- Esters does not contain sulfur, practically does not form soot and produces less carbon monoxide, polyaromatic and hydrocarbon compounds during combustion in comparison with traditional diesel
- The use of ester biofuel reduces net life cycle carbon dioxide emissions by about 80% compared to conventional diesel
- Fatty acid ester is a biodegradable fuel, so its leakage does not pose a serious environmental hazard
- Ester production, particularly, biodiesel production is well localized because of the availability of different raw materials, each country has the ability to produce biodiesel as a locally produced fuel
- Light esters have a high octane number, so can be used as the octane boosters to the gasoline blends
- Biodiesels have a higher cetane number than conventional diesel, that increases engine efficiency
- Biodiesel has additional lubricating properties that reduces engine wear
- The use of biodiesel does not require significant engine modifications

**Disadvantages of ester biofuels:**

- Biofuel production is more expensive today than production of fossil fuels
- Ester biofuels have a slightly lower energy density than fossil fuels resulting in an increase in fuel consumption of about 2-10%
- Biodiesel has a higher viscosity, cloud point and pour point than traditional diesel, making cold start difficult
- Several studies point out slightly higher NO<sub>x</sub> emissions compared to conventional fuels [61]
- Biofuel can oxidize and change its properties during long-term storage and decompose in the absence of stabilizers

## 1.2. SPECIFICS OF OXIDATION AND COMBUSTION OF FATTY ACID ESTERS

First of all, ester based biofuels are considered as a biodiesel. Biodiesel is defined as a mixture of long alkyl chain fatty acid methyl or ethyl esters. A typical set of fatty acids which esters are most often found in the biodiesel production is shown in Table 1.

After the transesterification of these acids with methanol or ethanol corresponding FAME and FAEE are formed. Until the XXI century chemical kinetics of esters' oxidation and combustion was not of particular interest since esters are not the main components of traditional hydrocarbon fuels. However, with the development of the biofuel industry chemical kinetics of the oxidation of ethers and esters began to be studied more widely and in detail. The key motivation was in the need for thorough understanding of the oxidation chemistry of new classes of compounds both in the pure form and in the mixtures with traditional fuels for the practical applications. Experimental and numerical studies of the oxidation and combustion kinetics of real biodiesel components are extremely complex due to the large sizes of the molecules. To solve this problem a hierarchical approach is used at which construction of a kinetic mechanism for the oxidation of a heavy compound is based on the kinetic submechanisms of lighter intermediate components. In this way the systematic studies of the oxidation chemistry of shorter model molecules allow us to describe the kinetics of intermediate stages of heavy fuel oxidation. At the same time, it can provide important information on the characteristics of the main reaction classes of a real fuel.

The reaction pathways of a molecule oxidation are determined by its structure and external conditions. Due to the long alkyl groups fatty acid esters can participate in the same transformation chains as normal hydrocarbons of the same length [61]. At the combustion conditions these are mainly reactions of the abstraction of a hydrogen atom (H-abstraction) when a molecule is attacked by a free flame radical. Nowadays the chemistry of hydrocarbon oxidation has been



studied quite deeply, therefore to describe this class of ester oxidation reactions existing kinetic schemes for the hydrocarbon oxidation can be exploited [62], [63].

Fatty acid	Number of saturated and unsaturated bonds	Chemical structure
Lauric	(12:0)	$\text{CH}_3(\text{CH}_2)_{10}\text{COOH}$
Myristic	(14:0)	$\text{CH}_3(\text{CH}_2)_{12}\text{COOH}$
Palmitic	(16:0)	$\text{CH}_3(\text{CH}_2)_{14}\text{COOH}$
Stearic	(18:0)	$\text{CH}_3(\text{CH}_2)_{16}\text{COOH}$
Oleic	(18:1)	$\text{CH}_3(\text{CH}_2)_7\text{CH}=\text{CH}(\text{CH}_2)_7\text{COOH}$
Linoleic	(18:2)	$\text{CH}_3(\text{CH}_2)_4\text{CH}=\text{CHCH}_2\text{CH}=\text{CH}(\text{CH}_2)_7\text{COOH}$
Linolenic	(18:3)	$\text{CH}_3\text{CH}_2\text{CH}=\text{CHCH}_2\text{CH}=\text{CHCH}_2\text{CH}=\text{CH}(\text{CH}_2)_7\text{COOH}$
Arachinic	(20:0)	$\text{CH}_3(\text{CH}_2)_{18}\text{COOH}$
Behenic	(22:0)	$\text{CH}_3(\text{CH}_2)_{20}\text{COOH}$
Erucic	(22:1)	$\text{CH}_3(\text{CH}_2)_7\text{CH}=\text{CH}(\text{CH}_2)_{11}\text{COOH}$
Lignoceric	(24:0)	$\text{CH}_3(\text{CH}_2)_{22}\text{COOH}$

Table 1. Chemical structure of typical fatty acids for biodiesel production [10], [64].

Another class of ester oxidation reactions corresponds to the ester group which contains two oxygen atoms. This class of reactions has been studied much less. For this reason the transformation kinetics of the ester group is of greatest interest when the oxidation chemistry of fatty esters is studied. It is important to note that the presence of oxygen atoms in the ester group changes the bond energy of neighboring C-C and C-H groups. This inductive effect can influence the reaction rates at the  $\alpha$  and  $\beta$  carbons of the alkyl group, in particular, it can change the activation energy of the H-abstraction reactions [65]. To obtain the information on the ester group reactions systematic experimental and theoretical studies are required. Usually light esters with an alkyl chain up to three carbon atoms are used as research objects, since they are quite simple and the most

convenient for experimental studies. It is assumed that the length of the ester alkyl chain does not significantly affect reactions of the ester group.

However, it is noted in many works that light esters with a short alkyl group are poorly suited as the model surrogates of a real biodiesel [66]–[69]. The reason is that they have a much higher reactivity and do not exhibit a negative temperature coefficient which is characteristic for the heavier esters. In this regard kinetic studies of oxidation and combustion of esters with long alkyl groups are in demand.

**CHAPTER 1. LITERATURE REVIEW.  
EXPERIMENTAL AND NUMERICAL  
STUDY OF THE OXIDATION  
KINETICS**

## 1.1. EXPERIMENTAL STUDY AND NUMERICAL SIMULATION OF OXIDATION OF FATTY ACID ETHYL ESTERS

### 1.1.1. Chemical-kinetic studies of small FAEEs as model components of biodiesel

For the beginning of this section it is important to note that there is a large number of technical and motor tests of various biodiesel fuels and their components in literature. Most of these works are purely descriptive and do not delve into the physical chemistry of the processes. Therefore, in this review we will discuss only works devoted to the study of the chemical kinetics of ethyl esters' oxidation.

Fatty acid methyl esters have been studied much more intensively than similar ethyl esters due to their prevalence and applied value. However, the increased interest to the FAEE-based biofuels has motivated researchers to study the kinetics of oxidation and combustion of ethyl esters in more detail. Also, a certain interest to the oxidation chemistry of FAEEs arose from a purely academic point of view. This is due to the fact that FAEEs are characterized by a unimolecular pericyclic decomposition through a six-centered transition state with the formation of ethylene and the corresponding carboxylic acid (Fig. 1.2).

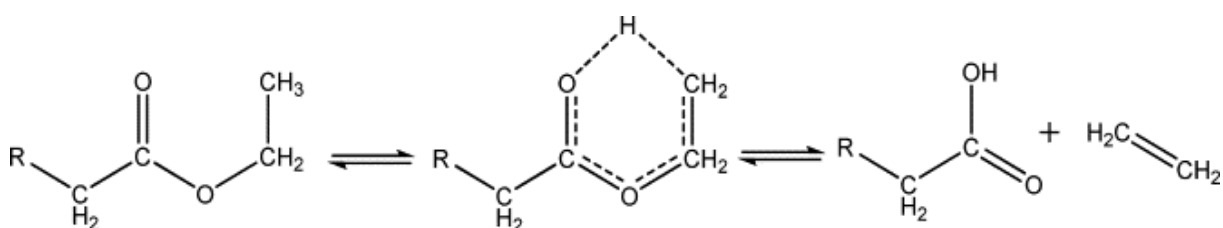


Figure 1.2. Unimolecular decomposition of an ethyl ester through the intermediate six-centered ring complex [70].

Formation of an intermediate cycle is caused by the interaction of the terminal hydrogen atom with the oxygen atom in the ester group due to the

deformation of the ethyl group. In the case of methyl esters such interaction is less possible due to another number of atoms in the group and, thus, another electronic structure. The reaction of six-center unimolecular decomposition is a distinctive feature of FAEEs. As it mentioned in literature the decomposition can occur at lower temperatures than radical initiation, therefore oxidation reactivity of ethyl ester can be higher than that of corresponding methyl ester.

This reaction pathway was introduced by Metcalfe et al. [71], [72] in their detailed mechanism of oxidation of small esters with the general formula  $C_5H_{10}O_2$ . This research group has investigated the oxidation of methyl butanoate (MB) and ethyl propanoate (EP) in a series of high-temperature experiments in a shock tube and in a jet-stirred reactor. To describe the experimental data obtained the authors proposed a new detailed kinetic model of EP and MB oxidation. The experiments have shown that EP has a shorter ignition delay time than that of the isomeric MB. This difference in the ignition delays was associated by the authors with the six-center unimolecular decomposition of the EP molecule in the low-temperature zone. Akih-Kumgeh and Bergthorson [73] have confirmed this trend. In their work they have investigated the ignition behavior of various methyl and ethyl esters in shock tube experiments and also they have carried out numerical simulations. The authors have analyzed isomerization effects and the influence of different alkyl groups on the ignition delay times of the esters. As in the work of Metcalfe, a more rapid ignition of isomeric ethyl esters was observed. The homologous sequence of three small ethyl esters, ethyl formate (EF), ethyl acetate (EA) and ethyl propanoate (EP), was investigated by Ren et al. [74]. Using near-infrared laser spectroscopy they tracked the time evolution of the concentration of  $H_2O$ ,  $CO_2$  and  $CO$  molecules behind reflected shock waves. The experimental results showed a significant difference in the pyrolysis rates of the three esters. To simulate the experimental results the authors have used the improved Metcalfe's mechanism [72]. They have noted a satisfactory agreement of the model with the data observed in the experiments with EF and EA and a poor agreement between the predictions of the model and experimental data on EP. In

the work [75] a comparative study of two heavier esters, methyl butanoate (MB) and ethyl butanoate (EB), was carried out. Experiments were carried out in a shock tube and in a jet-stirred reactor. The experiments have demonstrated again that ethyl ester is slightly more reactive than the methyl one. A new kinetic model was proposed taking into account the experimental results obtained. Basing on the analysis of production pathways and sensitivity analysis the authors suggested that the difference in the reactivity between MB and EB corresponds to easier unimolecular initiation of ethyl ester with the formation of H atoms. The authors also emphasize the different decomposition pathways of methyl and ethyl ester. Unfortunately, the experimental results with the jet-stirred reactor were reproduced unsatisfactorily by the mechanism proposed in the work. In conclusion the authors have pointed out the need for additional studies of esters in reactors of various types. In the work of Bennadji et al. [76] new experimental data were obtained on the oxidation of EB in a tubular plug-flow reactor. Concentration profiles of reactants, stable intermediates and final products were identified and measured using a coupled gas chromatography-mass spectrometry (GC/MS). Thanks to the data obtained the authors have managed to improve and confirm the above-mentioned mechanism [75].

The laminar flame speed of fuel is one of the most important global parameters, but only a few papers cover this topic in the case of FAEEs. Laminar burning velocities of the mixtures of air with small esters were measured by Wang et al. [77]. Seven methyl and ethyl esters, including ethyl formate (EF), ethyl acetate (EA) and ethyl propionate (EP), were investigated in flames by the particle image velocimetry (PIV) in a counterflow burner. The speeds were measured over a wide range of equivalence ratios, at atmospheric pressure and at elevated fresh mixture temperatures. In addition the authors carried out numerical simulations of the experimental data based on several literature known mechanisms. The calculated laminar velocities turned out to be overestimated in comparison with the experiments for almost all compounds. After the kinetic schemes analysis the authors came to the conclusion that it is

necessary to determine more accurately the rate constants for the reactions of primary esters destruction, in particular, reactions of the fuel radicals' decomposition. In the work Dayma et al. [78] the laminar combustion velocities of mixtures of several ethyl esters with air were measured in a spherical chamber. In this work the flame propagation velocities were measured at different initial temperatures, equivalence ratios and pressures. To describe the results obtained a new kinetic mechanism was proposed which was obtained by reducing the detailed mechanism of ethyl pentanoate oxidation [79] developed by the same group. As the result a good agreement was achieved between the experimental values of the burning rates and the model predictions for all esters. To test the new mechanism the authors simulated literature known experimental data on the ignition delays and oxidation in a jet-stirred reactor of the esters studied. The proposed mechanism described most of the experimental data quite satisfactorily. The work [79] published in the same year was dedicated to the study of a heavier ester, ethyl pentanoate (EPe). As in the previous work the authors measured laminar burning velocities of EPe/air mixtures in a spherical bomb over a wide range of pressures and equivalence ratios. Also, experiments on measurements of the concentration profiles of stable components in a jet-stirred reactor at 10 atm and various equivalence ratios were carried out. In this work a new detailed kinetic mechanism of EPe oxidation was proposed and was verified against the experimental data obtained. Comparison of model predictions with the experimental results has shown a good predictive ability of this kinetic scheme in the studied range of conditions and parameters.

Experimental data on the spatial distribution of species concentrations in flames (i.e. the chemical structure of a flame) under various conditions provides important information about the oxidation mechanism of a particular fuel. In addition, the flame structure measurements make it possible to check kinetic submechanisms in more detail in contrast to the global parameters (burning velocity, ignition delay time). Gasnot et al. [80] has conducted the first experimental study of the chemical composition of a flame with the addition of

fatty acid ethyl ester. Using gas chromatography (GC) and GC/MS in combination with microprobe sampling they measured the mole fraction profiles of reactants and stable products in a EA(2%)/CH<sub>4</sub>/O<sub>2</sub>/N<sub>2</sub> flame at low pressure. The data obtained were compared with a previously investigated flame of a CH<sub>4</sub>/O<sub>2</sub>/N<sub>2</sub> mixture. Analyzing the results of measurements in flames the authors noted the additional formation of oxygen-containing species and C<sub>2</sub>-hydrocarbons in flames with the ester doping. In their next work the authors proposed a new kinetic mechanism of EA oxidation in a flame [67] based on the previous experimental results. Another investigation of the effect of ethyl ester addition on the methane-air flame was carried out by Schwartz et al. [81]. Five isomeric esters with the general formula C<sub>5</sub>H<sub>10</sub>O<sub>2</sub>, including EP, were investigated as an additive (0.5%) in a laminar diffusion flame of a CH<sub>4</sub>/O<sub>2</sub>/N<sub>2</sub>/Ar mixture at atmospheric pressure. The authors carried out a comparative analysis of the main flame components and their mole fractions obtained by mass spectrometry (MS). As a result, the role of the unimolecular decomposition was noted; it was determined by the authors as the main reaction pathway of the EP decomposition in a flame. The possibility of the unimolecular decomposition resulted in less formation of soot precursors in comparison with other esters and in the formation of a large amount of oxygenates. Osswald et al. [68] has measured the mole fractions of basic and intermediate compounds in premixed laminar flames of methyl acetate (MA) and ethyl formate. The flames were stabilized on a flat burner at low pressure and the method of mass spectrometry with molecular beam sampling (MBMS) and photoionization with vacuum ultraviolet was exploited to determine the chemical composition of flames. Analyzing the primary degradation pathways of esters the authors concluded that MA decomposes mainly with the formation of formaldehyde, while EF leads to significantly higher concentrations of acetaldehyde. Using these experiments Westbrook et al. [69] has developed a new kinetic mechanism for the oxidation of small esters in flames. To validate and improve the mechanism proposed the same researchers group conducted experimental measurements of the chemical flame structure of three isomeric



ethers with the general formula  $C_5H_{10}O_2$ : ethyl propanoate, methyl butanoate and methyl isobutanoate [82]. Using photoionization mass spectrometry they measured the mole fraction profiles of stable components and several intermediate species in the laminar premixed flames at low pressure. The results obtained made it possible to clarify the ways of destruction of these esters and expand the previously developed mechanism [69]. As a continuation of these studies, the authors have studied the chemical flame structure of three unsaturated esters with the general formula  $C_5H_8O_2$ , including ethyl propenoate (EPE)[83]. The main goal of the study was to expand and verify the developed mechanism, as well as to determine the effect of a double bond in a fuel on the combustion kinetics of fatty acid esters. An experimental study and kinetic modeling of the combustion of small FAEs was the focus of the work of Sun et al. [84]. Using a photoionization MBMS-setup the mole fraction profiles of various compounds in rich premixed flames of EF, EA and EP stabilized at 30 Torr were measured. The authors also proposed a new kinetic combustion mechanism of small FAEs based on quantum-chemical calculations of the rate constants for the primary reactions pathways of ester decomposition.

Ethyl pentanoate oxidation mechanism [79] was examined on the new experimental data by Knyazkov et al. [85]. Using the same experimental setup as in the works [68], [69], [82], [83] the authors have measured the mole fraction profiles of various intermediate products in a stoichiometric premixed EPe/ $O_2$ /Ar flame at 20 Torr. The authors noted the lack of accuracy of the model in predicting the maximum mole fractions of many intermediate hydrocarbons. It should be noted that valeric acid ( $C_4H_9COOH$ ), which is formed during the six-centered unimolecular decomposition of EPe, was not identified in this work since the signal of the initial parent ion peak corresponding to this compound was too low. It was proposed to revise the chemistry of the fuel radicals' formation and consumption to improve the kinetic mechanism. Additionally, the authors suggested to include some oxygenated compounds that were determined in the experiment but were absent in the mechanism. Another recent work was also

devoted to the chemical structure measurements of EPe flames [86]. The authors have investigated laminar flames of lean, stoichiometric and fuel-rich EPe/O<sub>2</sub>/Ar mixtures at a pressure about 40 Torr. Analysis of the flame chemical composition was performed using GC analysis with probe sampling from the flame. Eight intermediate flame components were measured including formaldehyde, acetaldehyde, valeric acid and formic acid. It is important to notice that the authors did not find acetylene in the stoichiometric and lean flame. This fact seems quite strange since acetylene usually easily forms in flames from ethylene which is especially abundant in FAEEs flames.

It is worth to note that pentanoic (valerate) esters are of great interest themselves [87]. The reason is that this type of esters can be easily obtained from lignocellulose which is one of the main components of wood. [7], [88]. Therefore woody residuals can be effectively used as a raw material for the production of the ester-based biofuels. In the work of Contino et al. [9] the efficiency of a gasoline internal combustion engine (PSA EP6 engine) was tested running on several fuel mixtures: pure methyl pentanoate, pure ethyl pentanoate, a mixture of 20% ester with reference fuel PRF95 and pure PRF95. In addition, the researchers have monitored the composition of the exhaust gases in different engine operating regimes. The authors did not find any significant deterioration in engine performance when using valerates compared to the reference fuel. In the work of Lange et al. [7] a long-term test was carried out on ten gasoline engines that had been run for four months on a EPe(15%)/gasoline mixture. The engine power, its wear, composition of exhaust gases, fuel consumption and stability were monitored during machine exploitation. No operational problems were identified with the exception of a slight increase in consumption. A slightly higher engine performance was also noted that was associated by the authors with a high octane number (~100) of the ester. Thus, due to the high octane number and higher energy density than ethanol, methyl pentanoate and ethyl pentanoate are considered as effective additives or even an alternative to traditional fossil gasoline [7], [9].

Ester	Reactor	Conditions	Reference
EP	Shock tube	$T=1100-1670$ K, $p=1-4$ atm, $\varphi=0.25-1.5$	[71]
EA, EP	Shock tube	$T=1060-1572$ K, $p=1-11.4$ atm, $\varphi=0.5; 1.0; 2.0$	[73]
EF, EA, EP	Shock tube	$T=1301-1636$ K, $p=1.48-1.72$ atm	[74]
EB	Shock tube	$T=1250-2000$ K, $p=8$ atm, $\varphi=0.25-2$	[75]
EB	Plug-flow reactor	$T=500-1200$ K, $p=1$ atm, $\varphi=0.5-1.6$	[76]
EF, EA, EP	Counterflow burner	$p=1$ atm, $\varphi=0.7-1.5$	[77]
EA, EP, EB	Spherical chamber	$T=323-473$ K, $p=1-10$ atm, $\varphi=0.7-1.5$	[78]
EP	Jet-stirred reactor	$T=750-1100$ K, $p=10$ atm, $\varphi=0.3; 0.6; 1.0; 2.0$	[72]
EPE	Jet-stirred reactor	$T=560-1160$ K, $p=10$ atm, $\varphi=0.6; 1.0; 2.0$	[79]
	Spherical chamber	$T=423$ K, $p=1-10$ atm, $\varphi=0.7-1.4$	
EP	Coflow burner	$p=1$ atm, $X(\text{EP})=0.5\%$	[81]
EA	Flat burner	$p=37.5$ Torr, $X(\text{EA})=0.2\%$	[80]
EF	Flat burner	$p=30$ Torr, $\varphi=1.82$	[68]
EP	Flat burner	$p=30$ Torr, $\varphi=1.56$	[82]
EPE	Flat burner	$p\approx 15$ Torr, $\varphi=1.56$	[83]
EF, EA, EP	Flat burner	$p=30$ Torr, $\varphi=1.50$	[84]
EPE	Flat burner	$p=20$ Torr, $\varphi=1.00$	[85]
EPE	Flat burner	$p\approx 40$ Torr, $\varphi=0.81; 0.95; 1.31$	[86]

$T$  – mixture temperature,  $p$  – pressure in reactor,  $\varphi$  – equivalence ratio,  $X$  – mole fraction.

Table 2. List of kinetic studies of oxidation and combustion of small ethyl esters.

### 1.2.2 Kinetic investigations of oxidation and combustion of heavy FAEEs and real biodiesel components

As it noted earlier, light esters cannot fully reproduce the oxidation kinetic features of the components of a real biodiesel fuel. In this regard, despite the high complexity of experiments and modeling, various scientific teams have attempted to investigate detailed kinetics of the oxidation and combustion of heavy fatty acid esters. As in the case of light esters much more attention has been paid to FAMEs, while only a few works have been devoted to the study of heavy FAEEs. Zhang and Boehman have investigated ignition behavior of heavy FAEEs in a CFR engine compared to other heavy esters. In work [89] two esters with the general formula  $C_8H_{16}O_2$ , ethyl hexanoate and methyl heptanoate, were studied. Methyl heptanoate was found to be more reactive at low-temperature conditions than ethyl hexanoate. This was manifested in earlier decomposition of methyl ester and higher heat release in the low-temperature region at the same compression ratios. Thereby the authors concluded that the longer alkyl chain of methyl heptanoate plays a decisive role in the reactivity of the fuel despite the six-centered unimolecular decomposition of ethyl hexanoate. The authors also note the important role of the H-abstraction reactions from  $\alpha$ -carbon during the oxidation of esters which significantly affect the composition of intermediate and final products. In work [70] ignition of four  $C_9$ -esters was investigated by analogous methods: ethyl nonanoate, methyl nonanoate, methyl-2-nonenoate and methyl-3-nonenoate. The key conclusions of the work were about the highest reactivity of ethyl ester and a significant decrease of the low-temperature heat release in the presence of a double bond. The highest reactivity of ethyl ester was explained by the presence of an additional secondary C-H bond which increases the number of possible six-membered transition states for unimolecular decompositions. The authors also note that the presence of a double bond makes it difficult to form intermediate cycles that leads to a lower reactivity of unsaturated esters in the low-temperature region. Analyzing the product compositions the authors proposed the possible reaction pathways for the

oxidation of the esters studied. The analogy with the oxidation of heavy alkanes and alkenes was noted. Ghosh et al. [90] has investigated detailed kinetics of combustion of ethyl levulinate (EL) which is considered to be another type of liquid biofuel produced in large quantities from woody biomass. In this work ignition delay times of EL/O<sub>2</sub>/Ar mixtures in a shock tube and a rapid compression machine were investigated. A new kinetic mechanism has been proposed to describe the experimental data. Ethyl levulinate is an ethyl ester with a carboxyl group on the alkyl tail. In this regard, to develop the mechanism for the oxidation of ethyl levulinate, the authors used the mechanism of the ethyl propanoate oxidation and the model of 2-butanone oxidation. To take into account the thermochemistry of reactions correctly the same group of researchers has performed a theoretical calculation of thermodynamic parameters for the mechanism of EL oxidation [91]. The developed kinetic model satisfactorily described the experimental data, and the analysis of production pathways and sensitivity has shown that the ester oxidation chemistry plays a crucial role in these conditions. Using the developed model the authors estimated the research and motor octane number of EL ( $\geq 97.7$  and  $\geq 93$ , respectively) and came to the conclusion that EL can be used rather as a fuel additive to gasoline to increase the octane number. Previously EL was considered in the literature mainly as a biodiesel additive [92].

This literature review indicates clearly a lack of experimental and theoretical studies of the detailed kinetics of the oxidation of heavy FAEEs. At the same time existing works highlight a number of specific properties of ethyl esters in comparison with methyl ethers that indicates the need for additional studies of FAEEs. Moreover, the development of kinetic schemes for the oxidation of heavy ethyl esters can be based on the oxidation models of lighter FAEEs and on the existing oxidation mechanisms of heavy hydrocarbon fuels. Despite the fact that similar work has already been done for a number of heavy FAMES [93]–[95], the description of the kinetics of ethyl esters oxidation requires separate systematic studies.

## 1.2. THE MAIN OBJECTIVES OF THE WORK

Analyzing the literature review it can be concluded that there is a fairly good understanding of the kinetics of oxidation and combustion of small ethyl esters such as ethyl acetate and ethyl propanoate. These compounds are the most popular objects of experimental and theoretical studies that made it possible to develop detailed mechanisms of their oxidation with acceptable predictive potential. Despite the fact that these studies laid the foundation for the development of the oxidation mechanisms for FAEEs, these light compounds are only surrogates of the real biofuel components and they are not of practical interest themselves. Moreover, some authors have noted the incorrect use of esters with such short alkyl chains as the model biodiesel fuels. However, systematic investigations of heavier esters are associated with experimental and computational difficulties which, apparently, are the main reason for the small number of works in this direction. At the same time, information, primarily experimental, on the features of the oxidation of FAEEs with an alkyl chain of more than three carbon atoms is of great practical and scientific importance. A striking example is ethyl pentanoate, which is considered as an effective additive to gasoline, and at the same time it is a good model compound for kinetic studying of oxidation of real biodiesel components. Nevertheless, only one study of the laminar burning velocities of this compound is presented in the literature, any measurements of the ignition delay times are generally absent, and measurements of the chemical flame structure are rather contradictory.

Taking into account the above gaps in the literature flames of ethyl butanoate and ethyl pentanoate were chosen as the main objects of this research. For self-control and expansion of the experimental database it was also decided to investigate the chemical structure of ethyl acetate flames. The main tasks of the presented work were formulated as follows:

1. Measure the chemical structure of ethyl acetate, ethyl butanoate and ethyl pentanoate premixed flames stabilized on a flat burner at low and

atmospheric pressure. Clarify the ambiguous data on the structure of ethyl pentanoate flames at low pressure presented in the literature.

2. To analyze the existing kinetic models of ethyl esters oxidation and to develop a new detailed combustion mechanism of the esters studied basing on the most modern works on the kinetics of oxidation of small FAEEs.
3. Carry out numerical simulation of the chemical structure of the flames studied using a new mechanism and the mechanisms presented in the literature, determine the advantages and disadvantages of the proposed model. To conduct a comparative analysis of the ability of different mechanisms to qualitatively and quantitatively describe the chemical structure of the flames of the studied esters.
4. Carry out a numerical analysis of the kinetic mechanisms in order to determine the reasons of the discrepancies between the simulations and the experimental results. Suggest possible ways of the mechanism improvements.

## **CHAPTER 2. METHODICS**



This chapter contains two parts. Part 2.1 presents the experimental methods used in the work. Experimental setups, experimental conditions, methods of data processing and uncertainty analysis are described in detail. Part 2.2 describes methods of numerical modeling and analysis of chemical transformations in flames. Detailed information on the kinetic mechanisms used in this work is provided in this part. The aspects of a new mechanism development are also discussed.

## 2.1. EXPERIMENTAL DETAILS

### 2.1.1. Physical properties of the esters studied

Flames of fatty acid ethyl esters with the alkyl chains of two (ethyl acetate), four (ethyl butanoate) and five (ethyl pentanoate) carbon atoms with general formulas  $C_4H_8O_2$ ,  $C_6H_{12}O_2$  and  $C_7H_{14}O_2$ , respectively, were investigated. These esters are colorless, non-toxic, slightly water-soluble liquids with a strong characteristic odor. In the experiments reactants produced by Sigma-Aldrich with a purity of 99% were used. Table 3 shows the main physical properties of these compounds.

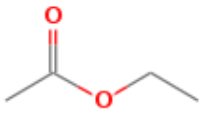
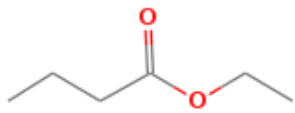
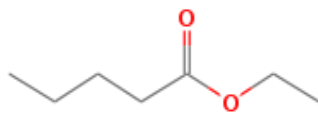
Physical properties [96]	Ethyl acetate 	Ethyl butanoate 	Ethyl pentanoate 
Gross formula	$C_4H_8O_2$	$C_6H_{12}O_2$	$C_7H_{14}O_2$
Molar mass, g/mol	88,1	116,2	130,2
Density (25 °C), kg/m <sup>3</sup>	902	875	875
Boiling temperature, °C	77	120	144-145

Table 3. Physical properties of the esters investigated in the work.

## 2.1.2. Molecular-beam mass-spectrometric setup for studying the chemical flame structure at atmospheric pressure

Experimental measurements of the chemical flame structures of ethyl esters at atmospheric pressure were carried out in the Laboratory of Kinetics of combustion processes (KCP) at the Voevodsky Institute of Chemical Kinetics and Combustion SB RAS in Novosibirsk, Russia. The experimental complex includes a fuel mixture supply system, a burner device and a mass-spectrometric analyzer combined with a gas sampling system. A detailed description of the main elements of the experimental setup, as well as the measurements and data processing techniques is provided below.

### *2.1.2.1. Description of the Botha-Spalding burner and the fuel supply system*

Atmospheric flames of the investigated substances were stabilized on a flat burner of the Botha-Spalding type [97] shown in Figure 2.1 (a). A flame ignited on the given burner is quasi-one-dimensional that means the concentration of substances and the flame temperature at any point in a plane parallel to the burner surface are constant and depend only on the coordinate along the normal to the burner surface. The one-dimensionality is violated only at the edges of the flame where significant heat losses and convective flows appeared. Therefore all measurements were carried out in the central part of the flame. The burner itself is a brass disc with a radius of 16 mm and a thickness of 3 mm with holes 0.5 mm in diameter and a distance of 0.7 mm between them. The disc is mounted in a water-cooled brass body controlled by a Termex VT4-1 thermostat. The burner temperature was maintained at 95 °C. Oxygen and argon flows were manually set with an accuracy of  $\pm 1\%$  using a calibrated mass-flow controller (MKS) MKS System Inc.

Liquid fuel was supplied from a syringe to evaporator through a metal capillary (Figure 2.1 (b)). The syringe plunger was driven by a stepper motor

operating at a given frequency corresponding to the required volumetric flow rate. A stream of argon and oxygen was passed through the evaporator carrying along the vapors of the liquid fuel. The vaporizer was made of a pyrex vessel filled with steel balls and equipped with an electric heater. The evaporator was maintained at a temperature of 10-15 °C below the boiling point of the particular ester studied. The choice of such a temperature regime ensured a complete evaporation of liquid ester continuously supplied to the evaporator. At the same time the temperature lower the boiling point did not lead to ester boiling that can cause instabilities in the fuel vapor supply to the burner.

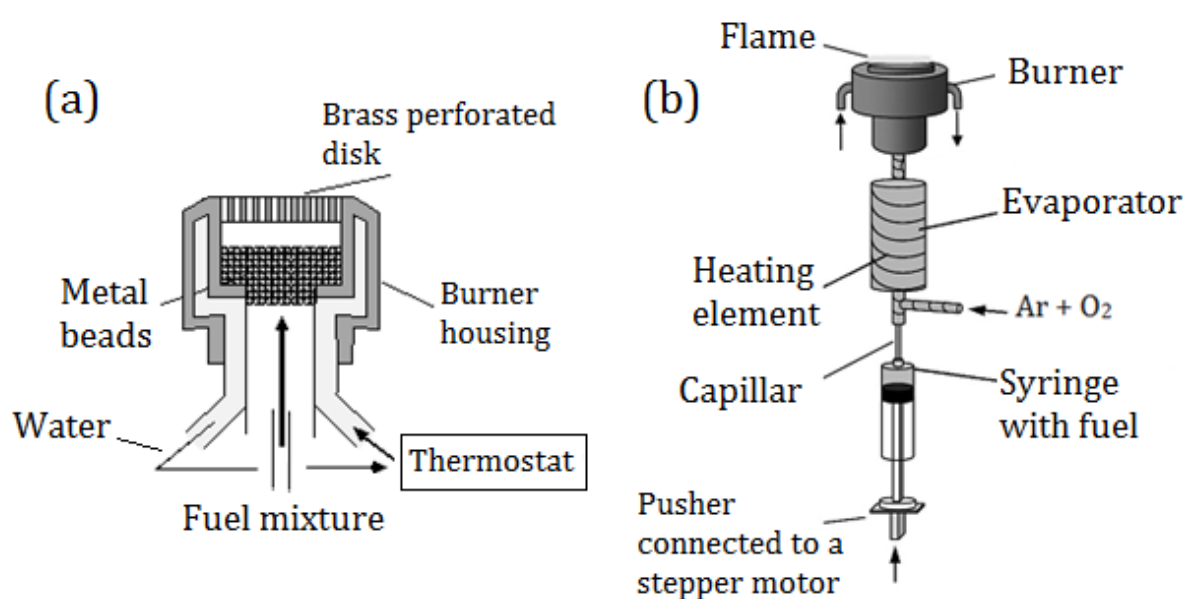


Figure 2.1. Botha-Spalding burner device (a) and the system of the fuel mixture supply to the burner (b).

Liquid fuel was supplied from a syringe to evaporator through a metal capillary (Figure 2.1 (b)). The syringe plunger was driven by a stepper motor operating at a given frequency corresponding to the required volumetric flow rate. A stream of argon and oxygen was passed through the evaporator carrying along the vapors of the liquid fuel. The vaporizer was made of a pyrex vessel filled with steel balls and equipped with an electric heater. The evaporator was maintained at a temperature of 10-15 °C below the boiling point of the particular ester studied. The choice of such a temperature regime ensured a complete

evaporation of liquid ester continuously supplied to the evaporator. At the same time the temperature lower the boiling point did not lead to ester boiling that can cause instabilities in the fuel vapor supply to the burner.

The component composition and mass-flow rates of combustible mixtures in experiments at atmospheric pressure are shown in Table 4. Here  $X$  is the mole fraction of a substance in the mixture,  $Q_v$  is the total volumetric flow rate of the fuel mixture under standard conditions (25 °C),  $Q_m$  is the total mass flow rate of the mixture,  $\varphi$  is the equivalence ratio.

<i>Fuel</i>	$X(\text{ester})$	$X(\text{O}_2)$	$X(\text{Ar})$	$Q_v, \text{cm}^3/\text{s}$	$Q_m, \text{g}/(\text{s}\cdot\text{cm}^2)$	$\varphi$
EA	0.037	0.163	0.8	25	0.0245	1.1
EA	0.077	0.223	0.7	15.24	0.0155	1.7
EB	0.022	0.178	0.8	24.98	0.0244	1.0
EB	0.047	0.253	0.7	15.24	0.0154	1.5
EPe	0.019	0.181	0.8	25	0.0203	1.0

Table 4. Composition and mass-flow rates of combustible mixtures of ethyl esters studied at atmospheric pressure.

#### *2.1.2.2. Description of the MBMS-setup for studying the chemical flame structure at atmospheric pressure*

The analysis of the chemical composition of the flames was carried out using a molecular-beam mass-spectrometric setup (MBMS) with soft ionization by electron impact. This setup was constructed in the Laboratory of Kinetics of combustion processes to analyze the chemical structure of flames in a wide range of pressures. The experience of successful operations of this setup is reflected in many publications of the laboratory staff [98]–[103].

The general scheme of the MBMS-setup is shown in Figure 2.2. This experimental setup consists of three series-connected vacuum chambers with constant evacuation. The analyzed gas volume enters the first chamber through the sampler. After sampling the gas volume moves forward in the form of a molecular beam into the third chamber with a quadrupole mass spectrometer installed in it. The signal from the mass spectrometer is processed by the data acquisition system and output to the computer. The sampling process and the technical details of the installation are described in more detail below.

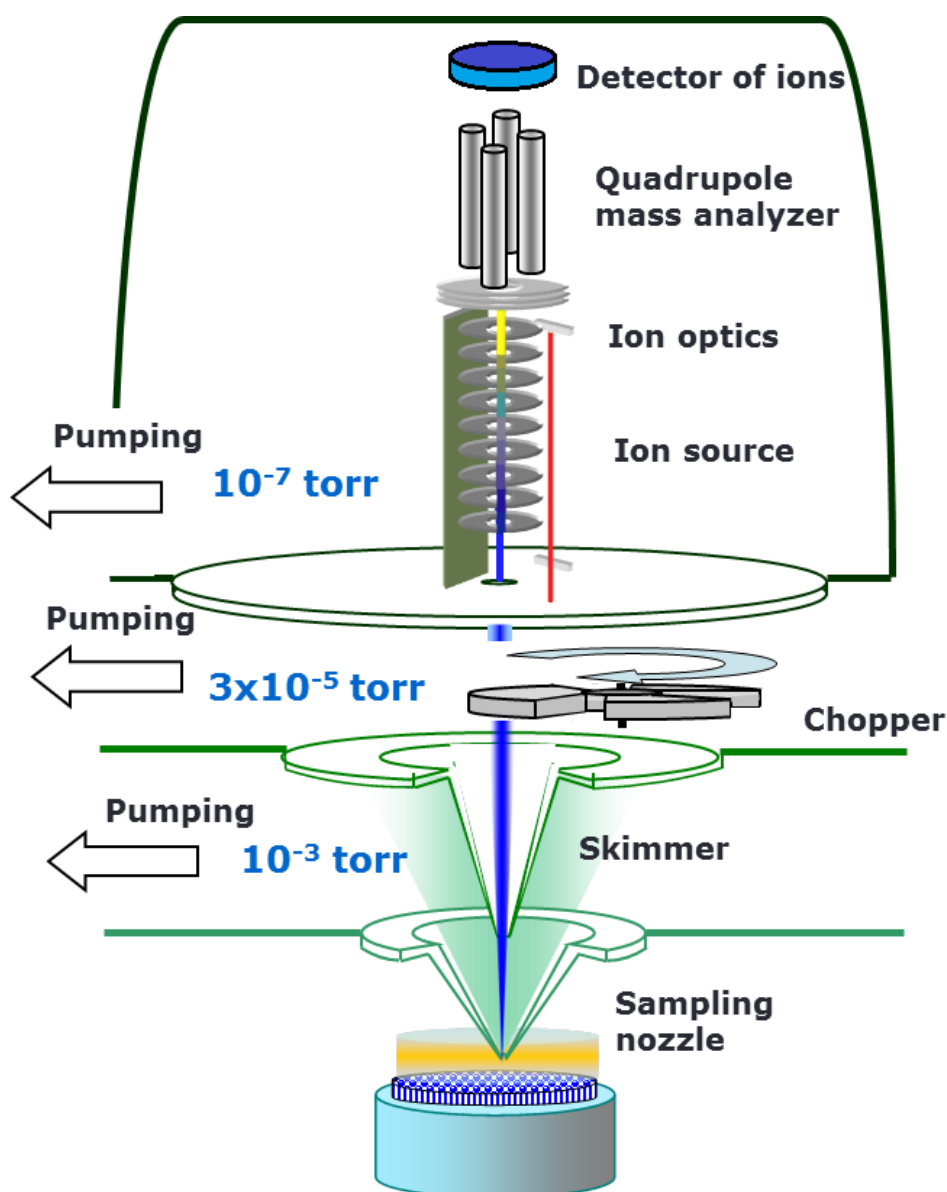


Figure 2.2. General scheme of the MBMS-setup for the measurements of the chemical flame structures.

Sampling from the flame is performed by a conical quartz probe with a hole in the tip. A schematic drawing and a real photograph of the probe are shown in Figure 2.3. The manufacture of such a probe is tailored manually and is an extremely demanding process since the quality and accuracy of manufacturing of the probe affects directly the gas sampling from the flame. For the experiments described a standard probe for this setup was prepared. The geometric parameters of the probe were selected on the basis of theoretical justifications and the previous experience of the laboratory staff of KCP [104], [105]: the inner opening angle of the cone is  $40^\circ$ , the outer angle is  $50^\circ$ , the size of the hole at the tip is 0.08 mm, the wall thickness near the hole is about 0.08 mm, the total height of the cone is 25 mm. The probe is glued with epoxy resin to a water-cooled metal flange which in turn is rigidly attached to the 1st chamber. Pressure in the 1st chamber is maintained at the level of  $10^{-2}$ - $10^{-3}$  Torr using a diffusion steam-oil pump with a pumping capacity of 1100 l/s. Due to the created pressure difference outside and inside the probe a portion of gas is sucked from the flame. During sampling the gas reaches supersonic speed at the nozzle inlet. Rapid expansion into vacuum leads to the "freezing" of the degrees of freedom and then the gas moves in the form of a non-reacting molecular beam.

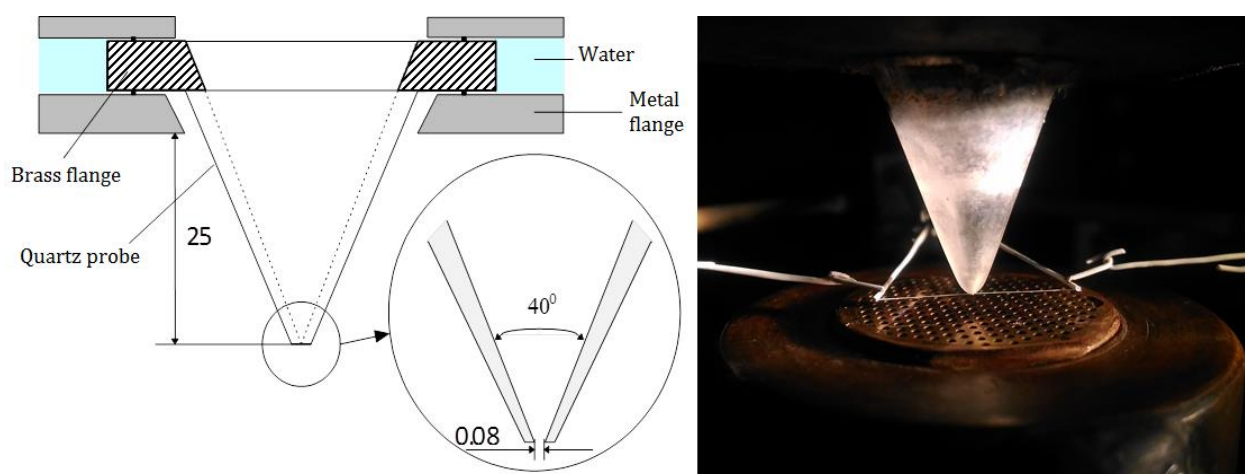


Figure 2.3. Schematic drawing of the probe with a mounting flange and the real photograph of the probe above the thermocouple and burner.

Measurement unit: mm.

Molecular beam enters the 2<sup>nd</sup> chamber through a skimmer which is presented as a stainless steel cone with an internal angle of 40°, an external angle of 60° and a hole in the tip with a diameter of 0.64 mm. The distance between the tip of the sampling probe and the skimmer is 20 mm. This distance is chosen so that the top of the skimmer is placed closer to the probe than the theoretical position of the Mach disk in the gas flow (~25 mm for this system). The skimmer cuts out the central unperturbed part of the molecular beam and passes it into the 2<sup>nd</sup> chamber. Operating pressure in the 2<sup>nd</sup> chamber is maintained at a level of 10<sup>-5</sup> Torr using a turbomolecular pump with a capacity of 500 l/s. The second chamber contains a modulator which is performed as a rotating disc with three slots. The modulator alternately overlaps and then passes the molecular beam into the 3<sup>rd</sup> chamber. Presence of the modulator in the system makes it possible to distinguish between the “background” and “beam + background” signals.

The beam passes from the 2<sup>nd</sup> chamber to the 3<sup>rd</sup> chamber through a collimator orifice with a diameter of 4 mm and then enters to the ion source. The distance between the holes "skimmer - collimator" is 350 mm and "collimator - ion source" is 50 mm. Normal pressure in the 3<sup>rd</sup> chamber is about 10<sup>-7</sup>-10<sup>-8</sup> Torr, and it is maintained using a turbomolecular pump with a pumping capacity of 500 l/s. This setup is equipped by a modified ion source in the form of a filament cathode with a voltage drop compensation system and ion optics developed at the Institute of Energy Problems of Chemical Physics, Russian Academy of Sciences [106]. The source creates a beam of ionizing electrons with a narrow energy spread ( $\pm 0.25$  eV) that allows operating in the “soft” ionization mode at energies close to the ionization potential of particular atoms and molecules in a flame (~8-16 eV). This ionization method reduces fragmentation and overlapping of mass peaks from different substances that greatly simplifies the mass spectra interpretations.

Separation by the masses of the resulting ions occurs in an EZAN MS-7302 quadrupole mass-spectrometer. The signal from the secondary electron multiplier VEU-6, which acts as a detector, is guided through the shaping

amplifier to the pulse counter. Herewith the background signal determined by the molecular beam modulation is automatically subtracted. Each signal value of a particular mass peak is formed from averaging over three detector measurements. The entire data acquisition and synchronization system of the modulator is based on the CAMAC standard and is controlled from a computer. Setting the ionizing energy of the ion source and adjusting the quadrupole to mass are also made from a computer through digital-to-analog converters (DAC).

### *2.1.2.3. Measurement of mass spectra and identification of compounds*

Moving the burner vertically by a screw mechanism we measured the dependence of the mass peak intensities on the distance "probe - burner" at a given ionization energy for each mass. The distance "probe - burner" was controlled using a cathetometer with an accuracy of  $\pm 0.05$  mm. The list of measured mass peaks was compiled individually for each flame based on a literature analysis and the assumed paths of the corresponding fuel destruction. For each compound the parent peak or the most intense fragmentation peak (or both) was chosen as the measured mass. The database of the National Institute for Standards and Technology (NIST) was used as a database of mass spectra [107].

Since argon is the main component (70-80%) of the fuel mixture in all flames, the initial signals of the measured mass peaks ( $I_i^0$ ) were normalized to the intensity of the signal of the 40th mass ( $I_{Ar}^0$ ) and the mole fraction of argon ( $X_{Ar}$ ):

$$(2.1) \quad I_i = \frac{I_i^0}{I_{Ar}^0} \cdot X_{Ar}$$

Such normalization makes it possible to compare flames with different argon dilutions and to avoid the scatter of measured signals associated with possible fluctuations in the gas flow. Further data processing is carried out with normalized signals.



The signal intensity of the  $i$ -th component ( $I_i$ ) is related to its mole fraction ( $X_i$ ) by a simple ratio:

$$(2.2) \quad I_i = S_i(E) \cdot X_i,$$

where  $S_i(E)$  is a calibration factor for a given substance at the fixed ionizing electron energy  $E$ . The calibration factor depends on many parameters and can generally be represented by the following expression [108]:

$$(2.3) \quad S_i(E) = A \cdot \sigma_i(E) \cdot D(m_i) \cdot F(T, p),$$

where  $A$  is a numerical coefficient of proportionality,  $\sigma_i(E)$  is an effective ionization cross-section of the  $i$ -th compound at the energy of ionizing electrons  $E$ ,  $D(m_i)$  is a coefficient that characterizes the dependence of the sensitivity of the MBMS-setup on the mass of detected ions; the mass-discrimination factor appears due to the fact that the central part of the molecular beam can be enriched with the heavier particles because of barodiffusion,  $F(T, p)$  is an empirical function that establishes the dependence of the molecular beam density in the ionization region on the flame pressure  $p$  and local temperature  $T$ . The  $F(T, p)$  function is an instrumental function, so it is determined by the geometry (probe, skimmer, collimator) and gas-dynamic characteristics of the system. Therefore  $F(T, p)$  is a unique function of the apparatus and it has the same value for all the species detected on the same setup.

$S_i(E)$  coefficients for most of the stable compounds were determined in direct calibrations using the gas mixtures of known composition. For the calibrations the flow of calibration gases was injected directly to the probe through a burner with a quartz tube attached to it. The tube was heated by an external source to 453-473 K in order to avoid formation of gas clusters at the probe entrance.

Writing equation 2.1 and taking into account 2.2 for two compounds  $i$  and  $j$  in a molecular beam we can obtain the relation:

$$(2.4) \quad I_i/I_j = \sigma_i(E_i)/\sigma_j(E_j) \cdot D(m_i)/D(m_j) \cdot X_i/X_j$$

The ratio  $D(m_i)/D(m_j)$  can be determined experimentally. For that the measurements were carried out using the calibration mixtures of known

composition consisting of gases with different molecular weights. It was shown that for compounds with close molecular weights the ratio  $D(m_i)/D(m_j) \approx 1$ . These value also corresponds to the theoretical substantiation of this effect [109].

Equation 2.4 shows that determining the signal intensities of the two compounds, the corresponding ionization cross sections and the mole fraction of one of the compounds, the mole fraction of the second compound can be calculated. This method for the mole fraction determining is called the method of relative ionization cross-section (RICS)[108]. This approach was applied in the case of impossibility of direct calibration for any compound. The electron impact ionization cross-sections for a given ionizing electron energy were taken from the NIST database [110]. Unfortunately, the error this method is quite high, by the order of 20%, since the theoretical calculations of the effective ionization cross-sections at low electron energies is a complex physical problem. In this regard the general accuracy of determining the molar fraction according to the RICS method was noticeably lower than that according to the direct calibrations.

The total statistical uncertainty of determining the mole fractions of reactants and stable products (Esters, O<sub>2</sub>, CO, CO<sub>2</sub>, H<sub>2</sub>O) was about  $\pm 15\%$ . The measurement accuracy of molecular hydrogen was approximately  $\pm 30\%$  due to the difficulties with it pumping out of the vacuum system. The mole fractions of the remaining compounds were determined with an accuracy of  $\pm 50\%$ . All profiles below are obtained by averaging over several measurements. A complete list of compounds measured in the flames at atmospheric pressure is given in Appendix 1. The Appendix also contains the values of the ionization potentials (PI), the energy of ionizing electrons (EIE) at which each compound was measured, the calibration method and the accuracy of the mole fraction determination.

### 2.1.3. Online sampling gas chromatographic setup for studying the chemical flame structure at low pressure

Experimental measurements of the chemical flame structure of esters at low pressure were performed at the Laboratory of Reactions and Process Engineering CNRS (LRGP) in Nancy, France. The measurements were carried out on a combustion facility with probe sampling from a flame front in a low-pressure chamber with further analysis on a gas chromatograph. This setup was constructed by the collective of the LRGP and it has been successfully applied for the combustion kinetics studies in previous works [111]–[113].

#### *2.1.3.1. Description of the fueling and vacuum pumping systems*

The general scheme of the experimental stand is shown in Figure 2.4. The combustible mixture, consisting of argon, oxygen and vapors of the studied ester, was supplied to the burner through the heated line highlighted by red in the figure. The fueling line was additionally heated to avoid condensation of heavy ester vapors. The mass flow of each gas was controlled by a corresponding mass-flow controller (Bronkhorst) connected to a computer. The liquid fuel was supplied from a metal vessel which was pressurized by argon injected through the special channel. The fuel portion pressed out of the vessel entered the fuel supply line. The exact ester flow rate was controlled by a Coriolis-type mass-flow controller (Bronkhorst Cori-Tech) installed at the outlet of the ester vessel. After the MFC the liquid entered an evaporator-mixer (Bronkhorst) where it was evaporated and mixed with argon. The resulting fuel mixture entered the burner along with the other gases. All the controllers were calibrated before the experiments. Then the flow control manipulations were carried out from the computer only.

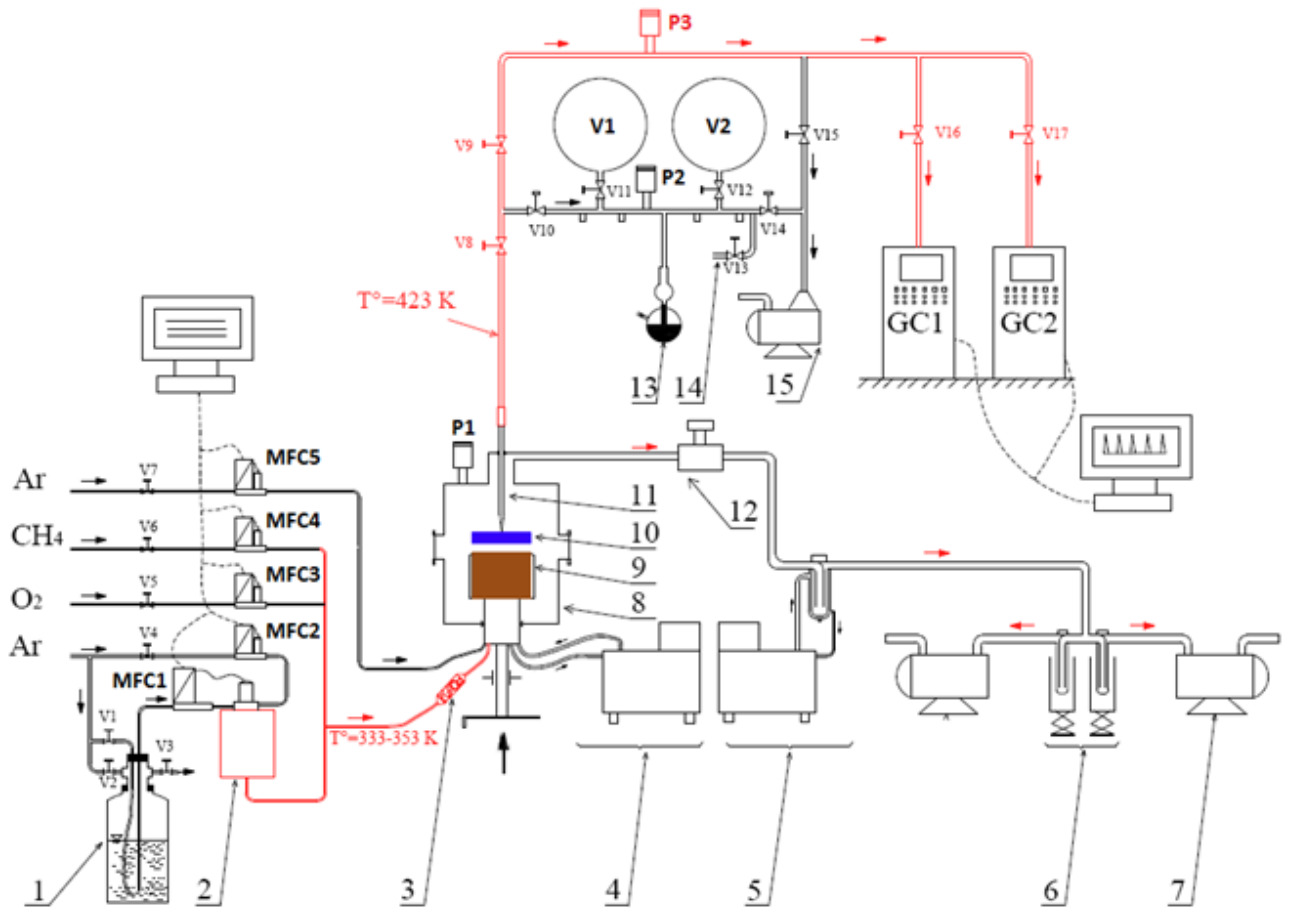


Figure 2.4. General scheme of the experimental facility for studying the chemical flame structure at low pressure.

- |  |  |
|--|--|
| 1 – metal vessel with a liquid fuel                      | 11 – sampling probe                          |
| 2 – evaporator   | 12 – pressure regulator                      |
| 3 – filter/flow stabilizer                               | 13 – mercury piston for the gas pressurizing |
| 4 – burner cooling thermostat                            | 14 – inlet for the calibration mixture       |
| 5 – water condensing system with a cooling thermostat    | 15 – turbomolecular pump                     |
| 6 – water condensation system with liquid nitrogen traps | V1-V17 – valves                              |
| 7 – rotary vane pump                                     | GC1-GC2 – gas chromatographs                 |
| 8 – low pressure chamber                                 | MFC1-MFC5 – mass-flow controllers            |
| 9 – McKenna burner                                       | P1-P3 – pressure gauge                       |
| 10 – flame   | V1-V2 – free vessels for the mixtures        |

Since the experiments were carried out in a low-pressure chamber, the flame was ignited by an electric discharge created between an electrode in the chamber and the burner surface. It was not always possible to ignite the investigated combustible mixture with such approach. To solve this problem a

stoichiometric flame of methane was ignited first. An additional methane line was connected to the general mixture supply system through its own MFC. After methane had been ignited, the ester supply was switched on and the methane flow rate was gradually decreased to zero until the combustible mixture composition completely reached the required values.

During the experiments pressure in the chamber was maintained at 50 Torr due to a constant evacuation by two vane pumps. The pumping rate was regulated by a pressure regulator (12 in Figure 2.4). Since a combustion process generates a large amount of water, two nitrogen traps and a cooling thermostat were installed on the pumping line in front of the pumps. This allowed us to minimize the amount of water entering the pumps.

### *2.1.3.2. Description of the McKenna burner*

The flame was stabilized on a McKenna burner mounted in a metal combustion chamber (8-10 in Figure 2.4). The burner was mounted on a metal rod and could be moved vertically with a screw mechanism under the chamber. The position of the burner surface was controlled using a cathetometer with an accuracy of  $\pm 0.05$  mm.

The McKenna burner itself consists of a round metal housing with a diameter of 120 mm. Connections for the inlet of gases and water are mounted in the burner body (Figure 2.5 (a)). A porous sintered bronze disc is pressed into the central part of the body (60 mm in diameter) and a spiral copper tube of water cooling is pressed inside the disk. The burner temperature was maintained during the experiments at 333 K using a water thermostat. Around the central disc there is a porous ring also made of sintered bronze. A gas flow can be supplied separately from the main combustible mixture through this ring that makes it possible to stabilize the flame additionally. However, this opportunity was not used in our experiments.

Fuel gas entered the burner mixes uniformly in the housing and exits through the porous disk as a laminar flow. This flow after ignition forms a flat quasi-one-dimensional flame (Figure 2.5 (b)).

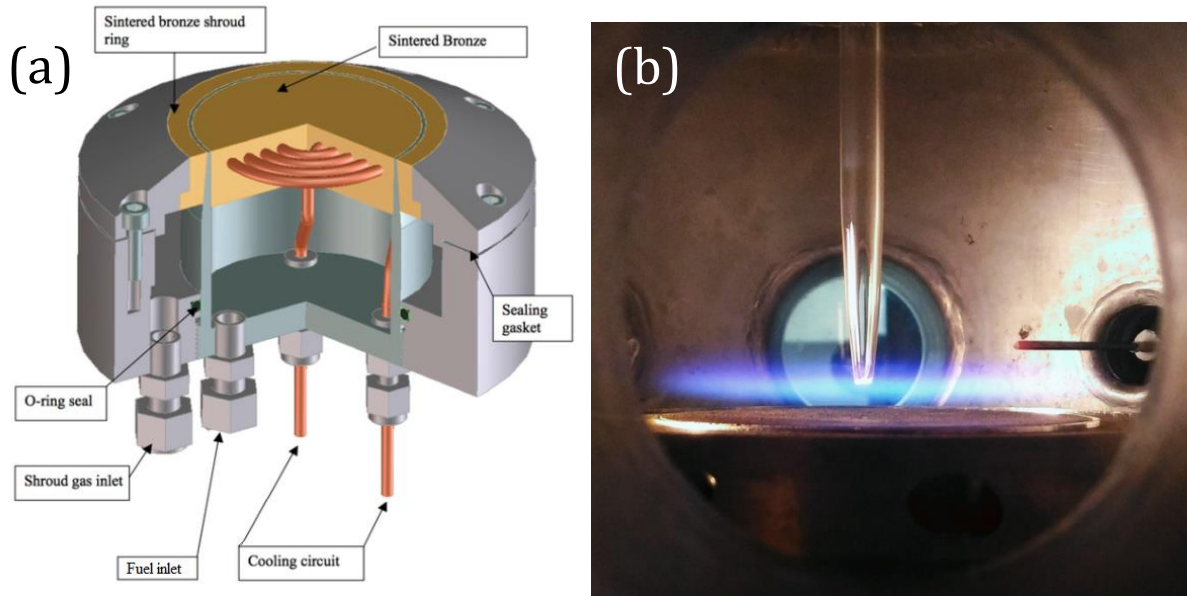


Figure 2.5. McKenna burner device (a) and real photograph of the flame stabilized on the burner in the low pressure chamber (b).

Table 5 shows compositions and flow rates of the combustible mixtures in experiments at low pressure. Here  $X$  is the mole fraction of the substance in the combustible mixture,  $Q_v$  is the total volumetric flow rate of the fuel mixture under the standard conditions (25 °C, 1 atm),  $Q_m$  is the total mass flow rate of the mixture,  $\varphi$  is the equivalence ratio.

<i>Fuel</i>	$X(\text{ester})$	$X(\text{O}_2)$	$X(\text{Ar})$	$Q_v, \text{cm}^3/\text{s}$	$Q_m, \text{g}/(\text{s}\cdot\text{cm}^2)$	$\varphi$
EA	0.042	0.208	0.75	91.7	0.00584	1.0
EPE	0.024	0.226	0.75	100.1	0.00577	1.0

Table 5. Composition and flow rates of unburnt gas mixtures of ethyl esters studied at low pressure.

### 2.1.3.2. Description of sampling system

Sampling from the flame was carried out using a thin quartz capillary probe with a conical narrowing and a hole in the tip (Figure 2.5 (b)). The geometric characteristics of the probe are shown in Figure 2.6.

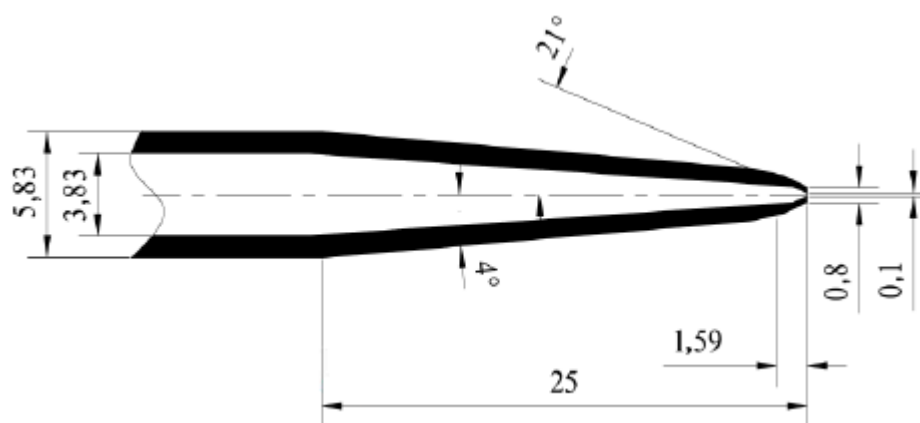


Figure 2.6. Geometry of the sampling probe used in experiments at low pressure. Measurement unit: mm.

This type of probe has a narrower shape compared to the probe for MBMS experiments that makes it possible to reduce gas-dynamic and thermal disturbances of the flame. However, due to the small opening angle a molecular beam is not formed in a narrow probe and highly reactive compounds, such as radicals, recombine on the inner surface of the walls.

The probe was fixed in the cap of the vacuum chamber in such a way that the sampling part was in the chamber and the outer part was stuck out of the chamber. Moving the burner inside the chamber it was possible to take a gas sample from different flame zones and to obtain a profile of the species mole fractions as the function of distance above the burner.

On the open side the probe was connected to an evacuated and heated sampling line leading to the vacuum system and GC analyzers. A valve was installed on the line near the capillary to cut it off from the chamber. Vacuum in

the sampling line and in the later volumes was maintained using a turbomolecular pump (TMP) connected to the system with a shut-off valve.

The sampling process at each point of the flame was carried out according to the following algorithm: first, the vacuum system and the sampling line were pumped out to a pressure of  $10^{-2}$ - $10^{-3}$  Torr. At this time the burner with flame was installed at the required height relative to the probe. Then the valve on the line was opened and the residual gas was pumped out in the capillary for several minutes. After that the valve in front of the TMP was closed, and sampling into the vacuum system began. Since pressure in the combustion chamber is low, the process of sampling leakage took about 1-2 minutes until pressure in the sampling system reached 10-12 Torr. Then the valve on the sampling line was closed stopping the sampling. The gas portion sampled was compressed up to 20-25 Torr using a mercury piston. This manipulation was done in order to increase the concentration of the investigated substances at the inlet to the chromatographs. After compression by mercury the gas portion entered two GC analyzers and the chemical analysis process was started.

### *2.1.3.3. Chromatographic analysis*

Online gas chromatography was used to obtain isomer-specific information for stable flame intermediates. Two standard GC analyzers were exploited for the sample analysis:

- Agilent 7890A equipped with HP-PlotQ and HP-Molesieve columns for separation of hydrocarbons, oxygenates and argon. Helium was used as a carrier gas. A flame ionization detector (FID) with a methanizer and a thermal conductivity detector (TCD) provided identification of the compounds. The methanizer provided conversion of CO, CO<sub>2</sub> and oxygenated compounds into methane that made it possible to record their signals on the FID, which allow a better precision and a much lower detection threshold.



■ HP 5890 Series II with Carbosphere column and TCD was used only for H<sub>2</sub> and O<sub>2</sub> detection. Argon was used as a carrier gas in this apparatus.

Retention times of the species were determined from the calibration mixtures and the previous works on this setup. The duration time of one sample analysis was mostly determined by the retention time of the corresponding fatty acid formed during ester combustion. For the flame of EPe the time of a single measurement reached 90 minutes. Detailed list of GC-analyses parameters is provided in Appendix 2. The list of the species detected in GC-analyses is provided in Appendix 3.

#### 2.1.3.4. Calibration and data processing

GC-signal from the  $i$ -th compound ( $I_i$ ) is defined as the area under the peak corresponding to the given compound on the chromatogram. The signal  $I_i$  is proportional to the concentration  $n_i$  and, therefore, to the partial pressure of the given compound in the gas sample  $p_i$ . The proportionality coefficient between the peak area of the  $i$ -th substance in the chromatogram and its partial pressure is called calibration coefficient  $S_i$ . When we know the coefficient  $S_i$  mole fraction of a compound ( $X_i$ ) can be easily found by the formula:

$$(2.1) \quad X_i = \frac{p_i}{P} = \frac{I_i}{S_i \times P},$$

where  $P$  – pressure of the taken sample at the inlet to the chromatograph.

To determine the calibration coefficients  $S_i$  direct calibrations were carried out with gas mixtures of known composition. For the calibrations the cylinders installed on a vacuum system were filled with a calibration mixture, then known amount of gas was let from the cylinder into the system and analyzed on GC. Most of the compounds measured in these experiments were calibrated directly.

When it was impossible to calibrate directly any species, the corresponding coefficient  $S_i$  was estimated indirectly by the number of carbon atoms in the

molecule. Such estimation is possible due to the fact, that the molecule is converted into methane passing through the methanizer which performs as a catalytic converter. The number of methane molecules formed corresponds to the number of carbon atoms in the starting compound. Thus the calibration coefficient of a substance of  $n$  carbon atoms can be estimated by the formula:

$$(2.1) \quad S_i = S_{CH_4} \times n ,$$

where  $S_{CH_4}$  – calibration coefficient for methane determined precisely from the direct calibrations.

It has been verified on many species that estimated calibration coefficients agree with coefficients of the direct calibrations with acceptable accuracy. For example, direct calibrations with  $C_2$ -compounds ( $C_2H_2$ ,  $C_2H_4$ ,  $C_2H_6$ ) provided coefficients  $S_i$  in the range of 13906-15562, whereas the coefficient calculated by the number of carbons is 15614. As it seen, the greatest deviation from the direct calibrations does not exceed 10%. The same situation was observed for the heavier compounds. Depending on the concentration of the component in a flame the uncertainty of the mole fraction determination was about 5% for the main components and about 10% for intermediate products ( $X_i < 10^{-4}$ ) that corresponds to the accuracy of the devices used.

## 2.1.4. Flame temperature measurements

### 2.1.4.1. Thermocouple temperature measurements

Temperature is the most important parameter in a reacting system. Accurate numerical simulation of the chemical flame structures requires information on the actual flame temperature in experiments. In this regard the profile of the temperature dependence on the height above the burner was measured in all flames. Temperature measurements in flames are rather complicated since the profiles are characterized by sharp gradients and high

absolute values of temperature on the scales of several millimeters. In this regard the micro-thermocouple method was chosen for temperature measurements in both atmospheric and low pressure flames.

One important specific of temperature measurements in experiments with sampling is the necessity of taking into account thermal disturbances of the flame by the probe. To account for these disturbances temperature is measured in a flame in the presence of a probe. Such approach provides a real temperature information as it is during the sampling. Thermocouple junction is placed near the probe orifice ( $\sim 0.1$  mm) measuring the gas temperature at the inlet of the sampling probe. Thermocouple position relative to the probe and the burner surface during temperature measurements are shown in Figure 2.7. For these measurements the thermocouple should be as thin as possible in order to obtain sufficient spatial resolution and minimize flow deceleration in front of the probe.

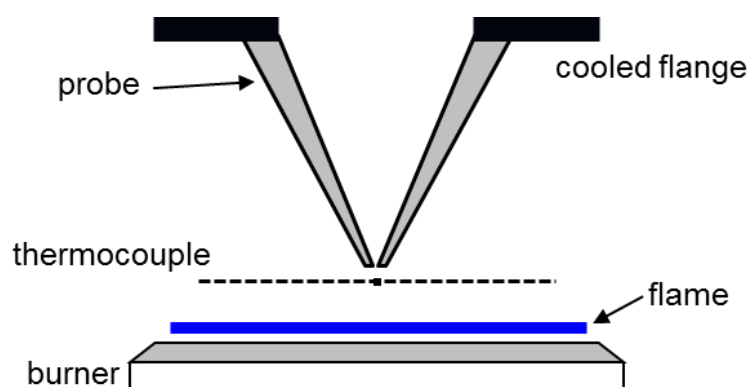


Figure 2.7. Thermocouple position relative to the probe and the burner surface during temperature measurements.

Since the thermocouple in a flame front heats up to temperatures of 1300–1500 K, the thermocouple wire begins to glow strongly thereby cooling and lowering the gas temperature readings. Therefore it is necessary to correct thermocouple measurements for radiation during experimental data processing.

### 2.1.4.2. Temperature measurements at atmospheric pressure

For the temperature measurements at atmospheric pressure thin S-type thermocouples made of Pt–Pt10%Rh wire of 0.03 mm thickness were used. The thermocouples were hand made for each experiment. Prepared thermocouple wire with thermojunction has been attached to the thermocouple body (Figure 2.8). For that platinum and platinum-rhodium wires were spot-welded under a microscope control. Then they were welded to the mustaches of a V-shaped holder made of thicker (0.2 mm) wires of the same metals. The mustaches were additionally stretched on the sides with springs to avoid sagging of the thermocouple in a flame because of heating. To prevent catalytic reactions on the wire surface the thermocouple was covered with a thin layer of silicon oxide  $\text{SiO}_2$ . Together with the coating the thickness of the thermocouples was about 0.05–0.07 mm. The thermocouple thickness was controlled before and after each measurement.

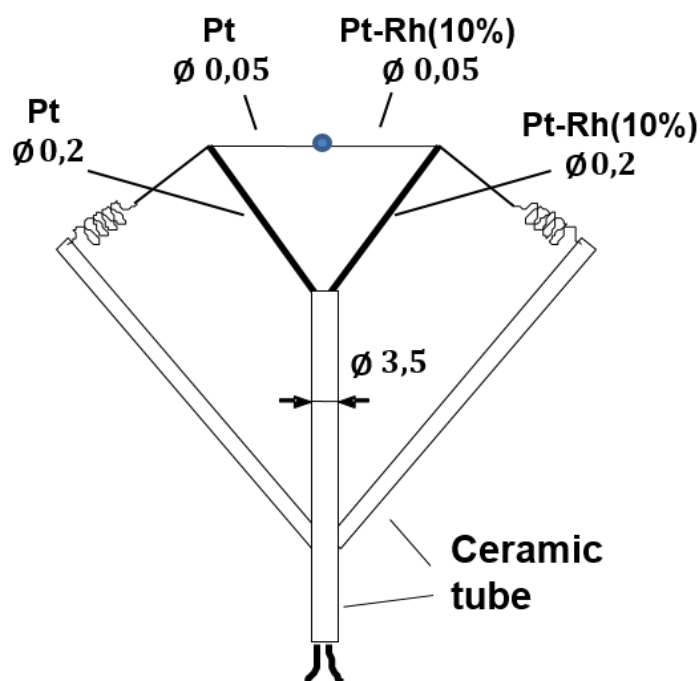


Figure 2.8. Schematic of the thermocouple in experiments at atmospheric pressure. Measurement unit: mm.

To take into account radiation heat losses the temperature correction was calculated using the formula proposed earlier in the work [114]:

$$(2.2) \quad \Delta T = T_g - T_c = \frac{1}{\lambda} [1.25 \cdot \varepsilon \cdot \sigma \cdot d^{\frac{3}{4}} \cdot (T_c^4 - T_w^4) \cdot (\eta / \rho v)^{\frac{1}{4}}],$$

where  $T_g$  is the gas temperature,  $T_c$  is the temperature of thermojunction,  $T_w$  is ambient temperature,  $d$  is thermocouple diameter,  $\varepsilon$  is the emissivity factor,  $\sigma$  is the Stefan-Boltzmann constant,  $\lambda$ ,  $\eta$  are the coefficients of gas thermal conductivity and viscosity,  $\rho$ ,  $v$  are the gas density and velocity. This formula is an analytical solution of heat balance between a hot gas flow and a cylinder.

Since argon was the main component of gas mixtures (70-80%), the coefficients of viscosity and thermal conductivity in the above formula were taken for argon taking into account their dependence on temperature. The temperature dependence of  $\varepsilon$  was taken into account according to the formula proposed in the work [115]. The resulting profile was obtained by averaging over several measurements. The absolute uncertainty of temperature measurements did not exceed  $\pm 50$  K.

#### *2.1.4.3. Temperature measurements at low pressure*

In experiments at low pressure the temperature profiles were measured using a thin B-type thermocouple. This type of thermocouples is made of platinum-rhodium wires with different ratios of platinum and rhodium: Pt30%Rh–Pt6%Rh by weight. In this work wires of 0.1 mm thickness were used. The flame zone at low pressure is much wider compared to the experiments at atmospheric pressure. Therefore a good spatial resolution can be achieved with thicker wire that greatly simplifies the manufacture and operation with such a thermocouple.

The thermocouple was spot-welded of corresponding wires and then welded to a U-shaped holder made of wires of larger diameter (0.5 mm) made of

the same alloys. The general construction of the thermocouple body is shown in Figure 2.9. To avoid catalytic reactions on the surface of the thermocouple a ceramic coating of BeO-Y<sub>2</sub>O<sub>3</sub> ceramics was applied to the wire. The use of BeO-Y<sub>2</sub>O<sub>3</sub> as a protective coating for thermocouples is described in the work [116].

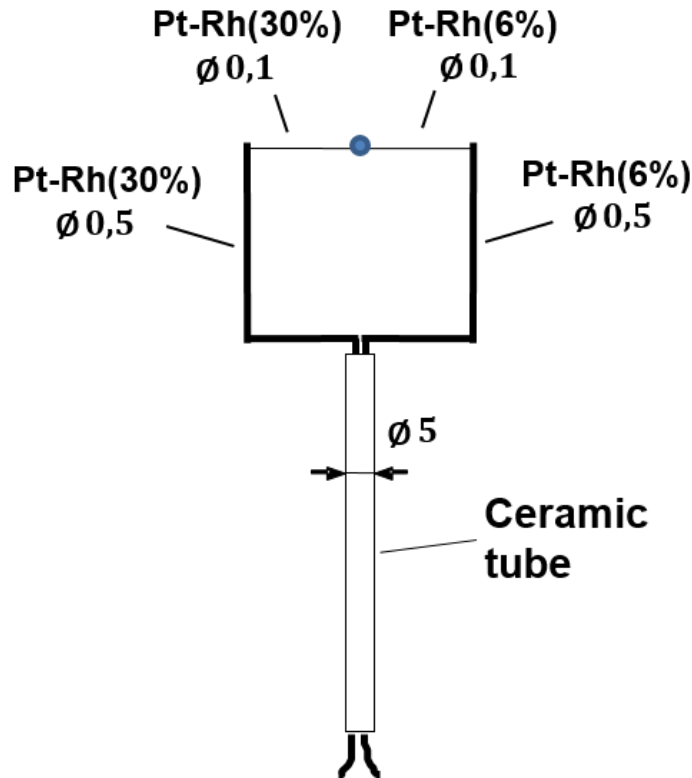


Figure 2.9. Schematic of the thermocouple in experiments at low pressure.

Measurement unit: mm.

Low pressure thermocouple measurements were also corrected during data processing to take into account radiative heat loss from the thermocouple. The method of electrical compensation was used for this purpose [117]. This method is based on the compensation of radiation heat losses by forced electric heating of the thermocouple. For the thermocouple with electrical compensation in a flame we can write the heat balance equation:

$$(2.3) \quad h \cdot (T_g - T_c) + R \cdot I^2 = \varepsilon \cdot \sigma \cdot (T_c^4 - T_0^4),$$

where  $T_g$  is the gas temperature,  $T_c$  is the thermocouple temperature,  $T_0$  is temperature of the chamber walls which absorb radiation,  $h$  is convective heat

transfer coefficient,  $R$  is the thermocouple resistance,  $I$  is the current through the thermocouple,  $\varepsilon$  is the emissivity factor,  $\sigma$  is the Stefan-Boltzmann constant

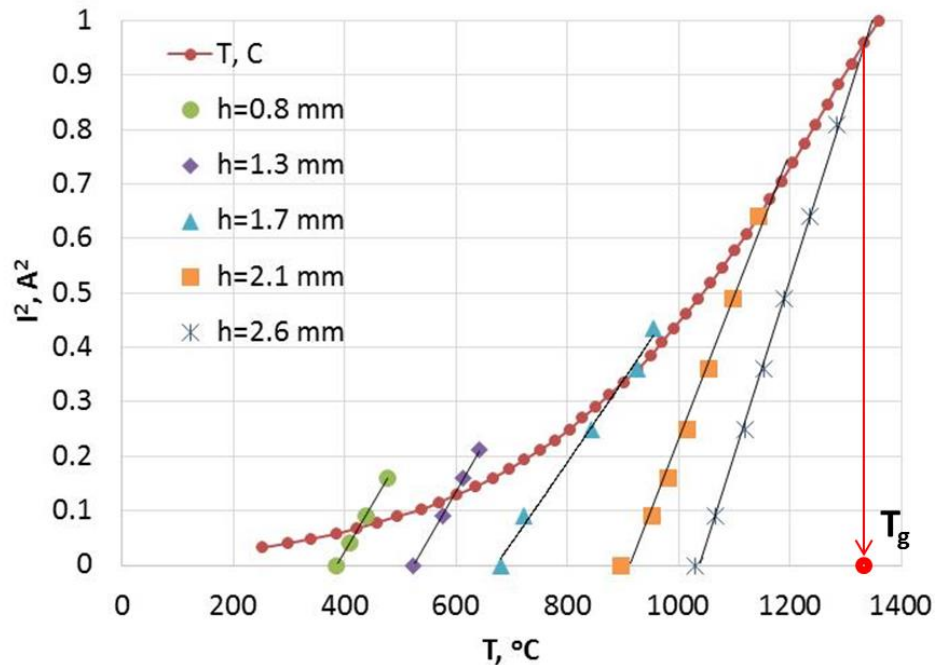


Figure 2.10. Thermocouple calibration curve and electro-compensated temperature measurements in EPe flame at different distances from the burner.

For calibration the thermocouple has been placed in a vacuum chamber and was heated by electric current. In this case the convective term in the heat balance equation is equal to zero that makes it possible to construct a dependence curve of radiation heat loss on the current passed.

Next, the temperature was measured in the flame with the heating system connected to the thermocouple. Increasing the amperage passed through the thermocouple, the thermocouple reading increased linearly. These reading can be approximated by a straight line. For the measurements at different distances from the burner a set of lines could be plotted. The point of intersection of the straight line with the calibration curve corresponds to the current at which electrical heating completely compensates radiation heat loss at a given temperature. Thus the temperature of the intersection of the straight line with

the calibration curve corresponds to the actual gas temperature  $T_g$ . Figure 2.10 shows the calibration curve of the thermocouple and the temperature measurements in the EPe flame at low pressure.

This method is applicable in the linear thermocouple region and not too high temperatures since the thermocouple can burn out from additional current heating. According to the estimations the total uncertainty did not exceed  $\pm 100$  K. The largest measurement uncertainties correspond to the zone of final products, where the flame temperature is the highest. So, in the main flame zone the uncertainty was even lower.

## 2.2. NUMERICAL SIMULATIONS

### 2.2.1. Theoretical problem description

Numerical modeling is an essential part of a detailed analysis of combustion processes. It allows us to highlight and understand the most important aspects of the complex physicochemical processes independently complementing experimental investigations. Numerical simulation of chemical kinetics in reacting systems (including flames) makes it possible to calculate practically important global parameters, such as laminar flame speeds, ignition delay times, chemical composition of pyrolysis and combustion products (presence of harmful emissions), ignition conditions, flame stability and so on. In addition numerical simulations are extremely useful for purely research purposes greatly speeding up and simplifying the analysis processes.

There is a number of specialized software packages for such calculations developed both by individual research groups and by large commercial companies. The most popular ones are CHEMKIN [118], [119], Cantera [120], OpenSMOKE [121]–[123], Chemical Workbench [124], FlameMaster [125], Cosilab [126]. In this work, the CHEMKIN II and CHEMKIN-Pro software package



were used. In fact, CHEMKIN-Pro is an extended and more convenient version of CHEMKIN II. The CHEMKIN program is a set of numerical models of various typical reactors for solving the problems of reacting flows. It can take into account the gas-phase and surface kinetics, thermochemical and physical properties of substances. The “Premixed Laminar Burner-Stabilized Flame” reactor was used to simulate the chemical structure of the flames studied. This reactor is a mathematical model of a premixed laminar one-dimensional flame stabilized on a flat burner at a constant pressure. The model is described by the following system of equations:

(2.4) ideal gas equation of state

$$P = \frac{\rho RT}{M}$$

(2.5) continuity equation

$$\frac{\partial \rho}{\partial t} + \frac{1}{S} \frac{\partial}{\partial x} (\rho v S) = 0$$

(2.6) mass conservation law

$$\rho \left( \frac{\partial Y_i}{\partial t} + v \frac{\partial Y_i}{\partial x} \right) = - \frac{1}{S} \frac{\partial}{\partial x} (j_i S) + w_i, 1 \leq i \leq I$$

(2.7) energy conservation law

$$\rho c_p \left( \frac{\partial T}{\partial t} + v \frac{\partial T}{\partial x} \right) = \frac{1}{S} \frac{\partial}{\partial x} \left( \lambda S \frac{\partial T}{\partial x} \right) - \frac{\partial T}{\partial x} \sum_{i=1}^I j_i c_{pi} - \sum_{i=1}^I h_i w_i - \frac{1}{S} \frac{\partial}{\partial x} (q_r S)$$

Here  $R$  – the universal gas constant,  $x$  – spatial coordinate,  $t$  – time,  $T$  – temperature,  $P$  – pressure,  $\rho$  – mass flow density,  $v$  – gas velocity,  $c_p$ ,  $\lambda$  – heat capacity at constant pressure and thermal conductivity of the gas mixture,  $M$  – average molecular weight of the mixture,  $S$  – cross-sectional area of the flow tube (the area of the flow tube is assumed constant as default),  $q_r$  – heat flow,  $Y_i$  – mass fraction of the  $i$ -th component of the mixture (there are  $I$  components in total),  $c_{pi}$  – heat capacity at constant pressure of the  $i$ -th component,  $h_i$  – specific enthalpy of the  $i$ -th component,  $j_i = \rho Y_i V_i$  – diffusion flux of the  $i$ -th component, where  $V_i$  – diffusion velocity of the  $i$ -th component,  $w_i$  – mass rate of formation of the  $i$ -th component in a chemical reaction per unit volume.

This system of equations consists of  $I+3$  equations for  $I+3$  variables:  $\rho$ ,  $v$ ,  $T$ ,  $Y_1, \dots, Y_I$ . To solve it boundary conditions are set on the left ( $x=0$ , burner surface) and right border of the flame ( $x=h$ , where  $h$  is the maximum calculated distance from the burner, it corresponds to the zone of flame products). In the flame front the total mass flow rate  $V_m = \rho v$  is conserved. On the left boundary  $V_m$  is defined from the initial conditions and on the right boundary vanishing of concentration gradients for all components is required. Boundary conditions for temperature are set either in a similar way or as a defined temperature profile  $T(x)$  measured in the experiment. In the latter case the heat balance equation in the system (2.4) - (2.7) is not solved and the temperature from the input file is used. Thus, the solution to the complete system of equations (2.4) - (2.7) corresponds to a freely propagating flame, and the solution to the system with a given profile  $T(x)$  corresponds to a real flame with heat losses to the burner and probe.

In addition to the initial composition, pressure, mass flow rate and temperature profile, the chemical-kinetic mechanism is loaded to CHEMKIN. Chemical kinetic mechanisms usually have a form of three text files with input data but sometimes it could be just a one file.

The first file contains a list of all compounds considered in the system and all chemical reactions in which they are involved. Parameter values  $A_i$ ,  $n_i$  and  $E_i$  are given for reaction rate constant  $k_i$  for each reaction in the modified Arrhenius form:

$$(2.8) \quad k_i = A_i T^{n_i} e^{-\frac{E_i}{RT}},$$

where  $A_i$  is the pre-exponential factor,  $n_i$  is the power of the temperature multiplier and  $E_i$  is the activation energy. Pressure dependence of each  $k_i$  could be additionally specified in the file. The reverse reaction rate is calculated from thermodynamic data, if it is not explicitly defined.

The second file contains information on the thermodynamic characteristics of all substances. The file looks like a set of coefficients  $a_{p,1}^0 - a_{p,7}^0$  which describe heat capacity  $C_p^0$ , enthalpy  $H_T^0$  and entropy  $S_T^0$  of a molecule in the polynomial form:

$$(2.9) \quad \frac{C_p^0}{R} = a_{p,1}^0 + a_{p,2}^0 T + a_{p,3}^0 T^2 + a_{p,4}^0 T^3 + a_{p,5}^0 T^4$$

$$(2.10) \quad H_T^0 = a_{p,6}^0 R + \int_{T=298}^T C_p^0 dT$$

$$(2.11) \quad S_T^0 = a_{p,7}^0 R + \int_{T=298}^T \frac{C_p^0}{T} dT.$$

To enhance the accuracy of the polynomial approximation the coefficients  $c_{p,1}^0 - c_{p,7}^0$  in the file are given for high and low temperatures.

The third file describes physical properties of the substances. For each molecule the Lennard-Jones potential coefficients (collision diameter  $\sigma$  and potential well depth  $\varepsilon$ ), dipole moment, polarizability and rotational relaxation parameter are given. The equation system (2.4) - (2.7) can be solved using the parameter  $\sigma$  which is necessary for the diffusion coefficients calculations.

Thus, the system of equations (2.4) - (2.7) together with the boundary conditions and the input data forms a complete boundary value problem which could be solved by the finite difference methods incorporated to the CHEMKIN package. As the solution the program generates a file with the spatial distribution of molar fractions of species, temperature and other parameters along the flame coordinate.

### 2.2.2. Detailed kinetic mechanisms of oxidation and combustion

To calculate the chemical flame structure of ethyl acetate, ethyl butanoate and ethyl pentanoate a detailed mechanism of EPe oxidation proposed by Dayma et al. [79] was used. This mechanism was the first detailed kinetic mechanism of EPe oxidation proposed in the literature. It is based on the chemical-kinetic mechanisms for the oxidation of C<sub>1</sub>-C<sub>5</sub> species [127]–[129] developed to describe

oxidation kinetics of various alcohols and their mixtures with small hydrocarbons. This mechanism was extended by Dayma and coauthors taking into account the corresponding oxidation chemistry of EPe and lighter ethyl ethers. This fact made it possible to use this mechanism for the flame simulations of EA and EB. Since only the flames were investigated in this work the low-temperature chemistry associated with the formation of a large amount of peroxide compounds did not have a significant effect. Thereby this low-temperature part was removed from the mechanism. The full version of the mechanism includes 522 compounds and 2719 reactions while the reduced version consists of 232 compounds and 1845 reactions. The last one was exploited for the calculations in the work.

The mechanism of Dayma was published in 2012 and the kinetic parameters of specific reactions of FAEEs were poorly understood at that time. In this regard, the rate constants of the primary reaction pathways of FAEE destruction used in this mechanism were estimated only from the principles of structural analogy with other oxygenated compounds (alcohols and aldehydes). This fact has motivated us to create a new version of the EPe combustion mechanism based on recent studies of the combustion kinetics of ethyl esters. The mechanism of oxidation of small FAEEs proposed by Sun et al. [84] was taken as a basement for the new mechanism. The mechanism of Sun was developed to describe high temperature oxidation of three light ethyl esters: ethyl formate, ethyl acetate and ethyl propanoate. The well-proven AramcoMech 1.3 mechanism [130] was used as the basic kinetic scheme for the oxidation of small C<sub>0</sub>-C<sub>4</sub> compounds in the mechanism of Sun et al. To describe the main destruction pathways of ethyl esters the rate constants of the corresponding reactions were calculated by the quantum chemical methods or have been taken from the recent theoretical works.

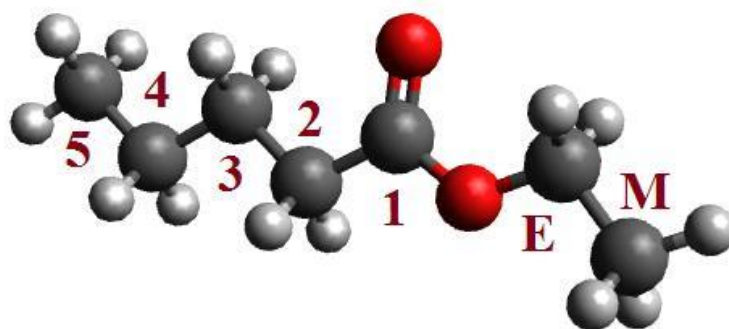


Figure 2.11. The structure of ethyl pentanoate molecule with carbon labeling.

To describe combustion kinetics of heavier FAEEs we have extended the Sun mechanism with the corresponding high-temperature oxidation reactions of ethyl butanoate and ethyl pentanoate. These reactions were taken from the mechanism of Dayma but those kinetic parameters were significantly revised. The goal was to develop a self-consistent mechanism and take into account the quantum-chemical calculations from the work of Sun et al. For these purpose the rate constants of H-atom abstraction reactions from EB and EPe molecules by the atoms and radicals (H, O, OH and CH<sub>3</sub>) in positions *M*, *E* and 2 (Fig. 2.11) were taken similar to those used in the Sun mechanism for lighter ethyl esters. The substitution is based on the assumption that the ethyl group in small FAEEs is weakly influenced by the alkyl part of the molecule. This assumption is partially confirmed by calculations in several works [131], [132].

In the mechanism of Dayma the rate constants for the H-abstraction reactions by radicals in the *2nd*, *3rd* and *4th* positions are taken to be the same. This is a logical assumption, however, it can be assumed that the ester group should influence the rate of reactions in the *2nd* position due to the inductive effect of oxygen. This hypothesis is supported by Sun et al. [84], which calculations for EA and EP predicted a larger value of the rate constants of the H-abstraction reactions with radicals in the *2nd* position. Also, in the mechanism of Dayma the H-abstraction reactions in positions 5 and *M* have the same rate

constants taken as an analogy with terminal carbons in a linear alkane. In the new mechanism these constants are different since the proximity of oxygen in the ethyl group affects the energy of the C-H bond in position *M*.

For better agreement of the model predictions and the experimental results on EPe flame at low pressure, the main reaction of ethanol formation  $C_2H_5OH (+M) \rightleftharpoons C_2H_5+OH (+M)$  was taken with the rate constant from the well-known Marinov mechanism [133]. The original rate constant of this reaction given in the mechanism of AramcoMech 1.3 led to a significant underestimation of the maximum mole fraction of ethanol. It should be noted that in the mechanism of Dayma the ethanol oxidation chemistry is fully described by the Marinov mechanism.

A complete list of reactions with modified rate constants in the new mechanism is shown in Table 5. The resulting developed mechanism contains 320 compounds participating in 2027 reactions. Thermochemical and transport data were taken from the mechanism [84] and extended with data from the mechanism [79].

To describe the chemical structure of ethyl acetate flames the mechanism from the work of Ahmed et al. [134] was used in addition to the Dayma mechanism and the mechanism proposed in the thesis. This mechanism is the most recent published mechanism of methyl acetate and ethyl acetate oxidation. It includes 506 compounds and 2809 reactions, it was included to the work with the aim to check it against the new experimental data on the flame structure of EA at atmospheric pressure.

<i>Reaction</i>	<i>A (cm<sup>3</sup>/mol·s)</i>	<i>n</i>	<i>E (cal/mol)</i>	<i>Reference</i>
EB+H=EB4J+H2	6.07E+10	1.18	8600.00	[131]
EB+H=EB3J+H2	1.43E+10	1.2	6050.00	[131]
EB+H=EB2J+H2	9.12E+09	1.22	4470.00	[131]
EB+H=EBMJ+H2	4.83E+10	1.22	9860.00	[131]
EB+H=EBEJ+H2	1.44E+10	1.25	5970.00	[131]
EB+OH=EB2J+H2O	4.87E+02	2.94	-2107.00	[132]
EB+OH=EBMJ+H2O	4.19E+01	3.72	-19.00	as EP in [84]
EB+OH=EBEJ+H2O	4.63E-02	4.32	-1640.00	as EP in [84]
EB+O=EB2J+OH	4.77E+04	2.71	2106.00	as MP in [135]
EB+O=EBMJ+OH	1.07E+03	3.6	6560.00	as EP in [84]
EB+O=EBEJ+OH	2.91E+02	3.6	3890.00	as EP in [84]
EB+CH3=EB2J+CH4	7.82E-05	4.92	3383.00	as MP in [135]
EB+CH3=EBMJ+CH4	1.77E-16	8.57	2637.00	as EP in [84]
EB+CH3=EBEJ+CH4	4.70E-25	11.28	-3624.00	as EP in [84]
EPE+H=EPE2J+H2	1.69E+10	1.21	4870.00	as EP in [131]
EPE+H=EP MJ+H2	6.07E+11	0.93	10850.00	average from [131]
EPE+H=EPEEJ+H2	1.18E+10	1.27	5940.00	average from [131]
EPE+OH=EPE2J+H2O	9.15E+01	3.23	-1542.00	as MP in [132]
EPE+OH=EP MJ+H2O	4.19E+01	3.72	-19.00	as EP in [84]
EPE+OH=EPEEJ+H2O	4.63E-02	4.32	-1640.00	as EP in [84]
EPE+O=EPE2J+OH	4.77E+04	2.71	2106.00	as MP in [132]
EPE+O=EP MJ+OH	1.07E+03	3.6	6560.00	as EP in [84]
EPE+O=EPEEJ+OH	2.91E+02	3.6	3890.00	as EP in [84]
EPE+CH3=EPE2J+CH4	7.82E-05	4.92	3383.00	as MP in [132]
EPE+CH3=EP MJ+CH4	1.77E-16	8.57	2637.00	as EP in [84]
EPE+CH3=EPEEJ+CH4	4.70E-25	11.28	-3624.00	as EP in [84]
C2H5OH(+M)=C2H5+OH(+M)	1.25E+23	-1.54	96005.00	[133]

Table 5. List of reactions which rate constants were modified in the new model.

### 2.2.3. Mechanism analysis methods

As can be seen from the previous section, detailed kinetic mechanisms include hundreds of compounds and thousands of reactions that makes an analysis of kinetic schemes rather difficult. Methods of numerical analysis of kinetic mechanisms are widely used for a deep understanding of the relationship

between the global parameters of a system and specific reaction pathways. The most widely used methods are the sensitivity analyses and the rate of production analyses.

The sensitivity analysis quantifies how the solution of the equation system describing the reactor depends on changes in specific model parameters. Actually, the sensitivity analysis is a calculation of partial derivatives of some global parameter  $X$  (temperature, compound concentration, ignition delay time, etc.) using a set of reaction rate constants  $k$ , included in the model. If the value of the derivative  $\frac{\partial X}{\partial k_i}$  comes to zero, then the variation of  $k_i$  has a little effect on the solution vector. This result means that there is no need for a high accuracy of  $k_i$  determining to estimate the parameter  $X$  at these conditions. Otherwise, the rate constants of reactions with high sensitivity should be determined as accurately as possible, since they strongly affect the final solution. In this work we analyzed the sensitivity of the laminar burning velocities to the reaction rate constants.

The rate of production analyses allows us to determine the percentage contribution of individual reactions to the total formation or consumption of any compound in the reactor. There are two main approaches in this way: a single point analysis and an integral analysis. The single point analysis provides determination of the instantaneous contribution of all formation/consumption reactions of a component under specific conditions (temperature, composition, pressure) corresponding to only one spatial or temporal point of the reactor. On the contrary the integral analysis implies the sum of contributions from all spatial or temporal points of the reactor. For the one-dimensional flame model the integral analysis is reduced to the calculation of the integral:

$$(2.12) \quad \omega_i = \int_0^\infty \omega'_i dt = \int_0^\infty \frac{\omega'_i}{v} dx ,$$

where  $\omega_i$  is a local volumetric rate of compound production in the  $i$ -th reaction,  $v$  is a local gas velocity and  $x$  corresponds to the distance from the burner. The integral analyses approach was used in the presented work.



**CHAPTER 3. RESULTS.  
EXPERIMENTAL STUDY AND  
NUMERICAL SIMULATION OF THE  
FLAMES OF FATTY ACID ETHYL  
ESTERS**

This chapter presents the measured chemical flame structures of FAEEs in the experiments at atmospheric and low pressure. In addition to the mole fraction profiles in each flame a temperature profile was measured. The measured temperature profiles were used as the input for a numerical simulation of the corresponding flames. Experimental data in the chapter are presented together with the results of the numerical simulations. Discussion is provided in the context of description accuracy of experimental data by the models. In all figures in this chapter symbols represent the experimentally measured values and lines represent the results of numerical simulations by different mechanisms. In the second part of the chapter a numerical analysis of the models is provided. Discussion is performed to reveal and explain the major inaccuracies of the models. Special attention is paid to the new mechanism.

### **3.1. EXPERIMENTAL MEASUREMENTS OF ETHYL ESTER FLAME STRUCTURES**

#### **3.1.1 Ethyl acetate**

Ethyl acetate is one of the most studied ethyl esters. A lot of works were dedicated to the combustion studies of that ester including chemical flame structure at low pressures. However, there is still no experimental data in the literature on the chemical structure of EA flames at atmospheric pressure. In this regard, the results and discussion of the EA flames at atmospheric pressure presented in this part.

Figure 3.1 shows the mole fraction profiles of reactants (EA, O<sub>2</sub>) and the main products (H<sub>2</sub>O, CO<sub>2</sub>, CO) in near-stoichiometric ( $\varphi = 1.1$ ) and fuel-rich ( $\varphi = 1.7$ ) EA/O<sub>2</sub>/Ar flames. Black line with dots on the figure represents the experimentally measured temperature profiles; the corresponding values are shown on a separate scale on the right side.

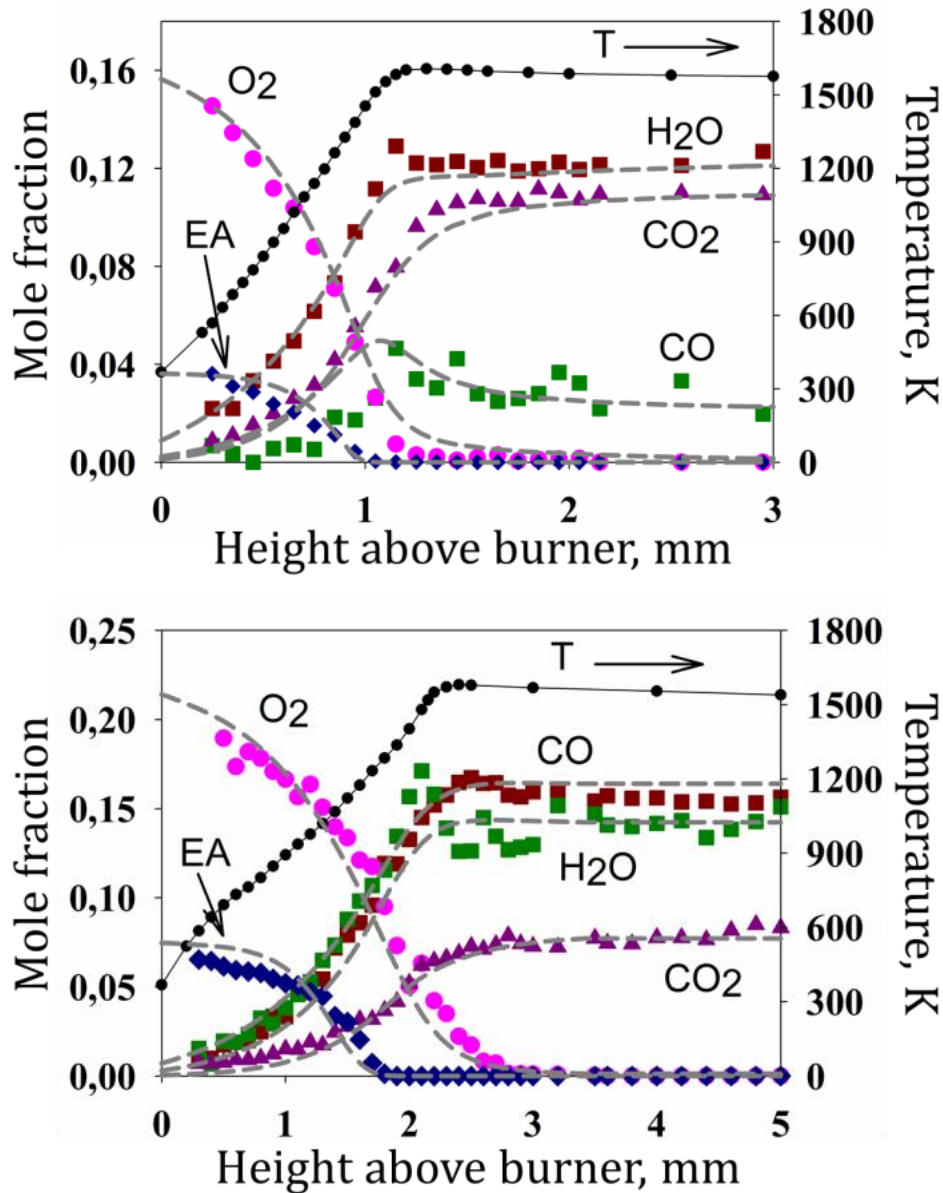


Figure 3.1. Temperature profiles and mole fraction profiles of reactants and main products in near-stoichiometric (top) and rich (below) flames of ethyl acetate at atmospheric pressure. Symbols: experimental data; dashed lines: numerical simulation with the model of Sun.

Kinetic simulation of EA flames was carried out using three kinetic schemes: the mechanism of Dayma et al. [79], the mechanism of Ahmed et al. [134] and the newly developed mechanism proposed in this thesis. But it is worth to note that in the case of EA the latter mechanism completely matches the mechanism of Sun et al. [84]. Therefore, the Sun mechanism will be referred in

the discussion. Calculations using all three mechanisms gave almost the same distribution of reactants and main products. Thus, Figure 3.1 shows only the simulation results obtained with the Sun mechanism.

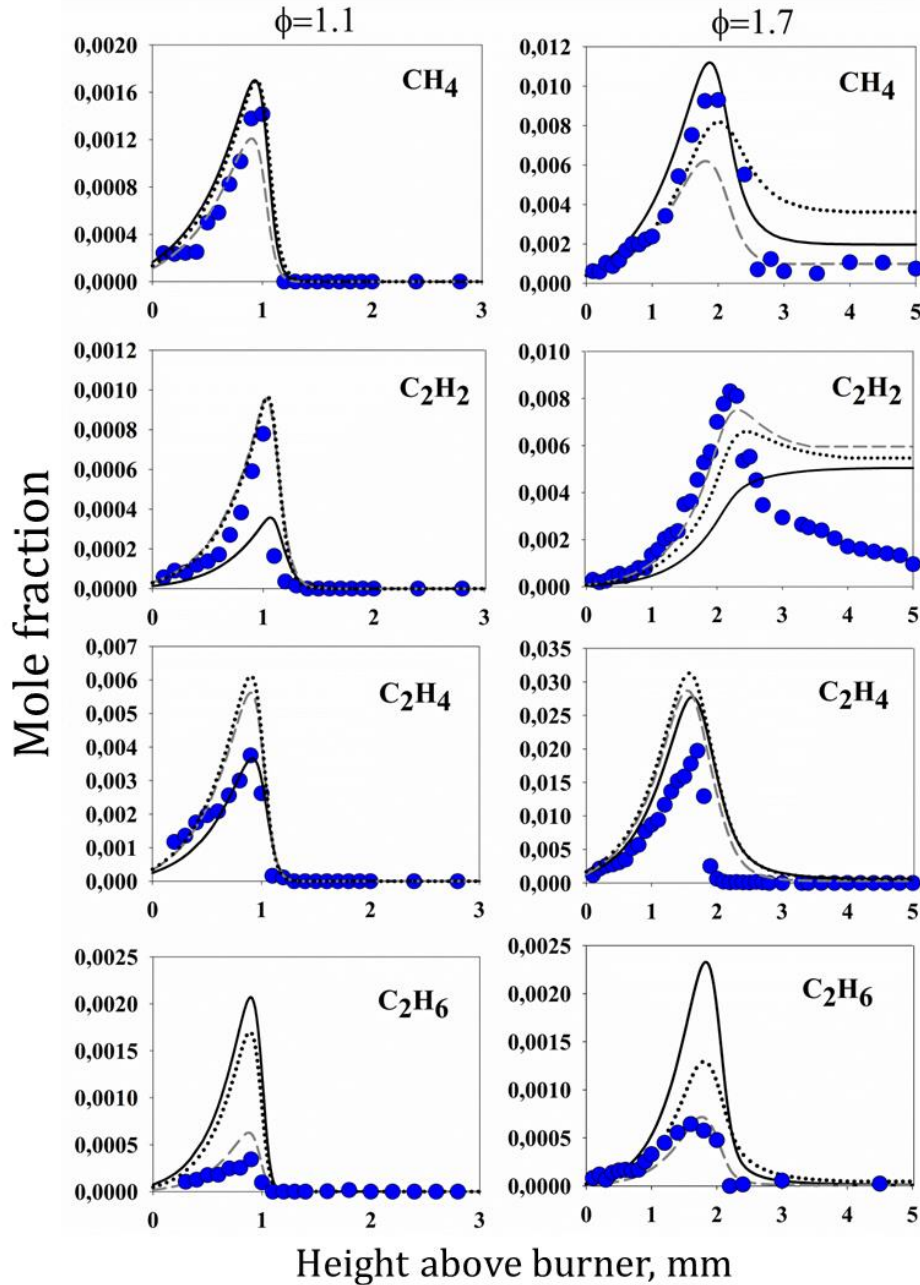


Figure 3.2. Mole fraction profiles of intermediate hydrocarbon products in the near-stoichiometric ( $\phi=1.1$ , left) and rich ( $\phi=1.7$ , right) ethyl acetate flames at atmospheric pressure. Symbols: experimental data; solid lines: Dayma mechanism; dotted lines: Ahmed mechanism; dashed lines: Sun mechanism.

As can be seen from the figure, the measured and calculated profiles are in good qualitative and quantitative agreement with each other. The main combustion zone in the stoichiometric flame is about 1.0-1.2 mm. In the rich flame it is naturally certainly wider, about 2.3-2.5 mm. The final temperature values of stoichiometric and rich flame are almost equal: 1575 K and 1545 K, respectively.

Figures 3.2 and 3.3 demonstrate a comparison of the mole fraction profiles of hydrocarbon and oxygen-containing intermediates with the simulation results by three kinetic mechanisms. Solid black lines represent the simulation results using the Dayma mechanism, dotted lines represent the Ahmed mechanism and dashed lines correspond to the Sun mechanism.

As can be seen from Figure 3.2, all three mechanisms fairly well described the mole fraction profile of methane in the near-stoichiometric flame and slightly worse in the rich flame. At the same time, a different shape of the profiles in the rich flame is observed, which indicates different rates of methane consumption in the mechanisms.

The experimental mole fraction profiles of C<sub>2</sub>-hydrocarbons are described with significant discrepancies by the models. Thus, the maximum mole fractions of acetylene (C<sub>2</sub>H<sub>2</sub>) and ethane (C<sub>2</sub>H<sub>6</sub>) are described most accurately by the Sun mechanism and slightly less accurately (especially C<sub>2</sub>H<sub>6</sub>) by the mechanism of Ahmed. Predictions of the peak mole fractions of these compounds by the Dayma mechanism differ by 4-5 times from the experimental data. At the same time, the Dayma mechanism gives the most accurate mole fraction prediction of ethylene (C<sub>2</sub>H<sub>4</sub>) in the near-stoichiometric flame. In general, from the Figure 3.2 we can assume that the Sun mechanism described the mole fractions of small hydrocarbons most accurately in the EA flames.

It worth to note the incorrect shape of the calculated mole fraction profiles of acetylene in the rich flame: all three mechanisms have predicted a nonzero concentration of C<sub>2</sub>H<sub>2</sub> in the end flame zone, while the experiment indicated the complete consumption of acetylene. This problem has already been observed in

simulations of the fuel-rich flames of other hydrocarbons both at atmospheric [136] and low [137] pressure flames. Wherein experiments always show almost zero acetylene concentration in the final zone that corresponds to thermodynamic calculations and conceptions about high acetylene reactivity. Most likely, these discrepancies in the models are associated with the insufficient accuracy of the kinetic parameters of  $C_2H_2$  consumption reactions in the mechanisms. Such systematic discrepancies demonstrate the imperfection of the existing kinetic schemes for the oxidation of small hydrocarbons despite the large number of works in this area.

Six-center unimolecular decomposition with the formation of acid and ethylene is the characteristic decomposition reaction of FAEEs. It can be seen from the plots that the mole fraction peak value of acetic acid ( $CH_3COOH$ ) increases with the increase of the equivalence ratio (Fig. 3.3). However, for the rich flame all three mechanisms predicted an overestimated maximum acetic acid concentration. In addition, the calculated mole fraction of ethylene in the rich conditions (Fig. 3.2) is also looking slightly overestimated in comparison with the experimental data. But for the near-stoichiometric flame a satisfactory agreement is observed for both species. It can be assumed that the discrepancies in the case of the rich flame are associated with the inaccurate values of the rate constant of unimolecular decomposition. On the other hand, the overestimated contribution of the unimolecular decomposition can be associated with the underestimated contribution of the H-abstraction reactions from the fuel molecule. Since the unimolecular decomposition competes with the H-atom abstractions the balance between these pathways manages the system. Moreover, the number of H-abstraction reactions is quite large (the number of C atoms  $\times$  the number of key flame radicals (H, O, OH,  $CH_3$ , etc.)). This fact increases a possibility of inaccuracies in this part of the mechanisms.

Acetaldehyde ( $CH_3CHO$ ) is an important intermediate combustion product of FAEEs which forms in large quantities after the C-O bond cleavage in the ester group. As itself acetaldehyde is a toxic compound. Therefore, precise control and

prediction of this compound in combustion products is of great practical importance. As can be seen from Figure 3.3, the best agreement between the experiment and calculations is observed for the model of Dayma. In this case, the mechanisms of Ahmed and Sun have underestimated the peak mole fraction of  $\text{CH}_3\text{CHO}$  in the near-stoichiometric flame by a factor of two. In the rich flame predictions of the Sun mechanism turn out to be close to the experimental ones, while the Ahmed mechanism still underestimates the peak concentration of  $\text{CH}_3\text{CHO}$ .

We have detected a peak signal corresponding to the ions with mass 42 u. Propene ( $\text{C}_3\text{H}_6$ ) and ketene ( $\text{CH}_2\text{CO}$ ) which are often formed in flames of heavy hydrocarbons [138], [139] contribute to this peak. Unfortunately, the MBMS setup used does not allow the separation of these two compounds. However, the simulations with all three mechanisms predicted similar peak values for propene mole fraction but different for ketene. Moreover, the mole fraction of ketene is several times higher (about  $10^{-4}$  in stoichiometric flame and  $10^{-3}$  in the rich one) than that of propene (about  $3 \times 10^{-5}$ ). In this regard the mass-peak 42 can be analyzed in terms of ketene formation.

Simulations based on the Ahmed and Sun mechanisms have predicted an overestimated value of the maximum mole fractions of ketene especially under the rich flame conditions. On the contrary, the Dayma model has underestimated these values. However, we can conclude that the Sun and Dayma models are equally close to the experimental values in the near-stoichiometric flame taking into account the experimental uncertainty. In the rich flame the mechanism of Dayma has shown a complete agreement with the experiment, whereas the other two models overestimated the peak mole fraction of ketene by 3-4 times.

According to the experiments the mole fraction of formaldehyde ( $\text{CH}_2\text{O}$ ) is insensitive to the equivalence ratio changes. This fact was confirmed in calculations by all three mechanisms. As it seen, the calculated values are almost two times higher than the experimental results. However the discrepancies between the simulations and experiments do not exceed the experimental

uncertainty. Such result can be assumed as satisfactory, since the accuracy of formaldehyde quantification in the flame was rather low due to the impossibility of the direct calibration.

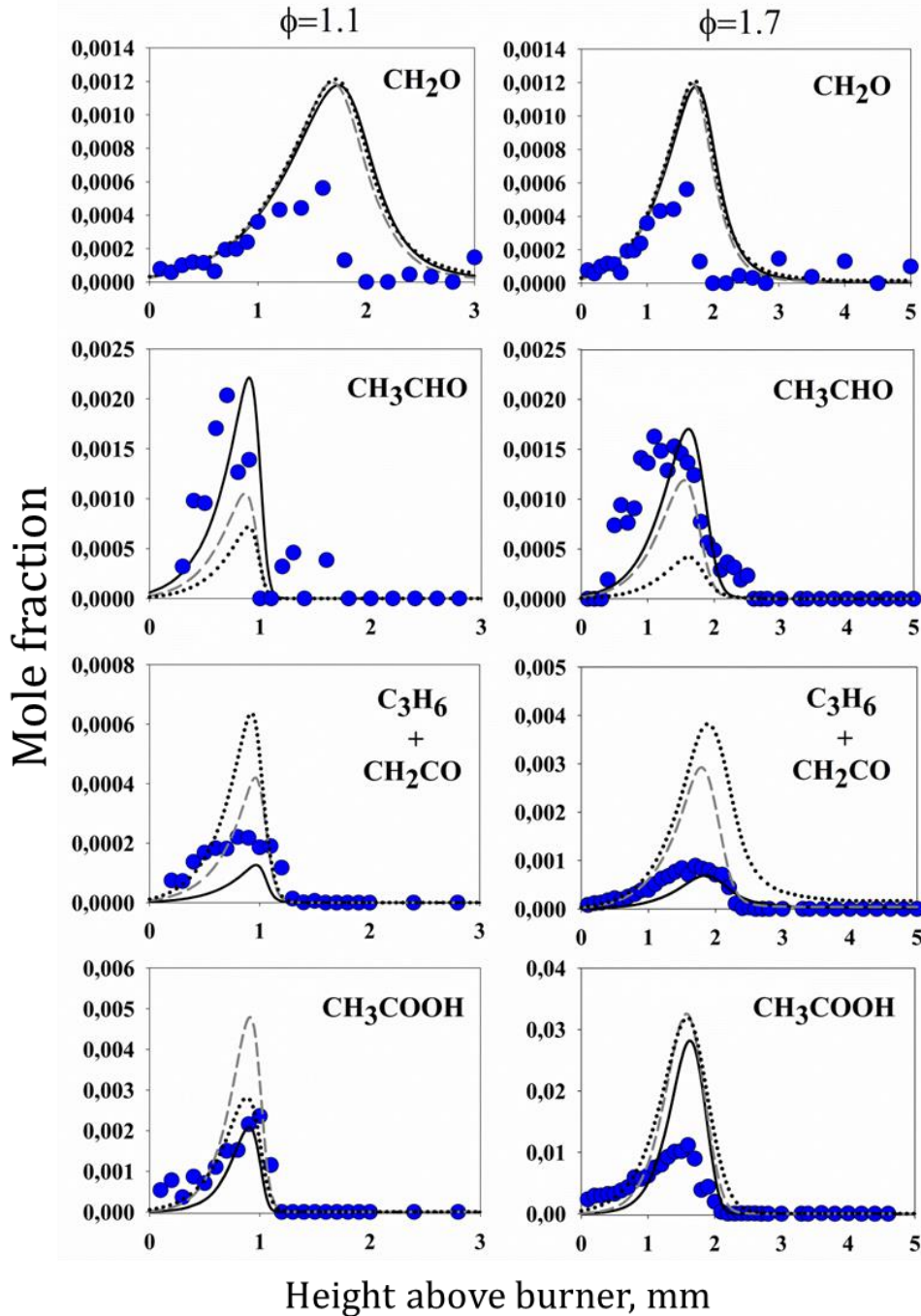


Figure 3.3. Mole fraction profiles of intermediate oxygenates in the near-stoichiometric (left) and rich (right) ethyl acetate flames at atmospheric pressure. Symbols: experimental data; solid lines: Dayma mechanism; dotted lines: Ahmed mechanism; dashed lines: Sun mechanism.



From the presented comparison of experimental data with modeling predictions by three kinetic mechanisms we assume a more accurate description of the formation kinetics of light C<sub>0</sub>-C<sub>2</sub> hydrocarbons in the Sun model. The kinetics of the formation of oxygenated compounds seems to be more accurately described in the mechanism of Dayma. The Ahmed mechanism has shown results similar to the Sun mechanism but it described the mole fraction profiles small hydrocarbons somewhat worse. Although, the mechanism of Ahmed has described the peak mole fraction of acetic acid in the near-stoichiometric flame more accurately than the Sun mechanism.

Despite the fact that low-pressure premixed flames of EA have been already studied, we decided to perform our own study at low pressure. Figure 3.4 shows the mole fraction profiles of reactants (EA, O<sub>2</sub>) and the main products (H<sub>2</sub>O, CO<sub>2</sub>, CO, H<sub>2</sub>) in stoichiometric EA/O<sub>2</sub>/Ar flame. Similar to the previous figures, black line with dots on the figure represents the experimentally measured temperature profiles; the corresponding values are shown on a separate scale on the right side.

Low-pressure flame of EA has a wide combustion zone (about 6-8 mm) with an S-curved temperature profile which demonstrates higher temperature of the flame compared to the near-stoichiometric EA flame at 1 atm. Nevertheless, the mole fraction composition of the products in both flames is quite similar, it can demonstrate proximity of the system to the equilibrium product composition in the post-flame zone.

As expected, all three mechanisms predicted almost equivalent mole fraction profiles of the main products and reactants, therefore only the simulations with the mechanism of Sun are demonstrated. Comparison of the experimental and simulated profiles shows a general agreement between them. However, a noticeable discrepancy between the measured and simulated profiles of oxygen can be observed. The reason is, that in this experiment there was a small air leakage in the sampling line. The amount of additional oxygen was estimated and subtracted from the final oxygen profile, but the accuracy of this

profile has become less. Nonetheless, the product composition demonstrates almost full oxidation of the fuel (stoichiometric mixture), while the simulations predicts slightly more CO and non-zero fraction of  $O_2$ . In this regard, the shape of the oxygen profile is looking reasonable.

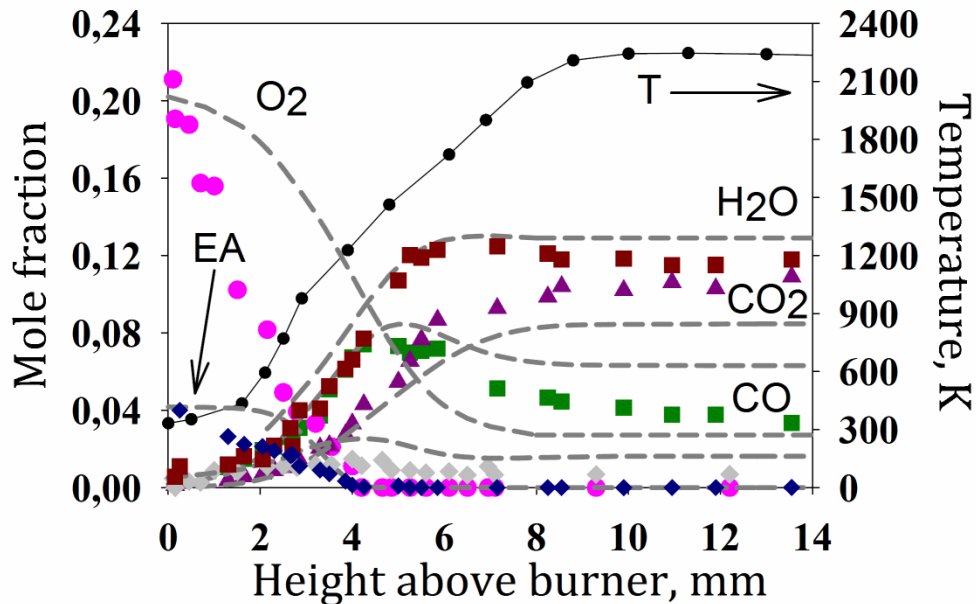


Figure 3.4. Temperature profile and mole fraction profiles of reactants and main products in the stoichiometric flame of ethyl acetate at 50 Torr.

Symbols: experimental data; solid lines: Dayma mechanism; dotted lines: Ahmed mechanism; dashed lines: Sun mechanism.

Figures 3.5 and 3.6 show experimentally measured and simulated mole fraction profiles of  $C_1$ - $C_3$  hydrocarbons and oxygenated intermediates. Symbols correspond to the experimental values, solid black lines represent predictions of the Dayma mechanism, dotted lines correspond to the mechanism of Ahmed and the mechanism of Sun is presented by dashed lines.

All three mechanisms predict different mole fraction profiles of the hydrocarbon species in the low pressure EA flame. The accuracy of predictions differs a lot also. The same situation was in the atmospheric near-stoichiometric flame of EA. Compared to the experimental data, the mechanism of Dayma provided the best prediction of the methane mole fraction profile, while the

mechanisms of Ahmed and Sun underestimated the peak mole fraction of  $\text{CH}_4$  by a factor of two. However, as in the atmospheric flame, the mechanisms of Sun and Ahmed predicted very well the peak mole fraction of acetylene, and the mechanism of Dayma underestimated it. Experimental mole fraction profile of ethylene appeared to be several times higher than in the atmospheric flame. The peak position is markedly shifted toward the burner that indicates an earlier  $\text{C}_2\text{H}_4$  formation than in the mechanisms. As in the case of atmospheric pressure, the mechanisms of Sun and Ahmed predicted the peak mole fraction of ethylene two times higher than that by the mechanism of Dayma. It is interesting to note, that the Sun mechanism appeared to be the least accurate in prediction of the  $\text{C}_2\text{H}_6$  peak mole fraction at 50 Torr, considering that this mechanism was the most successful at the atmospheric pressure. Vice versa, two other mechanisms demonstrate excellent agreement with the experimental peak mole fraction of ethane.

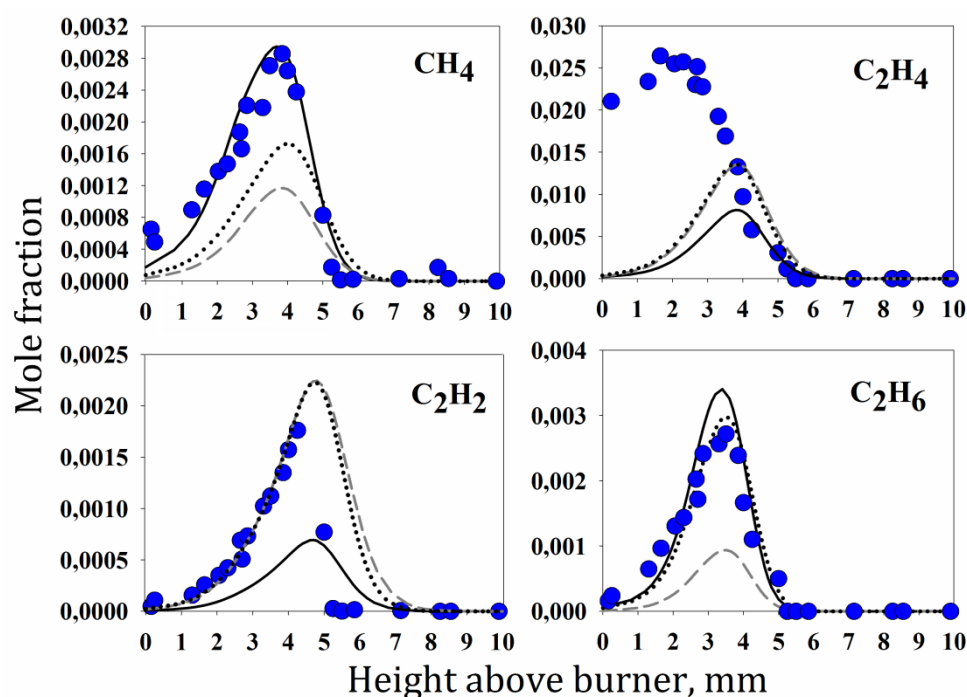


Figure 3.5. Mole fraction profiles of intermediate species in the stoichiometric flame of ethyl acetate at 50 Torr. Symbols: experimental data; solid lines: Dayma mechanism; dotted lines: Ahmed mechanism; dashed lines: Sun mechanism.

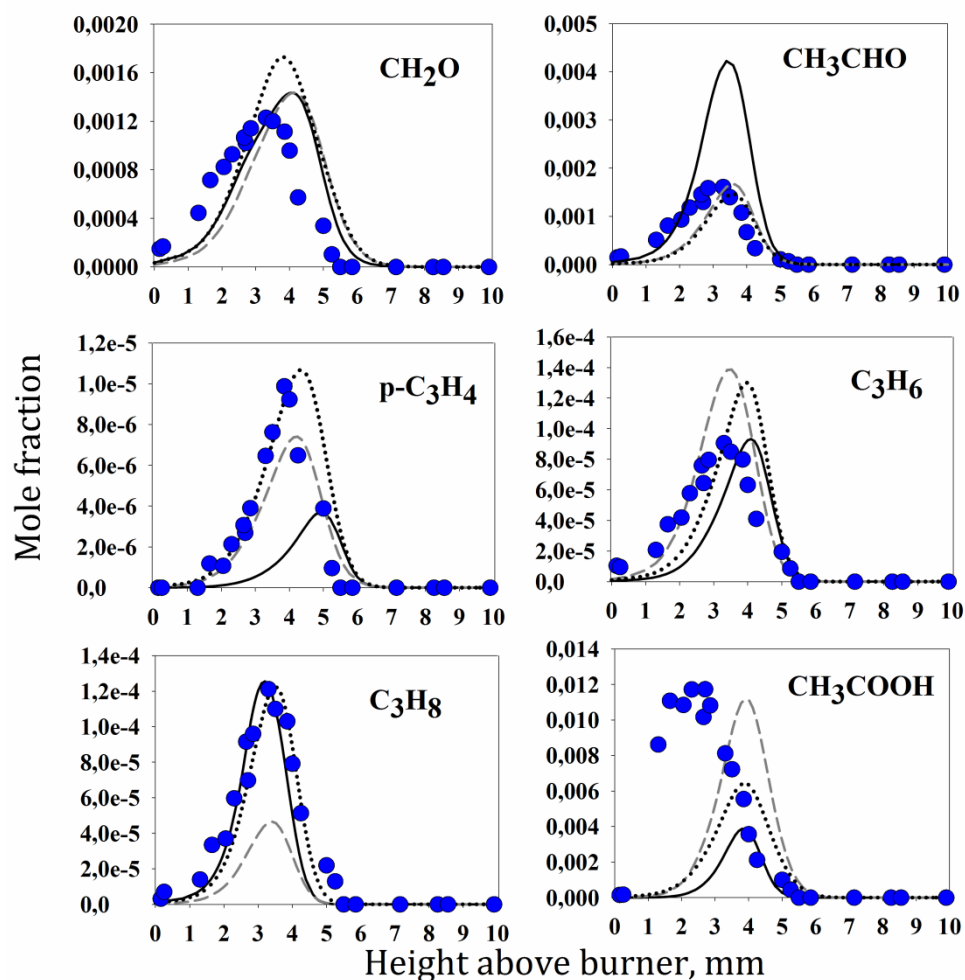


Figure 3.6. Mole fraction profiles of intermediate species in the stoichiometric flame of ethyl acetate at 50 Torr. Symbols: experimental data; solid lines: Dayma mechanism; dotted lines: Ahmed mechanism; dashed lines: Sun mechanism.

The experimental peak mole fractions of  $C_3$ -hydrocarbons are several times lower than that of  $C_2$ -species, but they are still interesting for the validation of mechanisms. As it seen from the Figure 3.6 the mechanisms predict almost the same profiles of  $C_3H_6$ , that agrees well with the experiment, except for a slight shift. The mole fraction profile of propyl ( $p-C_3H_4$ ) is simulated in the best way by the Ahmed mechanism. The mechanisms of Sun and Dayma underestimate the peak mole fraction of  $p-C_3H_4$ , and a slight shift in the mechanism of Dayma is observed. Worth to note, that simulated profiles of  $p-C_3H_4$  and  $C_3H_6$  have different peak positions, that indicates different rates of production of these species in the

mechanisms. The best prediction of the  $C_3H_8$  peak mole fraction was provided by the mechanisms of Dayma and Ahmed, while the Sun mechanism underpredicted propane mole fraction by a factor of three.

All three simulated mole fraction profiles of formaldehyde appeared to be very close to the experimental profile in contrast to the atmospheric pressure flame. However, a slight shift between the simulations and experiment can be observed. Acetaldehyde peak mole fraction predicted very well by the mechanisms of Sun and Ahmed. The mechanism of Dayma predicted two times higher value, but in the atmospheric flame this mechanism demonstrated the best simulations of  $CH_3CHO$  mole fraction. The peak mole fraction of acetic acid was predicted very well by the Sun mechanism. The Ahmed and Dayma mechanisms predict two and three times lower values, respectively. However, as it seen, the acid profile is shifted toward the burner as it is with the ethylene mole fraction profile. Since both these compounds are the products of the EA unimolecular decomposition, earlier fuel decomposition in the flame can be considered.

Compared to the atmospheric pressure results, simulations at low-pressure conditions differ noticeably. The mechanisms, which were adequate in predictions of some species at 760 Torr, appeared to be incorrect at 50 Torr. Such differences could be attributed to the different pressure-dependent parameters in the mechanisms.

### 3.1.2 Ethyl butanoate

Figure 3.7 shows the mole fraction profiles of reactants (EB,  $O_2$ ) and the main products ( $H_2O$ ,  $CO_2$ , CO) in stoichiometric ( $\varphi=1.0$ ) and fuel rich ( $\varphi=1.5$ ) EB/ $O_2$ /Ar flames. Two mechanisms were used to simulate the chemical structure of EB flames: the mechanism of Dayma et al. [79] and the mechanism proposed in the thesis. The simulation results based on the Dayma mechanism are shown in Figure 3.7 by solid black lines and the calculations based on the new mechanism

are shown by dashed red lines. As in the EA flames the simulated mole fraction profiles of reactants and main products by different mechanisms have practically coincided with each other. It can be seen that the calculated mole fraction profiles match the experimental profiles of all components quite accurately.

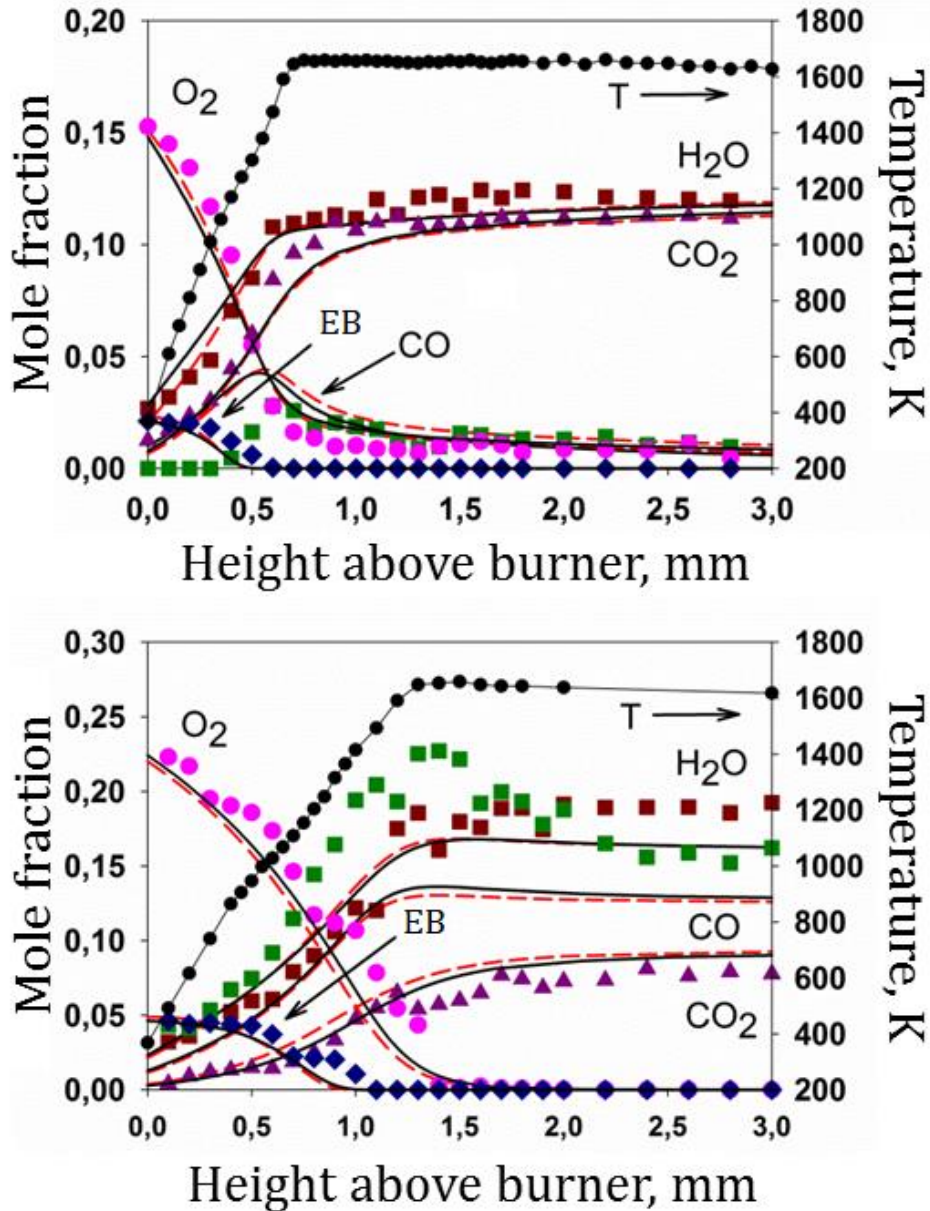


Figure 3.7. Temperature and mole fraction profiles of reactants and main products in stoichiometric (top) and rich (below) flames of ethyl butanoate at atmospheric pressure. Symbols: experimental data; black lines: Dayma mechanism; red lines: new mechanism.

A slight deviation is observed at the peak mole fraction of carbon monoxide (CO). In the stoichiometric flame the experimental peak mole fraction lies lower than the calculated one, but in the rich flame it is noticeably higher. The reason is the experimental error in particular experiment since CO is determined from the mass peak  $m/z=28$  which corresponds also to ethylene  $C_2H_4$ . This mass overlap introduces an additional inaccuracy of the CO mole fraction determination since the ethylene mole fraction is measured with the greater uncertainty than the main products. The width of the main combustion zone was about 0.6-0.7 mm in the stoichiometric flame and about 1.3-1.4 mm in the rich flame. This is almost two times narrower than that in the corresponding EA flames. It indicates a higher EB burning rate. This hypothesis is confirmed by data from the work of Dayma and co-authors [78]. It was shown that the experimental and calculated laminar flame speeds of EB/air mixtures ( $\sim 58$  cm/s at  $\varphi=1.0$ ,  $p=1$  atm) are higher than those of EA/air mixtures ( $\sim 52$  cm/s at  $\varphi=1.0$ ,  $p=1$  atm). The final temperature of the EB flames was about 1600 K which is slightly higher than that in the EA flames taking into account the close values of dilution and  $\varphi$  coefficients.

Figure 3.8 shows the experimentally measured and calculated mole fraction profiles of key radicals which are the main chain carriers in flames. Unfortunately, the mole fraction determination of atomic oxygen O, which is also an essential radical in combustion, is practically impossible in hydrocarbon flames due to the presence of large amounts of methane with the same molar weight ( $m/z=16$ ). As can be seen from the figure the experimental values and calculations are in good agreement taking into account the relatively high measurement uncertainty of the radicals. However, there are some discrepancies between the experimental and calculated profiles near the burner surface. This effect could be caused by the probe perturbations. Also, it could be attributed to the incorrect chemistry of H and OH formation in vicinity of the burner.

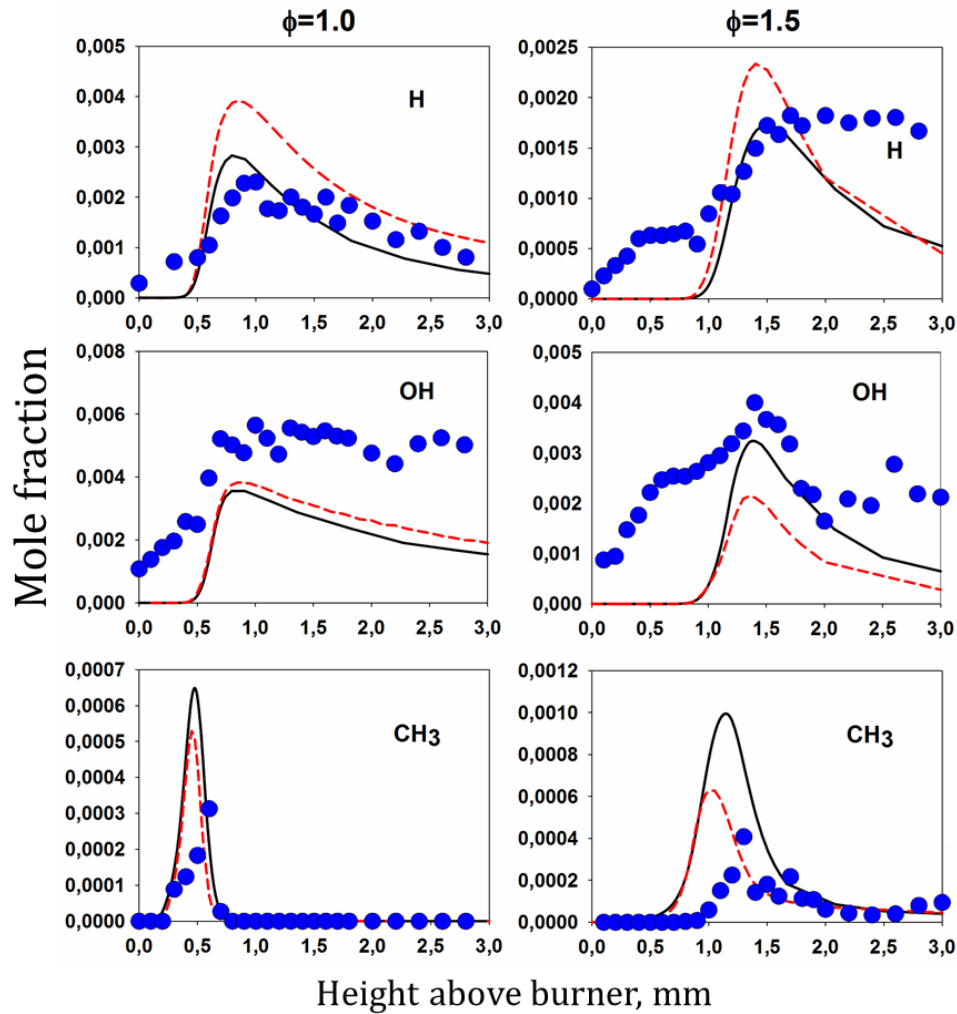


Figure 3.8. Mole fraction profiles of H, OH and CH<sub>3</sub> radicals in stoichiometric ( $\varphi=1.0$ , left) and rich ( $\varphi=1.5$ , right) flames of ethyl butanoate at atmospheric pressure. Symbols: experimental data; black lines: Dayma mechanism; red lines: new mechanism.

In Figures 3.9 and 3.10 the mole fraction profiles of hydrocarbon intermediates measured in the stoichiometric and rich flames of ethyl butanoate are presented. The figures show that experimental data are best described by the new model while the model of Dayma has provided much less accurate predictions. The most noticeable discrepancies between the modeling with this mechanism and experimental data observed for the mole fraction profiles of methane, acetylene, ethane, allene and propyne (C<sub>3</sub>H<sub>4</sub>, not separated in



experiments) and butylene ( $C_4H_8$ ). The disagreements have been observed for these species in both stoichiometric and rich flames.

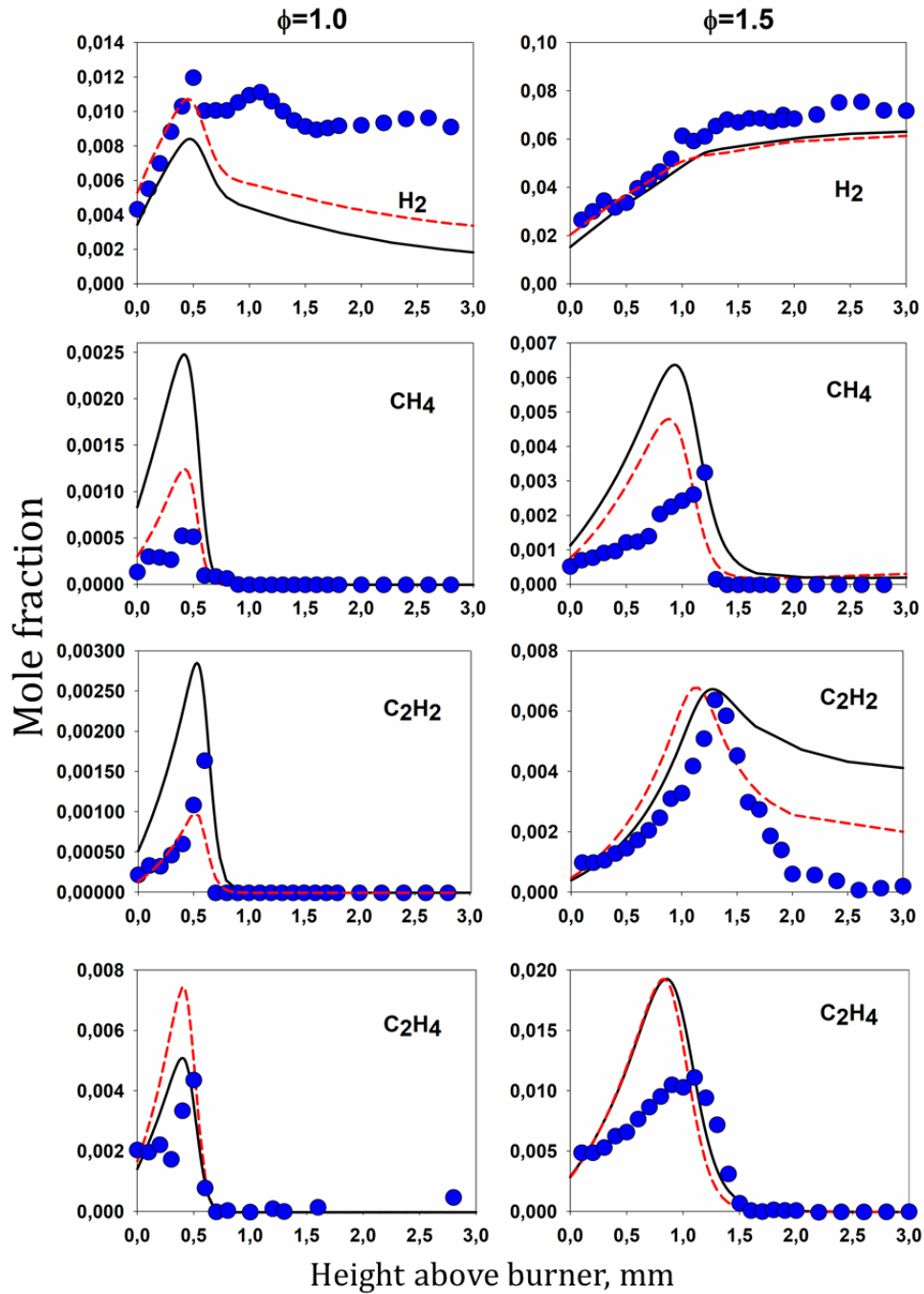


Figure 3.9. Mole fraction profiles of intermediate hydrocarbons in stoichiometric (left) and rich (right) flames of ethyl butanoate at atmospheric pressure. Symbols: experimental data; black lines: Dayma mechanism; red lines: new mechanism.

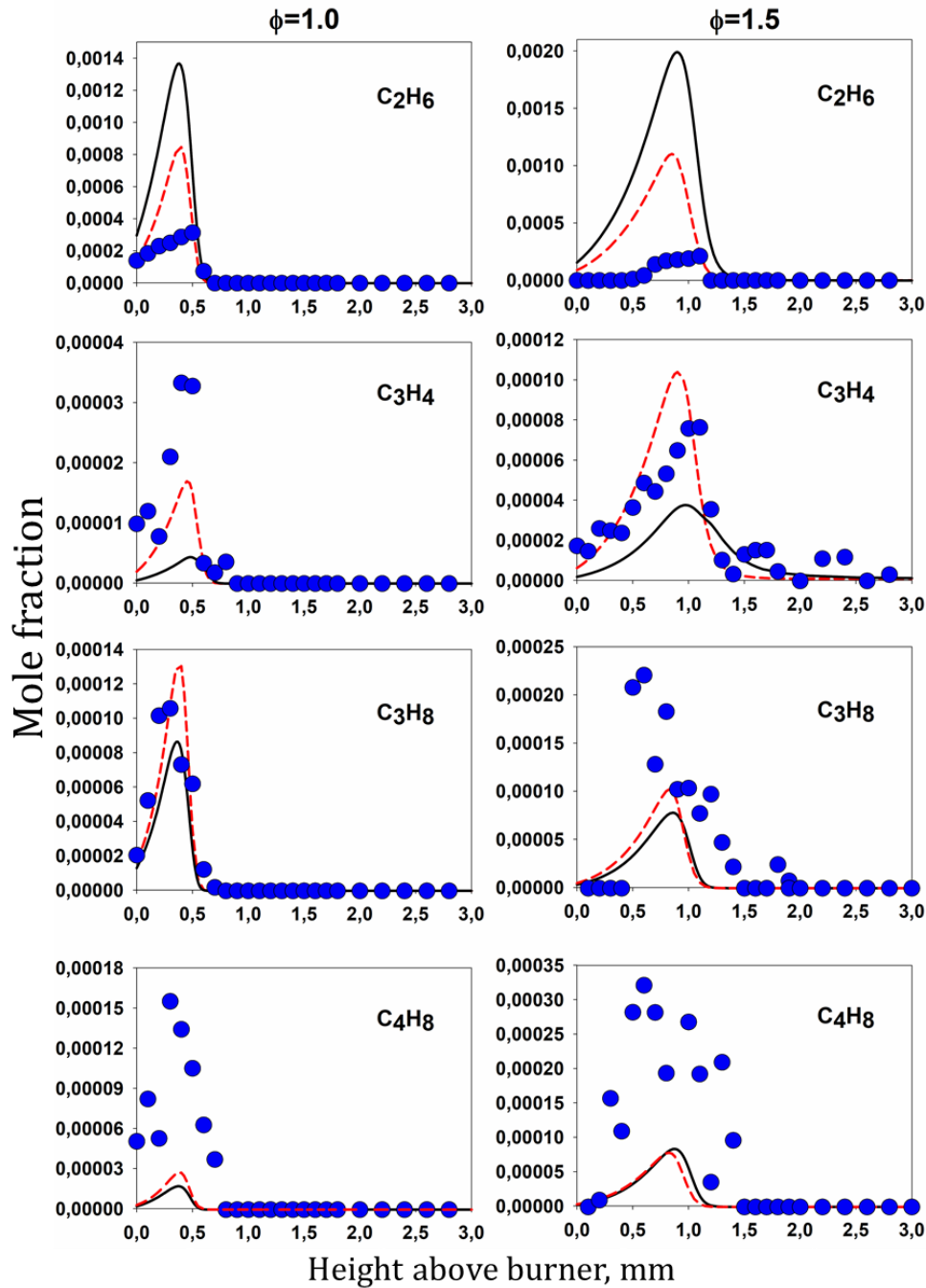


Figure 3.10. Mole fraction profiles of intermediate hydrocarbons in stoichiometric (left) and rich (right) flames of ethyl butanoate at atmospheric pressure. Symbols: experimental data; black lines: Dayma mechanism; red lines: new mechanism.

On the contrary, the new model has described the experimental profiles of practically all measured compounds fairly well in both flames. An unsatisfactory

agreement with the experiment is observed for ethane and propane in the rich flame only in the case of butylene. The last one was underestimated in simulations by a factor of 3-5 compared to the experiment.

As in the rich EA flame the calculated mole fraction profiles of acetylene in the rich EB flame do not reach zero in the final flame zone. As it seen, the experiment with a good accuracy gives a near-zero concentration of acetylene in this zone. However, it can be seen that the new model predicts half less acetylene mole fraction than the Dayma model in the end flame zone. Although, it is worth noting that the Dayma mechanism described the mole fraction profile of ethylene ( $C_2H_4$ ) a little more accurately in the stoichiometric flame. The same tendency in the EA flame was also observed.

Figure 3.11 shows comparison of the experimental and calculated mole fraction profiles of oxygenated compounds. The largest discrepancy between the experiment and modeling is observed in the case of formaldehyde ( $CH_2O$ ). Here, both models have predicted a twice higher mole fraction of  $CH_2O$  than was observed experimentally. Despite that fact the calculated values still lie within the experimental accuracy range. The similar discrepancy between the model calculations and experimental data was observed in the EA flames. That indicates the general tendency of the mechanisms to overestimation of the  $CH_2O$  concentration in the flames of these esters.

The experimentally measured mole fractions of butanoic acid ( $C_3H_7COOH$ ) have been described with acceptable accuracy by both models. However, as in the case of EA, a better agreement of the Dayma model with experiment under stoichiometric conditions can be noticed. At the same time, in the rich flame both models have overestimated the maximum mole fraction of acid again. Thus, some systematic inaccuracy in the description of the primary destruction pathways can be mentioned. Also, as it discussed in the case of EA, the problem could lay in the relationship between the unimolecular decomposition and the radical destruction reactions.

Generally, taking into account the experimental error in the measurement of the oxygenated compounds, we can assume a satisfactory agreement between the model calculations and experiment.

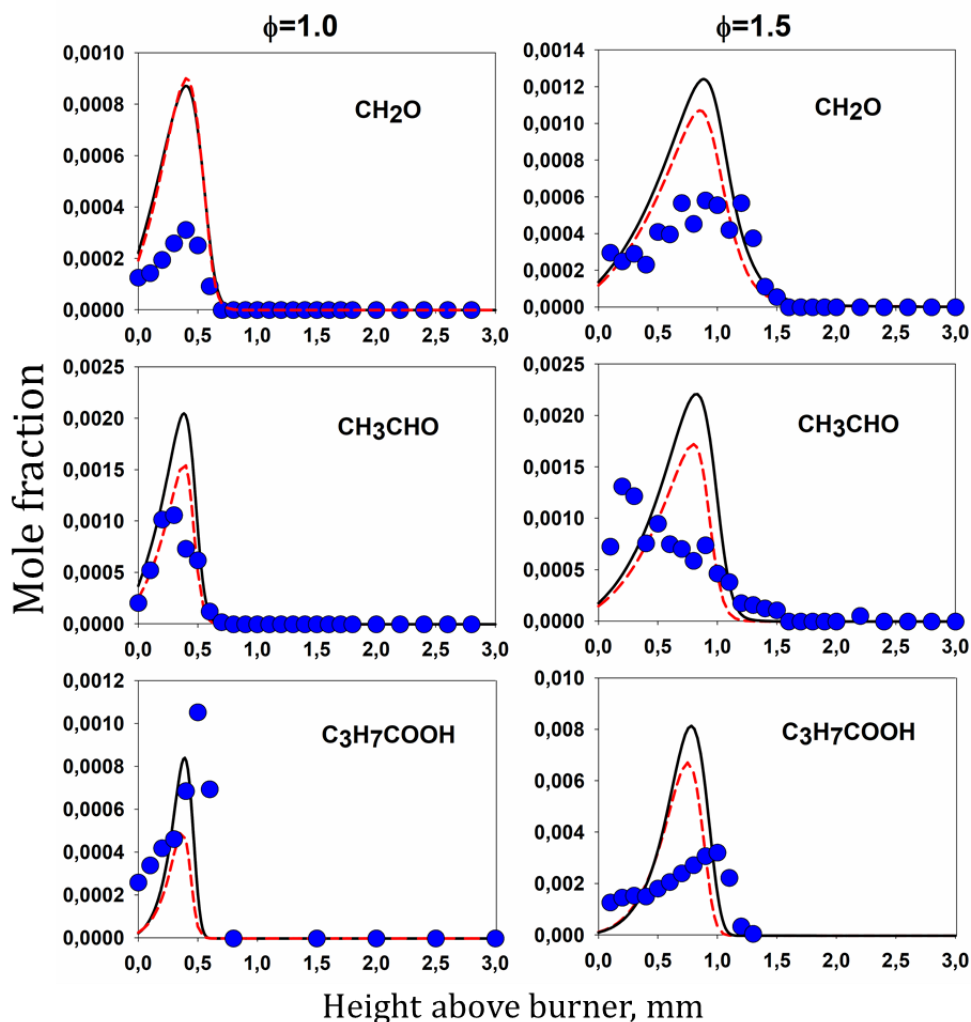


Figure 3.11. Mole fraction profiles of oxygenated hydrocarbons in stoichiometric (left) and rich (right) flames of ethyl butanoate at atmospheric pressure. Symbols: experimental data; black lines: Dayma mechanism; red lines: new mechanism.

From the above comparisons of the experimental and calculated mole fraction profiles of intermediate compounds it can be concluded that the new model describes the chemical structure of ethyl butanoate flames under stoichiometric and fuel-rich conditions noticeably better than the mechanism of

Dayma. However, for individual species, such as ethane and butylene, significant discrepancies have been observed. It indicates the need for the rate of production analysis for these compounds in the mechanisms.

### 3.1.3 Ethyl pentanoate

Figure 3.12 shows the mole fraction profiles of reactants (EPe, O<sub>2</sub>) and main products (H<sub>2</sub>O, H<sub>2</sub>, CO<sub>2</sub> and CO) in stoichiometric EPe/O<sub>2</sub>/Ar flame. The mechanism of Dayma and the new mechanism were also used to simulate the chemical structure of this flame.

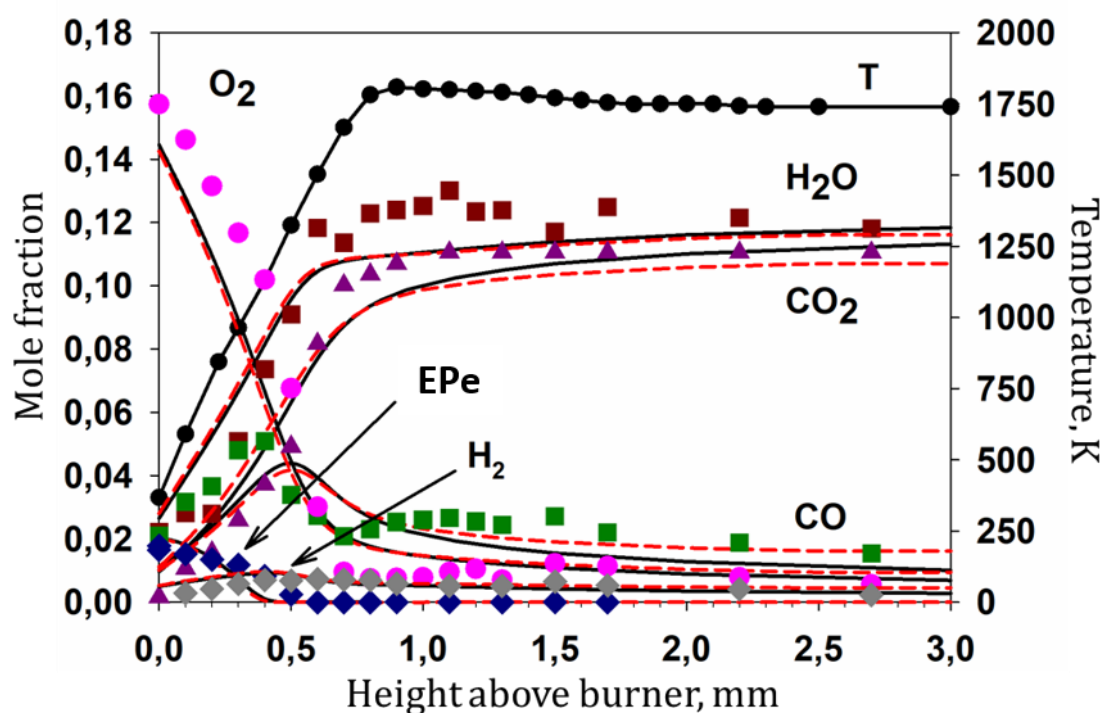


Figure 3.12. Temperature profile and mole fraction profiles of reactants and main products in the stoichiometric flame of ethyl pentanoate at atmospheric pressure.

Symbols: experimental data; black lines: Dayma mechanism; red lines: new mechanism.

As in the previous flames, here is a good agreement between the experimental data and simulation results for these components. The width of the

main combustion zone was approximately 0.6-0.7 mm which is the same as in the stoichiometric flame of ethyl butanoate. The EPe flame appeared to be hotter (1750 K in the end zone) than the EB flame (1600 K in the end zone) with the same percentage of argon dilution (80%).

The mole fraction profiles of the main radicals measured in the EPe flame are depicted on the Figure 3.13. As can be seen, the experimental mole fraction profiles of OH and CH<sub>3</sub> are in complete agreement with the calculated ones. The maximum mole fraction of atomic hydrogen H in the experiment is 3 times higher than that predicted by the mechanisms. Nevertheless, considering experimental uncertainties in atom and radical quantification, this can be considered as a quite satisfactory agreement for the radical mole fractions.

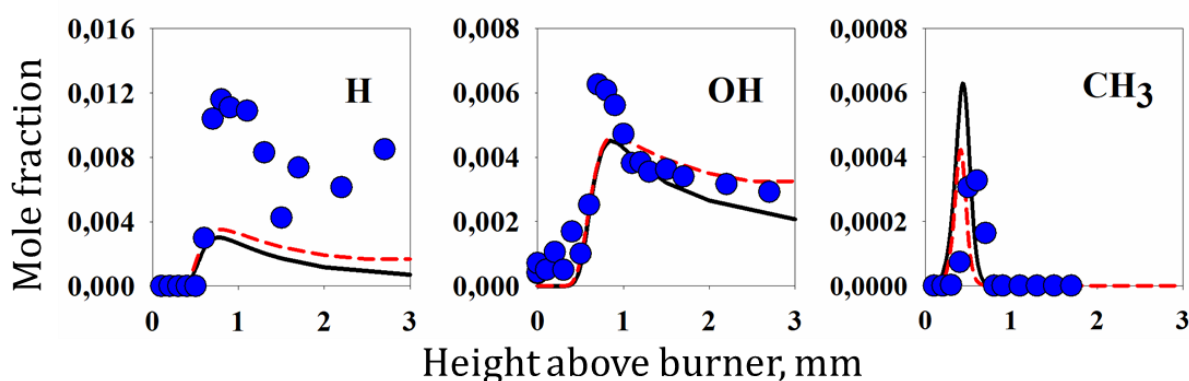


Figure 3.13. Mole fraction profiles of major radicals in the stoichiometric flame of ethyl pentanoate at atmospheric pressure.

Symbols: experimental data; black lines: Dayma mechanism; red lines: new mechanism.

Mole fraction profiles of hydrocarbon intermediates measured in the atmospheric flame of EPe are shown in Figure 3.14. As it seen, both models have described the mole fraction profiles of methane (CH<sub>4</sub>) and propane (C<sub>3</sub>H<sub>8</sub>) rather well. However, in the case of the latter one the new model seems to be more precise.

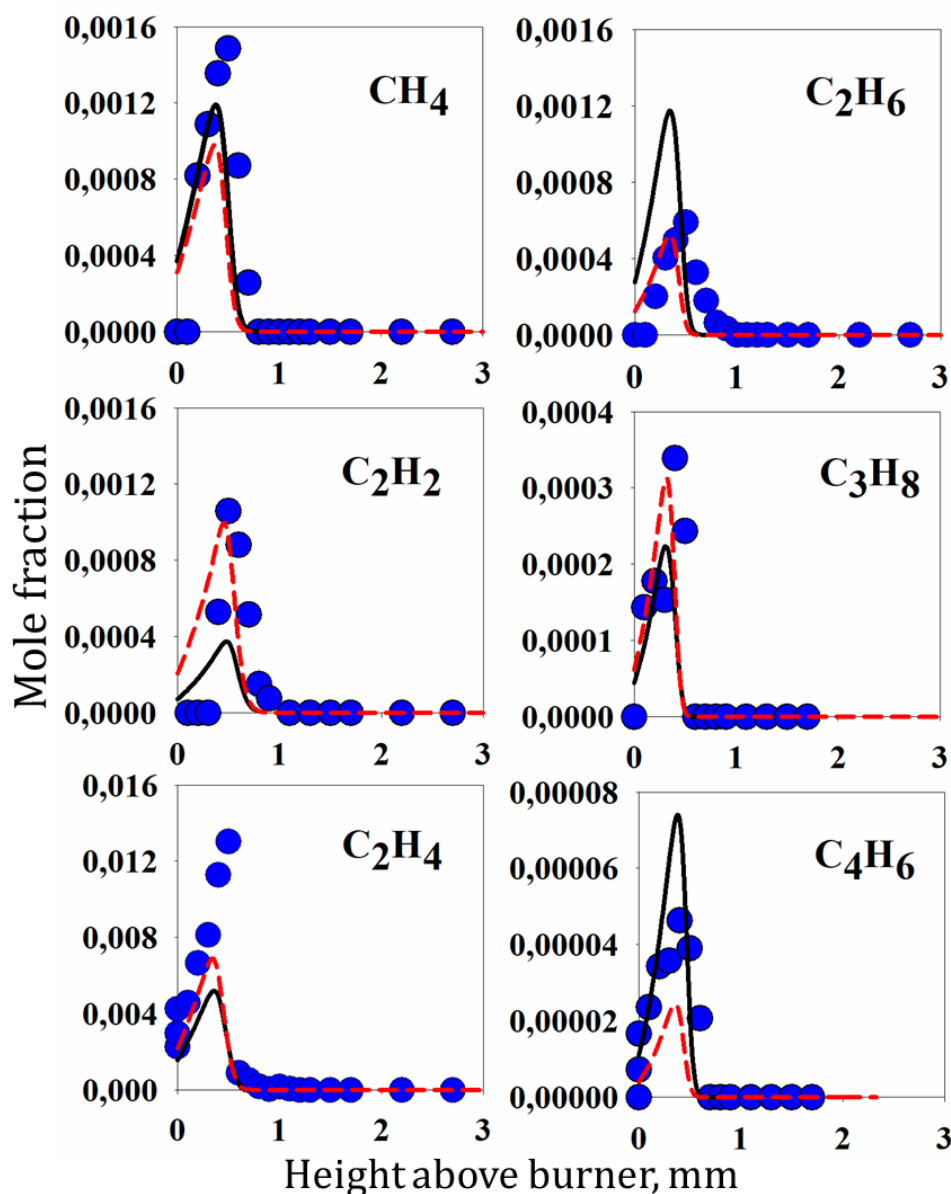


Figure 3.14. Mole fraction profiles of intermediate hydrocarbon products in the stoichiometric flame of ethyl pentanoate at atmospheric pressure.

Symbols: experimental data; black lines: Dayma mechanism; red lines: new mechanism.

Inaccuracies of both the models have been observed when the peak mole fractions of ethylene ( $C_2H_4$ ) and butadiene ( $C_4H_6$ ) were simulated. For ethylene the models have predicted close maximum mole fractions, but these values appeared two times lower than that in the experiment. In the stoichiometric flames discussed previously, the Dayma mechanism gave fairly accurate

predictions of the maximum mole fractions of ethylene, while the new model systematically overestimated it by one and a half time. The model inaccuracy in the EPe flame could be attributed to the fact that ethylene in flames is formed through a variety of competing paths. Thus, as heavier the fuel, the more difficult it is to describe the mole fraction profile of this intermediate.

The mole fraction profile of acetylene ( $C_2H_2$ ) has been described by the new model more accurately, as in the previous flames. The model of Dayma has predicted three times lower mole fraction maximum of acetylene. Also, the new mechanism has provided a more accurate description of the ethane mole fraction profile ( $C_2H_6$ ). In this case the mechanism of Dayma has significantly overestimated (by 3 times) the maximum mole fraction.

In the case of 1,3-butadiene, its experimental peak mole fraction has landed exactly in the middle between the corresponding model predictions. Herein the Dayma mechanism has overestimated the peak mole fraction of  $C_4H_6$  by a factor of two, and the new mechanism has predicted exactly two times less value than the experiment. Thus, both the models have described the experimental profile with the equal accuracy. However, the peak mole fraction of butadiene is only about  $10^{-5}$ . Thus, the accuracy of its determination does not play a significant role in comparison with acetylene, for example.

In contrast to the stoichiometric flames of EA and EB, in the EPe flame the calculated mole fraction profiles of oxygenated species have appeared in a good agreement with the experimental results (Fig. 3.15.). The maximum mole fractions of formaldehyde ( $CH_2O$ ) and acetaldehyde ( $CH_3CHO$ ) were adequately predicted by both the models within the experimental uncertainty. The similar situation has been observed with the total peak mole fraction of ketene ( $CH_2CO$ ) and propene ( $C_3H_6$ ). It should be noted that the mechanism of Dayma has predicted more propene ( $\sim 10^{-3}$ ) than ketene ( $\sim 10^{-4}$ ) in this flame, whereas the new mechanism has predicted very close maximum mole fractions of these compounds:  $\sim 6.5 \times 10^{-4}$  for propene and  $\sim 1.5 \times 10^{-4}$  for ketene.



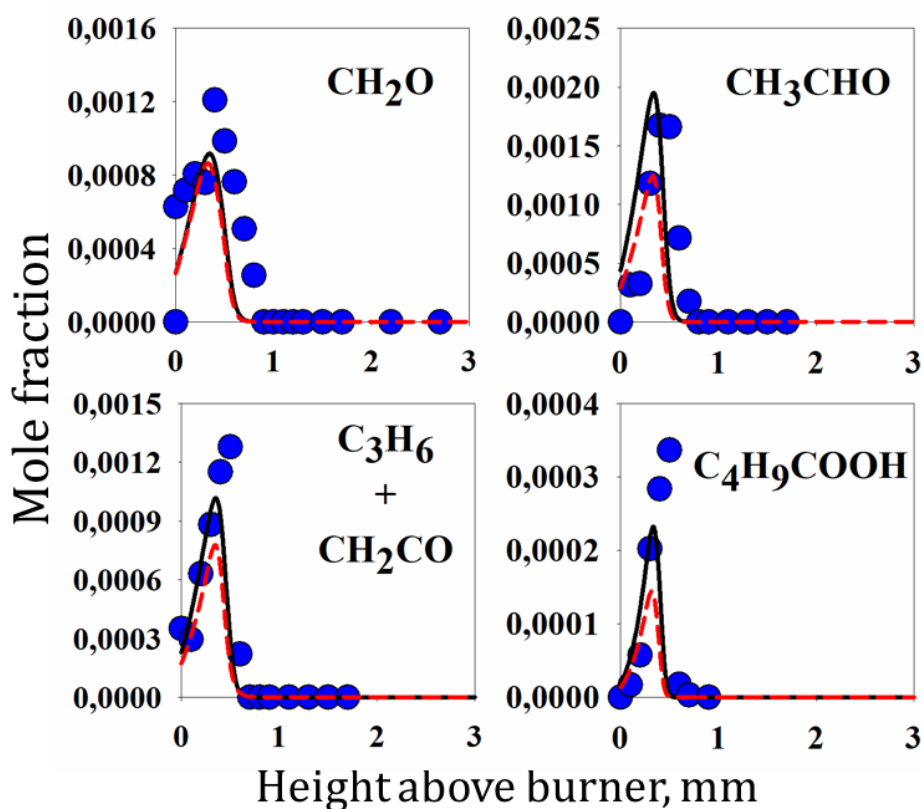


Figure 3.15. Mole fraction profiles of oxygenated products in the stoichiometric flame of ethyl pentanoate at atmospheric pressure.

Symbols: experimental data; black lines: Dayma mechanism; red lines: new mechanism.

The mole fraction profile of valeric acid (C<sub>4</sub>H<sub>9</sub>COOH) calculated according to the Dayma model has shown a lower peak value than the experimental one. But it could be assumed as a satisfactory agreement within the measurement uncertainty ( $\pm 50\%$ ). The same profile calculated with the new model has laid even lower and that indicates insufficient production or too fast consumption of C<sub>4</sub>H<sub>9</sub>COOH in the new mechanism.

In general, both the models have shown a satisfactory description of the experimental data. For this flame the new model appeared to be more accurate in description of the mole fraction profiles of acetylene, ethane and propane, and it was less accurate with the mole fraction of valeric acid. According to the calculations with the new mechanism, the maximum mole fraction of the acid is

almost three times lower than the experimental value. In turn, the model of Dayma has predicted the maximum acid mole fraction a little more accurately, but also underestimated it by more than one and a half time. The same underestimation of the acid mole fraction has been observed in the case of EB flame which has a close molecular weight to EPe. This problem indicates once again the need of detailed analyses of the decomposition reactions of heavier FAEEs.

Low-pressure flame measurements with a wide combustion zone provide a large data set for testing kinetic schemes, despite the fact that low pressure flames are not suitable for practical applications. Hereinafter the measurement results of the EPe flame structure at pressure of 50 Torr are provided. The results are also demonstrated in comparison with the simulations based on the mechanism of Dayma and the proposed mechanism. Low-pressure flame structures of EPe have been measured earlier in two works [85], [86], but the ambiguous results motivated us to perform our own measurements.

Figure 3.16 shows the mole fraction profiles of reactants (EPe, O<sub>2</sub>) and main products (H<sub>2</sub>O, H<sub>2</sub>, CO<sub>2</sub>, CO) in stoichiometric EPe/O<sub>2</sub>/Ar flame at pressure of 50 Torr. As expected, the simulated profiles agreed well with the experimental data. A slight discrepancy between the experimental and calculated oxygen profiles was found in the initial flame zone. This shortcoming could be associated with an older and less accurate chromatograph to determine oxygen mole fraction. As can be seen from the temperature profile, the EPe flame at low pressure was significantly hotter than the atmospheric pressure flame. This came from the lower argon dilution and other flame stabilization conditions: the flame at 50 Torr is farther from the burner and loses less heat. Also, the thinner and narrower probe in these experiments introduced less thermal disturbances of the flame compared to the sonic probe at the MBMS setup. One more reason was due to the higher radical concentrations which recombine less often at low pressure than at high.

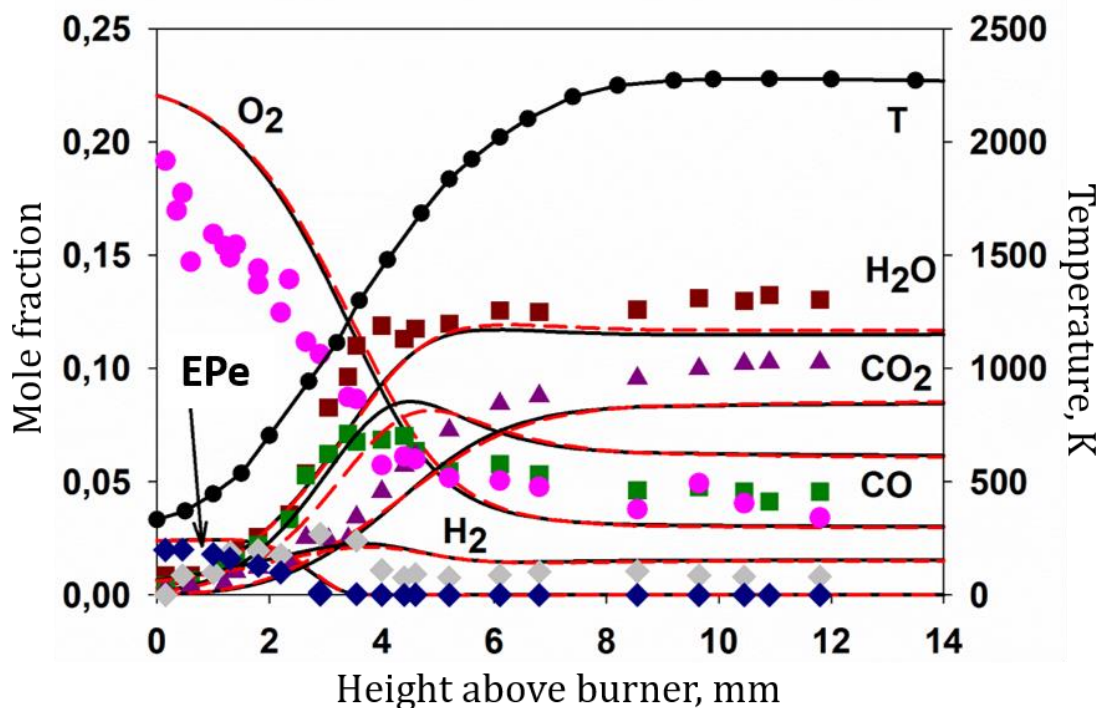


Figure 3.16. Temperature profile and mole fraction profiles of reactants and main products in the stoichiometric flame of ethyl pentanoate at 50 Torr.

Symbols: experimental data; black lines: Dayma mechanism; red lines: new mechanism.

Figures 3.17 and 3.18 demonstrate the measured mole fraction profiles of intermediate  $C_1$ - $C_4$  hydrocarbons in comparison with modeling by two mechanisms. The measured mole fraction profiles of propene ( $C_3H_6$ ), propane ( $C_3H_8$ ), n-butane ( $n-C_4H_{10}$ ) and 1-butene ( $1-C_4H_8$ ) were reproduced fairly accurately by both the models. Propene, which has not been separated from ketene in the atmospheric pressure experiment, was very well described by the mechanisms at low pressure. At the same time, in the experiment at atmospheric pressure a good agreement was observed between the models and experiment for the total propene+ketene profile. So, it can be assumed that kinetics of these compounds in EPe flames is described a fairly well in the mechanisms.

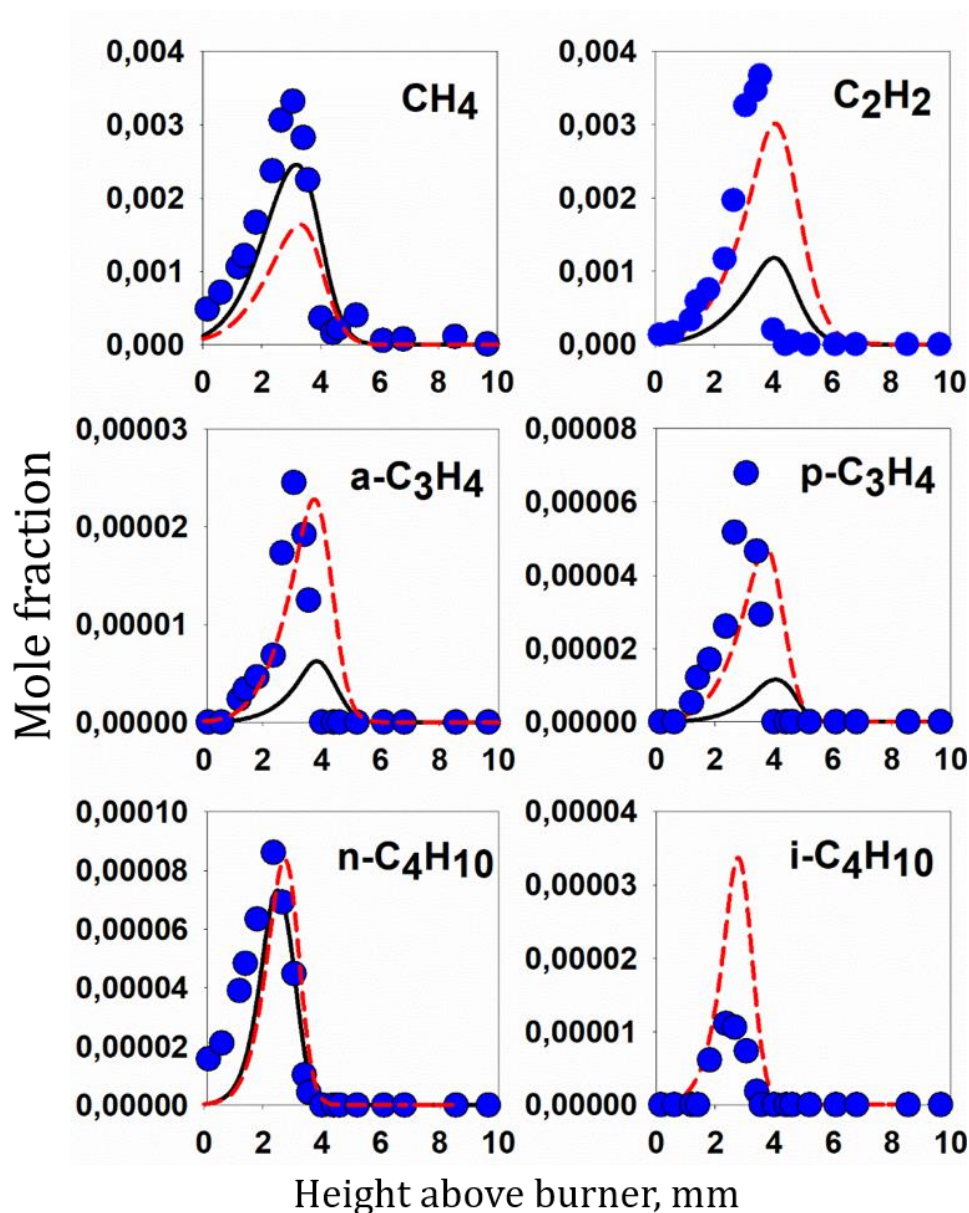


Figure 3.17. Mole fraction profiles of intermediate hydrocarbon products in the stoichiometric flame of ethyl pentanoate at 50 Torr.

Symbols: experimental data; black lines: Dayma mechanism; red lines: new mechanism.

In general, positions of the peak mole fractions of the other compounds were reproduced well in the simulations, but there are noticeable discrepancies in absolute values between the model predictions and the experiment. The new mechanism has described very well again the mole fraction profiles of acetylene

( $C_2H_2$ ), allene and propyne (a- $C_3H_4$  and p- $C_3H_4$ ), while the mechanism of Dayma has underestimated the maximum mole fractions of these compounds by 3-5 times. The peak mole fractions of methane and ethane, on the contrary, were calculated a slightly better by the Dayma model, whereas in the new mechanism the peak mole fractions of these species were underestimated by 1.5-2 times.

The experimental maximum mole fractions of ethylene ( $C_2H_4$ ), isobutane (i- $C_4H_{10}$ ) and 1,3-butadiene (1,3- $C_4H_6$ ) differ markedly from the calculated ones. As it seen, the measured mole fraction of ethylene appeared to be quite high and its position is shifted toward the burner relative to the calculated profiles. In this case, the models predict one and a half time lower value of the peak ethylene mole fraction than it was measured. We assumed that such a high ethylene mole fraction has appeared due to the additional unimolecular decomposition of EPe during the sampling process, since the small angle of the probe does not allow a molecular beam formation. To check this hypothesis we have estimated the possible amount of ethylene that could be formed in the probe at its temperature and have received a slight correction to the measured data. However, that estimation was not yet enough to match the modeling peaks. Thus, despite the obvious experimental issue, it can be still argued that both the models underestimate the maximum mole fraction of ethylene in the low-pressure EPe flame. It points again the possible inaccuracies in the ethylene formation chemistry used in the models.

As it seen from the experiment isobutane was formed less than n-butane in an order of magnitude. This is probably the reason why isobutane has not been incorporated into the mechanism of Dayma. However, isobutane was included to the AramcoMech 1.3 mechanism which was used as a sub-mechanism in the new model. Thus, the isobutane mole fraction profile was calculated using the new mechanism. The mechanism has reproduced well the shape and position of the experimental isobutane profile but overestimated its maximum by a factor of 3.

The calculated peak mole fraction profiles of 1,3-butadiene were shifted far from the burner than the experimental maximum. Even so, the absolute

maximum mole fraction of 1,3-C<sub>4</sub>H<sub>6</sub> was very well described by the Dayma model and was 2 times underestimated by the new model.

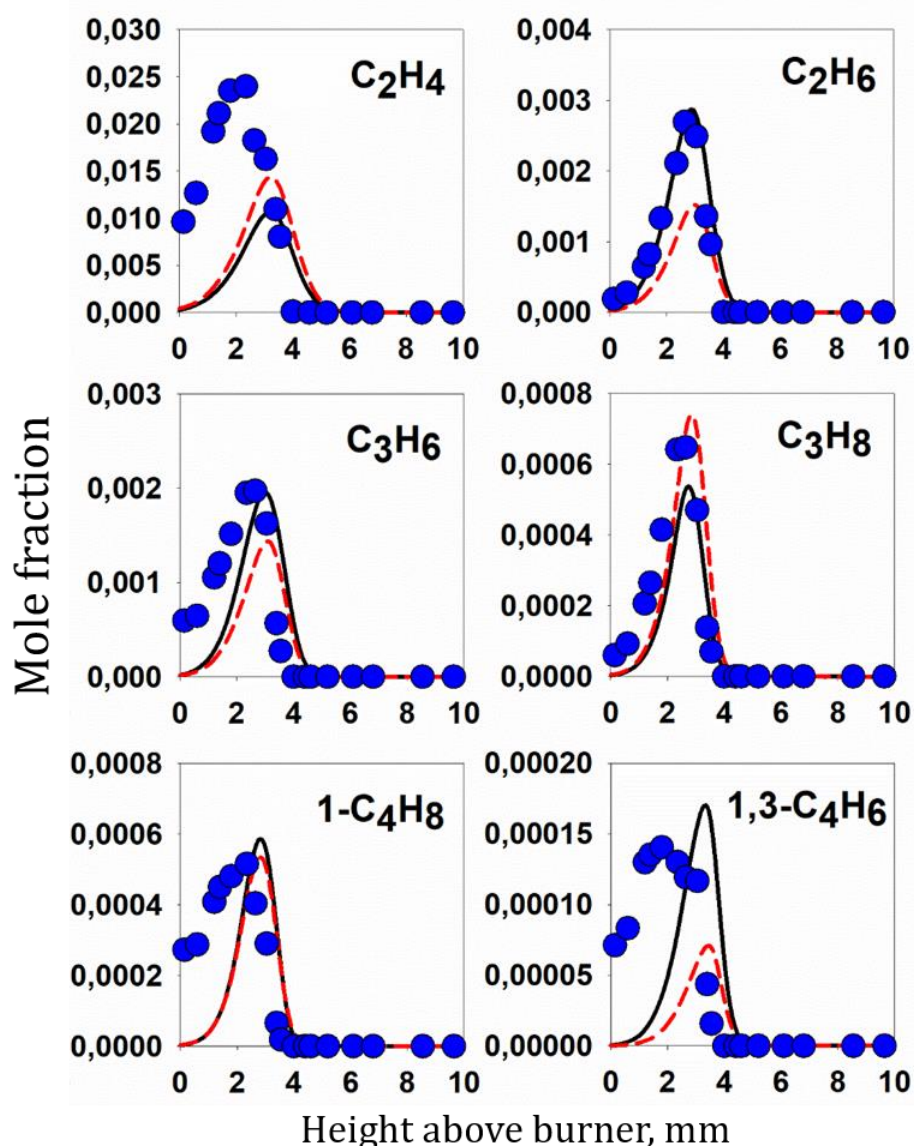


Figure 3.18. Mole fraction profiles of intermediate hydrocarbon products in the stoichiometric flame of ethyl pentanoate at 50 Torr.

Symbols: experimental data; black lines: Dayma mechanism; red lines: new mechanism.

As it seen, nonzero concentrations were observed close to the burner for a number of compounds in the experiment, for example, 1-butene or propene. However, the models have predicted a zero mole fraction of these compounds

near the burner. We suggested two explanations for this effect. The first is associated with the complexity of the probe measurements in vicinity of the burner surface. Since the probe takes a gas sample in a certain volume in front of it, sampling close the very surface might be distorted.

Another explanation is associated with a really faster formation of these substances than it is assumed in the models. This hypothesis is partially confirmed by the fact that nonzero concentrations near the burner surface were observed for ethylene and C<sub>4</sub>-hydrocarbons which, most likely, are formed at the early stages of the fuel destruction. It is worth noting that the similar problem was discussed in the work [85].

Figure 3.19 shows experimental and simulation results for oxygenated intermediates. As at atmospheric pressure, the mole fraction of acetaldehyde (CH<sub>3</sub>CHO) is higher than that of formaldehyde (CH<sub>2</sub>CO). It can be seen that the new model has predicted the peak mole fraction of acetaldehyde much better than the Dayma mechanism which has overestimated it by almost two times. The experimentally determined mole fraction of ethanol (C<sub>2</sub>H<sub>5</sub>OH) was quantitatively described by the models but the peak position in the experiment was shifted toward the burner surface similar to the above-described shifts of some hydrocarbons.

The mole fraction profiles of acetone (CH<sub>3</sub>COCH<sub>3</sub>), ethyl acrylate (C<sub>5</sub>H<sub>8</sub>O<sub>2</sub>) and valeric acid (C<sub>4</sub>H<sub>9</sub>COOH) measured in the experiment are in much worse agreement with the simulation results. The maximum mole fraction of acetone was underestimated by 3 times in the Dayma model and almost by 5 times in the new mechanism. However, the mole fraction of CH<sub>3</sub>COCH<sub>3</sub> has been only about 10<sup>-5</sup>, thus the description accuracy of this component was not of particular interest. In the low-pressure experiment we have measured the mole fraction profile of ethyl acrylate (C<sub>5</sub>H<sub>8</sub>O<sub>2</sub>) which should be formed at the early stages of EPe oxidation. As can be seen from the figure the peak mole fraction of C<sub>5</sub>H<sub>8</sub>O<sub>2</sub> was predicted by the mechanism of Dayma quite well. According to the new model, the peak molar fraction of ethyl acrylate should be 3.5 times higher, which

is beyond the experimental uncertainty and indicates a certain inaccuracy in the mechanism.

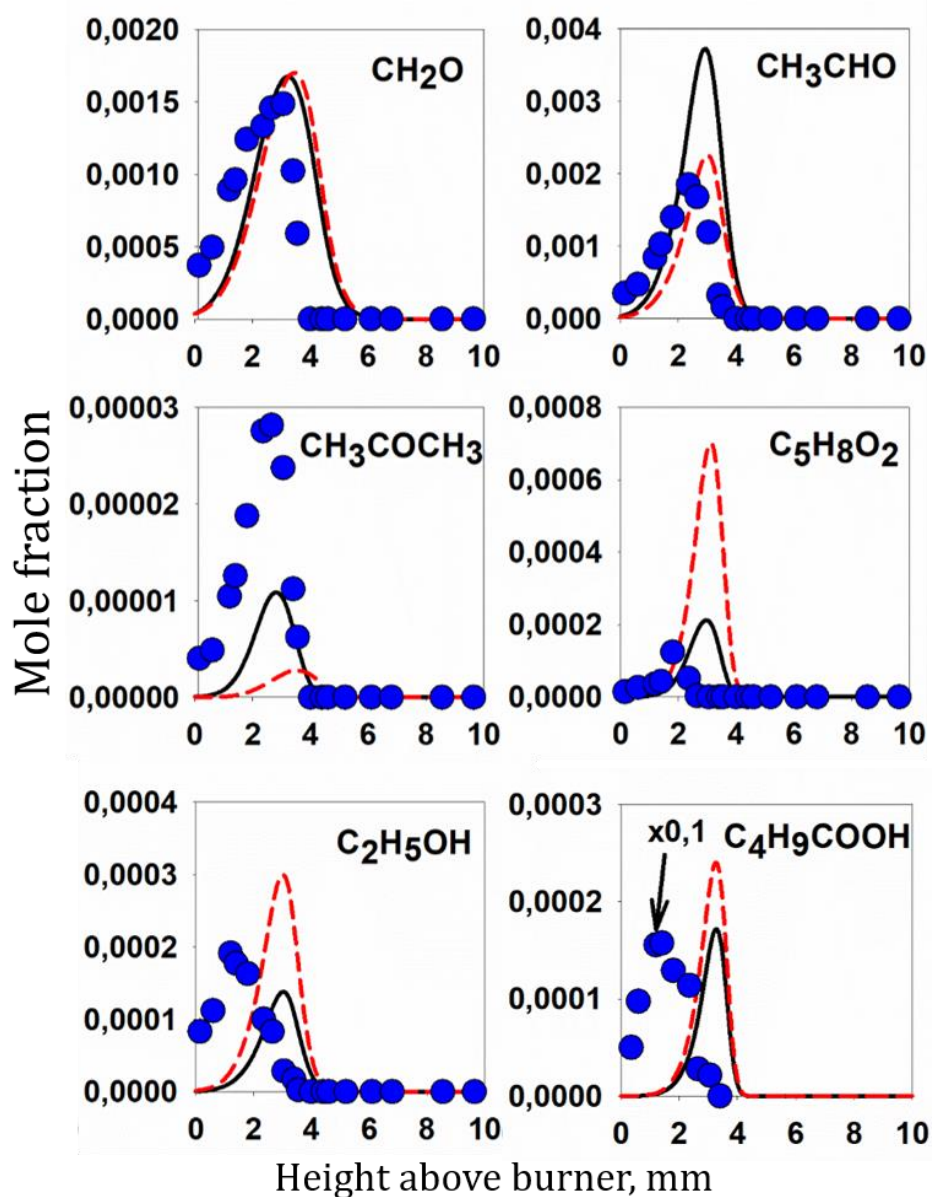


Figure 3.19. Mole fraction profiles of oxygenated products in the stoichiometric flame of ethyl pentanoate at 50 Torr.

Symbols: experimental data; black lines: Dayma mechanism; red lines: new mechanism

In the case of valeric acid, its maximum mole fraction in the experiment has been overestimated and shifted towards the burner, as in the case of ethylene.



This is consistent with the assumption that some decomposition of EPe has been gone in the probe due to insufficient sample cooling (if the temperature drop in the probe is not fast enough). It should be noted that the heated sample line from the probe to the GC analysers does not change the composition of the sample. We have check this possibility with calibration measurements using a gas mixture of known composition (EPe/Ar). However, even taking into account the excess acid formation in the probe, both models have underpredicted the maximum mole fraction of valeric acid.

In general, a satisfactory description of the mole fraction profiles of most of the hydrocarbons measured can be observed. The model oa Dayma and the new model have demonstrated a different predictive accuracy for individual compounds. Unfortunately, the probe effect did not allow us to determine with acceptable accuracy the ethylene and valeric acid mole fractions, which are the products of unimolecular decomposition. Nevertheless, from the data obtained it could be concluded that both models still underestimate the mole fractions of these compounds.

### **3.2. ANALYSIS OF DETAILED COMBUSTION MECHANISMS USED**

This section provides a detailed discussion of the mechanisms used basing on the integral analysis of the fuel conversion pathways in the flames. The mechanisms are discussed in the context of the accuracy of the experimental data description presented in the previous section. Particular attention is paid to the discussion of the new mechanism proposed in the thesis. The analyses performed allows to draw specific conclusions about the advantages and disadvantages of the mechanisms and to identify reaction pathways, which kinetic parameters require additional clarification.

### 3.2.1. Analyses of the primary decomposition pathways of esters in flames

#### 3.2.1.1. Ethyl acetate

As a rule, the general scheme of species oxidation in flames presents a destruction of parent fuel molecules to lighter compounds, which form stable products depending on the conditions. The specific ratio of quasi-stationary concentrations of intermediate species in a flame under given conditions depends on the reaction pathways in which the fuel predominantly decomposes. In this regard, the initial fuel oxidation stages are of particular interest for the analyses of detailed kinetic mechanisms.

Figure 3.20 shows an integral rate of production analysis (IROP) of the primary reaction pathways of ethyl acetate destruction in the near-stoichiometric flame ( $\phi = 1.1$ ). Three mechanisms were used to simulate EA flames. In this regard, this figure represents the generalized scheme of EA destruction in the flame. The values on the scheme indicate the percentage contributions of specific reactions to the complete consumption of particular component. Black values correspond to the mechanism of Dayma, blue values correspond to the Sun model, which is used in our new model of EPe combustion, and green values correspond to the model of Ahmed. Let's look an example of the scheme interpretation: from the presented analyses it follows that according to the model of Dayma 42.4% of ethyl acetate is consumed in the reaction of unimolecular decomposition with formation of ethylene and acetic acid. According to the Sun mechanism the contribution of this reaction to the consumption of EA is 30.74%, and in the model of Ahmed it is 28.94%.

In addition to the unimolecular decomposition, the mechanisms include three more pathways for the primary destruction of EA through the H atom eliminations with free radicals. Three H-atom abstractions correspond to three carbon atoms where C-H bond could be ruptured. As a result of the hydrogen elimination fuel radicals are formed. These species are represented on the figure as the EA molecule with an asterisk in the position where an H atom was

detached. In the Sun, Dayma and new mechanisms the ethyl acetate fuel radicals are designated as EAEJ, EAMJ and EA2J. Here the letter 'J' means a radical and the number or letter in front of it means the position (see Figure 2.11) where the C-H bond was broken. The same nomenclature is used for ethyl butanoate and ethyl pentanoate.

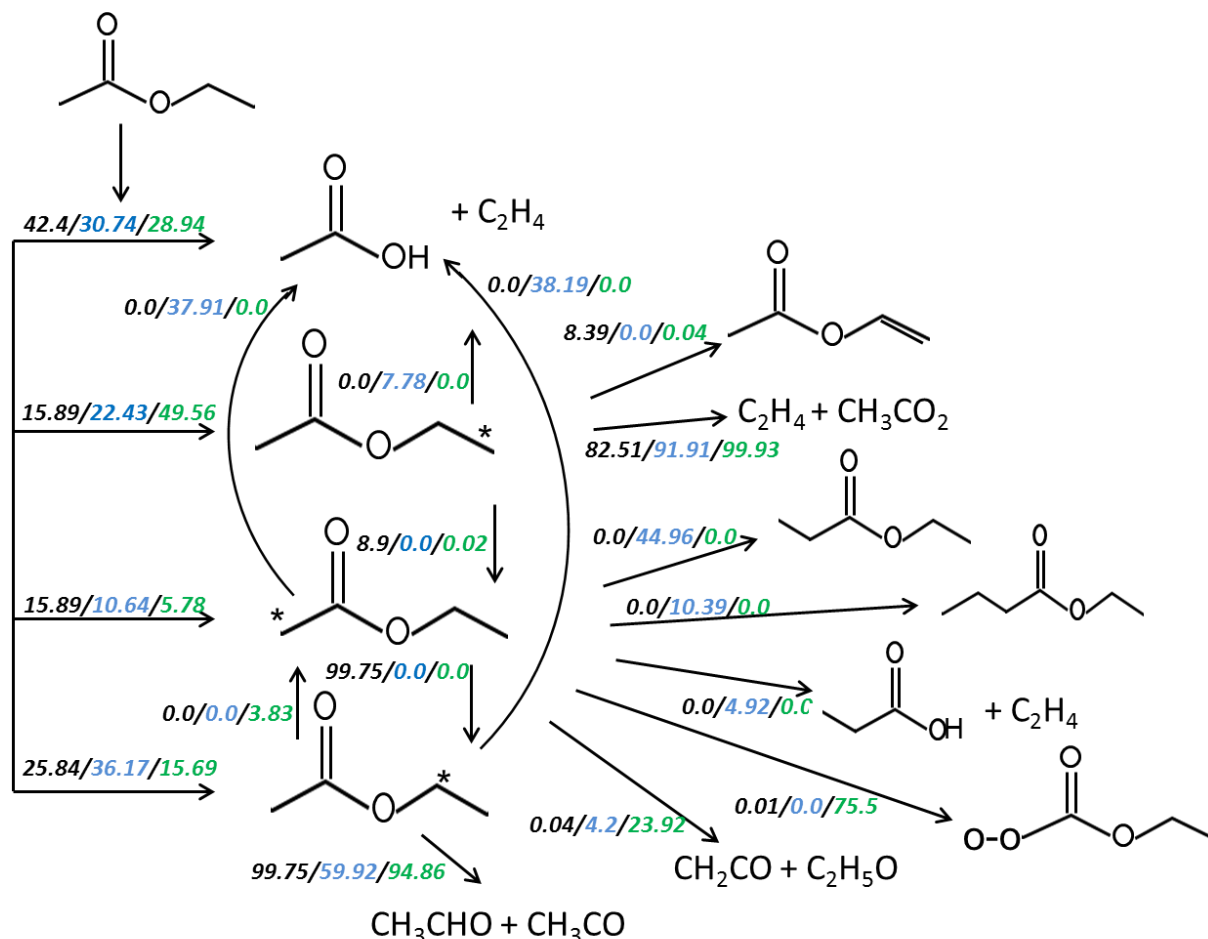


Figure 3.20. IROP analyses of the main oxidation pathways of EA in near-stoichiometric flame ( $\varphi = 1.1$ ) at atmospheric pressure. Black values: percentage contribution to the total component consumption according to the mechanism of Dayma; blue values: according to the model of Sun; green values: according to the model of Ahmed.

According to the analysis, the largest contribution to the fuel destruction in the model of Dayma is made by the unimolecular decomposition (42.4%) and by the H-abstraction in the *E* position (25.8%). In this mechanism the H-abstraction

reactions at positions *M* and *2* have the same contribution, since in the Dayma model these reactions have the same rate constants. However, in the Sun and Ahmed models these reactions have different rate constants, and the contributions of these pathways, respectively, are different. For instance, the most probable pathway of EA decomposition in the Sun model is H-abstractions in the *E* position (36.2%), and a slightly smaller contribution is made by the unimolecular decomposition (30.7%). The H-abstraction reactions in the positions *M* (22.4 %) and *2* (10.6%) have minor contributions. In the mechanism of Ahmed the contributions of the primary reaction pathways have distributed in the following order: H-abstraction in *M* (49.6%) > unimolecular decomposition (28.9%) > H-abstraction in *E* (15.7%) > H-abstraction in *2* (5.8%). Suchwise, all three mechanisms diverge in determining the most probable decomposition pathway of EA decomposition in the near-stoichiometric flame.

After formation in the unimolecular decomposition acetic acid is consumed in H-abstraction reactions with free radicals like the initial fuel. Such compounds as C<sub>2</sub>H<sub>2</sub>, CO, CH<sub>3</sub> and others are formed during these processes. Fuel radicals, in turn, are unstable compounds, so they mainly break down into lighter compounds during unimolecular decompositions. The fuel radical decompositions lead to the formation of light hydrocarbons and new unstable radicals of lighter mass. In addition to the decomposition reactions fuel radicals can isomerize into each other. However, such transformations under the considered conditions are realized only in the model of Dayma. The greatest percentage contribution is made by the isomerization reaction EA2J → EAEJ (99.8%). It means that according to the Dayma mechanism almost all EA2J fuel radicals convert to EAEJ radicals. The mechanism of Ahmed provides only a small contribution (3.83%) of this reaction in opposite direction, and the model of Sun does not include these isomerisations at all.

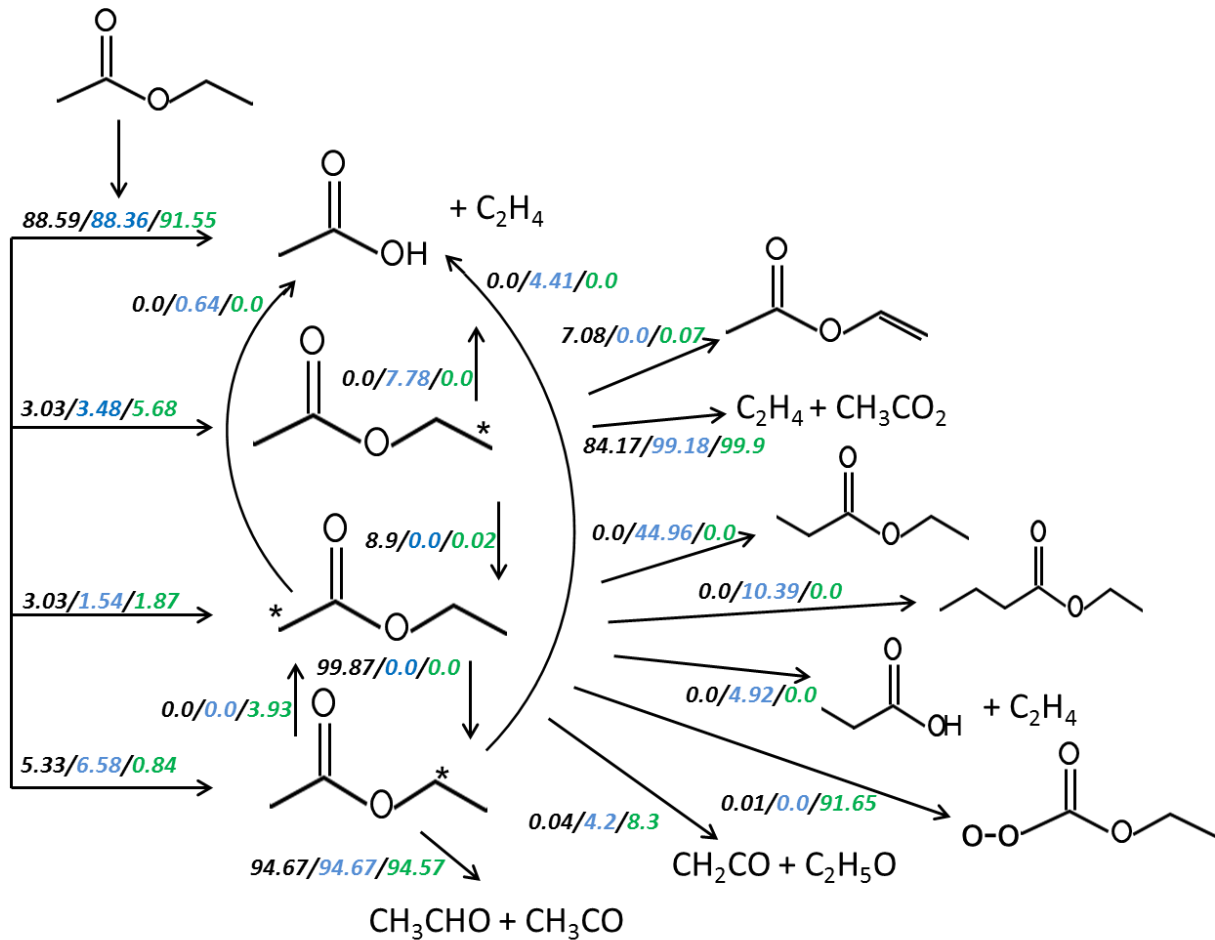


Figure 3.21. IROP analyses of the main oxidation pathways of EA in rich flame ( $\varphi = 1.7$ ) at atmospheric pressure. Black values: percentage contribution to the total component consumption according to the mechanism of Dayma; blue values: according to the model of Sun; green values: according to the model of Ahmed.

The analysis shows that in the Sun mechanism part of the fuel radicals is converted into acetic acid. These reactions have a particularly noticeable contribution in the near-stoichiometric flame that, possibly, is the reason for the overestimation of the maximum acid mole fraction by the Sun mechanism (see Figure 3.3). In this case, the predictions of the Dayma and Ahmed models are quite accurate. However, all three models overestimate the acid mole fraction in the rich flame. The ROP analysis of EA decomposition in the rich flame (Figure 3.21) shows that all three models predict EA oxidation almost completely (up to 90%) in the unimolecular decomposition. Based on the experimental results it

can be assumed that the contribution of this pathway to the mechanisms is overestimated. Another possible reason of the acid mole fraction overestimation may be the low rates of its consumption. According to the mechanisms the main decomposition pathways of acetic acid in flames are the H-abstraction reactions with radicals. Also, the acid could be decomposed via intra-molecular eliminations, but these pathways correspond mostly to the low-temperature oxidation regimes. Unfortunately, there is a lack of experimental studies of acetic acid high-temperature oxidation, thus the sub-mechanisms for acetic acid in all three mechanisms need to be checked. To deal with it additional experimental studies of acetic acid oxidation should be performed.

Acetaldehyde ( $\text{CH}_3\text{CHO}$ ) is the product of unimolecular decomposition of the EAEJ radical. This reaction is the main reaction pathway for the acetaldehyde formation in EA flames according to the analysis. As already noted, acetaldehyde is an important combustion intermediate that is often formed during the oxidation of oxygen-containing fuels including FAEEs. From Figures 3.20 and 3.21 it can be seen that contribution of the EAEJ formation reaction in the Ahmed mechanism is very low compared to other mechanisms. Apparently, that is the key reason for the significant underestimation of the acetaldehyde mole fraction by the model of Ahmed in both near-stoichiometric and rich flames. It is worth noting that the percentage contribution of the EAEJ formation reaction in the Sun model is larger than in the Dayma model. However, the mechanism of Dayma describes the mole fraction profile of acetaldehyde under the near-stoichiometric conditions more accurately, while the Sun model underestimates acetaldehyde maximum mole fraction by a half. According to the analysis the underestimation in the Sun model occurs because 38% of the EAEJ radical in the near-stoichiometric flame is converted to acetic acid. Besides, the model of Dayma takes into account the additional formation of EAEJ from EA2J that also contributes to the formation of acetaldehyde.

The analysis also makes it clear the reason of  $\text{C}_3\text{H}_6+\text{CH}_2\text{CO}$  mole fraction overestimation by the Sun and Ahmed models (see Figure 3.3). Calculations show

that the ketene ( $\text{CH}_2\text{CO}$ ) mole fraction is 3-5 times higher than the mole fraction of propene ( $\text{C}_3\text{H}_6$ ), so their sum can be analysed mainly as the ketene mole fraction. According to Figures 3.20 and 3.21 the EA2J fuel radical decomposes with the formation of ketene and ethoxide ( $\text{C}_2\text{H}_5\text{O}$ ). In the Dayma model this reaction has a near-zero contribution, while it is slightly greater in the Sun model (4.2%), and it is significantly higher in the Ahmed mechanism (23.9 % and 8.3% in two flames). In this case it is necessary to note again the role of  $\text{EA2J} \rightarrow \text{EAEJ}$  isomerization in the mechanism of Dayma.

From the Figures 3.20 and 3.21 it is also seen, that according to the Sun mechanism the EA2J radical has a possibility to recombine with  $\text{CH}_3$  or  $\text{C}_2\text{H}_5$  radicals forming ethyl propanoate and ethyl butanoate respectively. EA2J can also decompose forming propanoic acid and ethylene. In the mechanisms of Dayma and Ahmed these pathways do not realise. The mechanism of Ahmed comprises  $\text{O}_2$  addition to the EA2J radical under conditions studied. Moreover, the mechanism of Ahmed predicts this reaction as a dominant consumption pathway of the EA2J radical in both stoichiometric and rich flames. Additional experimental studies are also needed to confirm or deny the presence of these reactions.

Hereby, the ROP analysis of the primary transformation pathways made it possible to explain in detail the reasons of discrepancies between experimental data and predictions of the models in EA flames. The above analysis clearly indicates the need for a more correct account of the isomerization reactions of fuel radicals. Also, revision of the kinetic parameters of the acid formation reactions from the fuel radicals in the Sun model is needed. These observations correspond automatically to the new mechanism presented in the thesis.

### 3.2.1.2. Ethyl butanoate

ROP analysis of the primary oxidation pathways of ethyl butanoate in stoichiometric atmospheric flame is shown in Figure 3.22. As in the previous diagrams, the black values correspond to the model of Dayma. The blue values correspond to the mechanism proposed in this work. As discussed above, the rate constants of the primary H-abstraction reactions by various radicals were revised in the new mechanism. Therefore, the reaction contributions with each of the radicals H, OH, O and CH<sub>3</sub> are shown in the figure separately for a more detailed analysis.

Ethyl butanoate has a longer alkyl chain unlike ethyl acetate. That leads to an increase in the number of C-H bonds that can be attacked by radicals. At the same time, rate of reactions for different carbons of the alkyl group is different, that leads to a certain distribution of fuel radicals. For ethyl butanoate there can be five fuel radicals in total. For the convenience of the reader they are signed in Figure 3.22.

According to the Dayma model the most probable pathways of EB destruction in the stoichiometric flame are unimolecular decomposition (20%) and H-abstraction with the formation of two fuel radicals: EBEJ (17.7%) and EB2J (21.3%). Further in the flame, most of the EB2J radicals is isomerized into EBEEJ radicals, which in turn decompose completely with acetaldehyde (CH<sub>3</sub>CHO) formation. As in the EA flames, this pathway is the main reaction pathway of acetaldehyde formation. The same path is realized in the new mechanism. It can be seen from Figure 3.11 that the Dayma model overestimates a few the mole fraction of acetaldehyde, while the new mechanism predicts the values that are closer to experiment. This is most likely due to the slower consumption of acetaldehyde by H-atom abstractions in the model of Dayma.



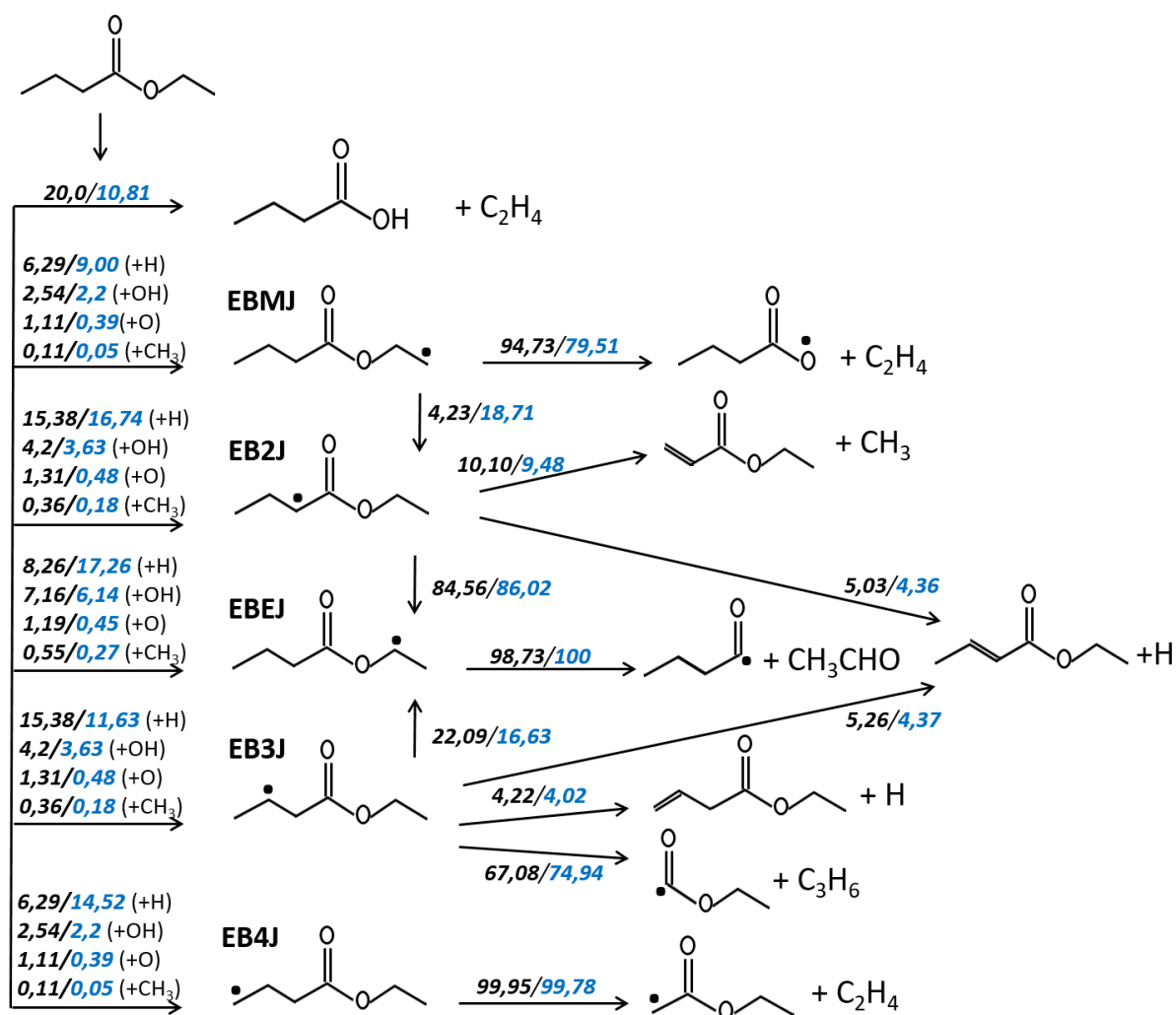


Figure 3.22. IROP analyses of the main oxidation pathways of EB in stoichiometric flame at atmospheric pressure. Black values: percentage contribution to the total component consumption according to the mechanism of Dayma; blue values: according to the new model.

The key pathways of EB oxidation according to the new mechanism are the H-abstraction reactions with formation of the fuel radicals EBEJ (24.1%) and EB2J (21%). In this case, the H-atom abstraction contributions in the other positions are slightly higher than in the Dayma model, and the contribution of the unimolecular decomposition is almost two times less, respectively. This results in a higher relative concentration of the fuel radicals in the new model than in the model of Dayma. Apparently, due to the increased role of hydrogen abstraction reactions in the new mechanism, the maximum mole fraction of butanoic acid

was slightly underestimated. To check the sensitivity of this reaction, we doubled the rate constant of the unimolecular decomposition reaction, and this led to almost complete agreement with experiment and Dayma's model. However, this method of fitting the mechanism to improve simulations cannot be considered reliable, since it leads to discrepancies in the description of other experimental data. Thus, the new mechanism retained the same rate constant as the Dayma mechanism.

A noticeable discrepancy between the model predictions and the experiment was observed for the mole fraction of allene+propyne ( $C_3H_4$  on the Figure 3.10). The analysis has shown that both of these compounds are formed mainly in the chain of propene transformation reactions  $C_3H_6 \rightarrow C_3H_5 \rightarrow C_3H_4$ . As it seen the main pathway of propene formation is decomposition of the EB3J fuel radical. In the new mechanism this reaction has a larger contribution than in the Dayma mechanism. That is reflected in a more accurate prediction of the maximum  $C_3H_4$  mole fraction. Although, an additional consideration of the rate constant of this reaction and of the allene/propyne consumption reactions is necessary for the accuracy improvement.

ROP analysis of the reaction pathways in the rich ( $\varphi = 1.5$ ) EB flame is shown in Figure 3.23. Both models define the unimolecular decomposition as the main pathway under these conditions. The main reason is that the main combustion zone is much wider and the temperature gradient is smaller in the rich flame. Thus, the fresh mixture heats up more slowly in the flame front, and the H atoms and OH radicals, which are mainly formed in the high-temperature zone, cannot diffuse close to the burner. That leads to the slowdown of radical reactions and an increase of the unimolecular decomposition role, since it has a relatively low activation energy and does not depend on the local concentration of radicals. However, the role of the six-center unimolecular decomposition seems to be overestimated, since the comparison of calculations with experiment (Figure 3.11) shows a twofold overestimation of the butanoic acid mole fraction in the models.

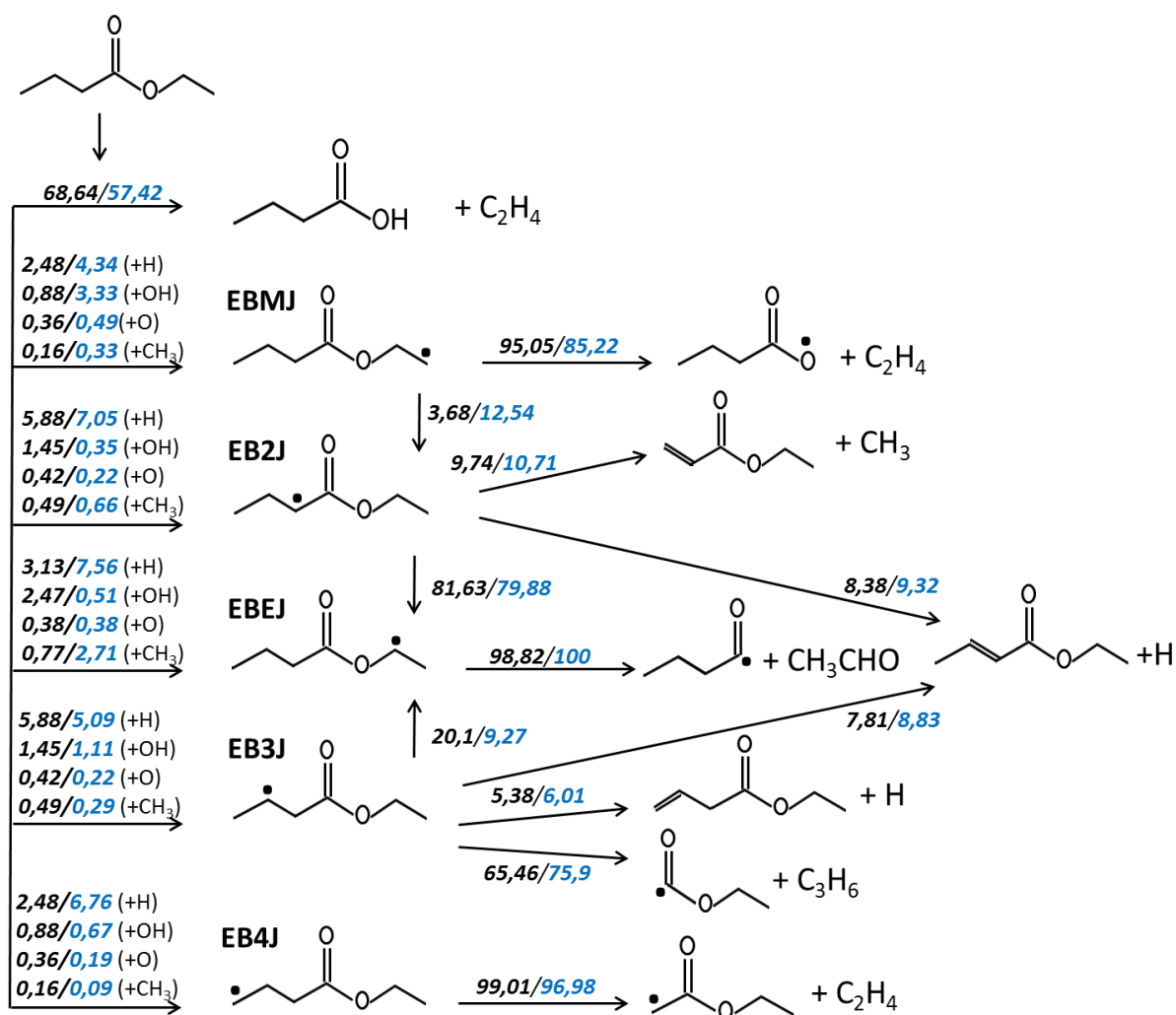


Figure 3.23. IROP analyses of the main oxidation pathways of EB in rich ( $\phi = 1.5$ ) flame at atmospheric pressure. Black values: percentage contribution to the total component consumption according to the mechanism of Dayma; blue values: according to the new model.

Figure 3.23 shows that the radical reaction contributions in both mechanisms are 2-3 times less than those in the stoichiometric flame. However, the general trends remain. It is important to discuss the formation of ethane (C<sub>2</sub>H<sub>6</sub>) and propane (C<sub>3</sub>H<sub>8</sub>) in the rich flame, since the model predictions for these compounds have diverged from experiment by more than 2 times (see Figure 3.10). The main pathway of ethane formation is the recombination of two methyl radicals (CH<sub>3</sub>). If we go back to Figure 3.8, we can see that the new mechanism describes the maximum mole fraction of CH<sub>3</sub> more accurately than the Dayma

mechanism. Therefore, the ethane mole fraction simulations by the new model in Figure 3.10 differ from the experiment less than the calculations by the Dayma model. In addition, the radical recombination reaction clearly depends on pressure, so it can be assumed that the pressure effect on the rate constant of this reaction is taken into account more correctly in the AramcoMech 1.3 mechanism. However, that is not enough as can be seen from the profile comparisons.

Propane mole fraction is closely related to the concentrations of ethane and methyl radical. The analysis has shown that the main reaction of  $C_3H_8$  formation in the mechanisms is the recombination of methyl and ethyl ( $C_2H_5$ ) radicals. The latter, in turn, is mainly formed from ethane and the decomposition products of fuel radicals. In the Dayma mechanism  $C_2H_5$  is mainly formed from the  $C_3H_7CO$  radical which appears together with acetaldehyde during the EBEJ decomposition. In the new mechanism, the main ethyl radical source is the  $C_2H_5OCO$  radical, which is a decomposition product of the EB3J radical. Also, a significant contribution to the  $C_2H_5$  production in the rich flame is provided by unimolecular decomposition of butanoic acid. So, the accuracy of the simulations of the propane mole fraction profiles is linked to the prediction accuracy of the short radicals.

Another minor compound whose mole fraction profile has been poorly described by the models is 1-butene ( $C_4H_8$ ). The discrepancy between the maximum mole fraction of butene according to calculations and experiments was observed not only in the rich, but also in the stoichiometric flame (see Figure 3.10). Butene is mainly formed in recombination of methyl radical with allyl radical ( $C_3H_5$ ), which is a product of the H-abstraction from propene. Therefore, the accuracy of butene mole fraction predictions is directly related to the accuracy of the methyl radical quantifications and the rate of destruction of the EB3J fuel radical.

In general we can conclude that it is necessary to refine the kinetics of radical formation in fuel-rich flames to improve the accuracy of the models. As can be seen from the analysis, the refinement of the formation and consumption

of methyl radical can significantly improve the description of the concentration of light hydrocarbons in ethyl butanoate flames.

### 3.2.1.3. Ethyl pentanoate

IROP analysis of oxidation pathways of ethyl pentanoate was carried out in the greatest detail since this ester is the most complex of those investigated in this work and is also of the greatest practical interest.

Figure 3.24 shows a diagram of the ethyl pentanoate conversion pathways in stoichiometric flame at a pressure of 50 Torr. Black values also correspond to the mechanism of Dayma, blue values correspond to the analysis of the new mechanism. The IROP analysis was carried out similarly to the EB analysis described above, i.e. the contributions of H-abstractions by different radicals are separately distinguished.

As can be seen from the figure, in contrast to the lighter esters, the unimolecular decomposition contribution to the total EPe destruction is insignificant compared to the H-abstraction pathways. Only about 7-8% of the fuel is consumed through this path according to the models. Such a low contribution is due to the long alkyl chain. It was expected that the contribution of the six-centered unimolecular decomposition in the homologous series of FAEEs decreases, since the number of sites for radical attacks increases with the alkyl chain lengthening.

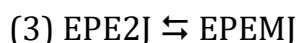
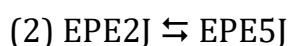
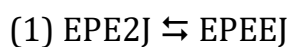
Thus, most of EPe in the stoichiometric flame is consumed in the H-abstraction reactions by the main flame radicals (H, OH, O and CH<sub>3</sub>). Therefore, the results of the latest studies [84], [131], [132] of the hydrogen abstraction reactions from the ester group in FAEEs (positions *E* and *M*, see Figure 2.11) were taken into account during the new mechanism developing. The H-abstractions at these positions lead to the formation of the fuel radicals EPEEJ and EPEMJ.



reactions in the *E* and *M* positions: 15.9% (*E*) and 8% (*M*) in the Dayma mechanism versus 17.7% (*E*) and 15.5% (*M*) in the new mechanism. As it also seen, in contrast to the mechanism of Dayma, in the new mechanism contribution of the reactions at position *M* is not equal to the contribution at position 5.

In the Dayma model, the total contribution of the H-abstraction reactions in positions 2, 3 and 4 is the same (20.3%), since the same rate constants were used for these reactions in all positions. However, as already discussed in Section 2.2.2, the new mechanism uses the refined rate constants of the H atom abstraction in position 2. That is why the total contribution of the EPE2J formation reactions in the new mechanism appeared to be higher than the contribution of the reactions leading to the formation of EPE3J and EPE4J: 26, 7% (2) and 13.4% (3 and 4). Further decomposition of the EPE2J radical leads to the formation of ethyl acrylate ( $C_5H_8O_2$ ) which was measured at low pressure. Apparently, the increase of the EPE2J production explains the overestimation of the ethyl acrylate mole fraction profile in calculations with the new mechanism. It indicates the necessity to improve H-abstraction constant and especially their relative ratios between the different radical formed. Also, we suppose that it is important to carry out a precise quantum-chemical calculation of the H-abstraction rate constants for the EPe molecule at position 2.

In addition to decomposition reaction, the EPE2J radical can isomerize into the other fuel radicals:



Herein, the contribution of the isomerization (2) is the same in both mechanisms (24-25%), but the contributions of reactions (1) and (3) are slightly different: 44% (1) and 14.3% (3) according to the mechanism of Dayma, and 65% (1) and 1.8% (3) in the new mechanism.

The IROP analysis of EPe conversion in the flame at 1 atm (Figure 3.25) demonstrates generally the same trends in the distribution of the H-abstraction

reaction contributions for both mechanisms. This is quite natural, since the rate constants of these reactions do not depend on pressure. In this case, the contribution of the EPe unimolecular decomposition in the Dayma mechanism is slightly increased in comparison with the flame at 50 Torr. In the new mechanism, on the contrary, it is slightly decreased. Nevertheless, the contribution of the fuel unimolecular decomposition in the atmospheric flame is also rather low in comparison with the radical abstraction of hydrogen.

It can be seen from Figure 3.25 that the pressure increase affects the percentage distribution of isomerization reactions. According to the Dayma mechanism, the contribution of reaction (1) is increased from 44% to 63%, and according to the new mechanism it is increased from 65% at 50 Torr to 69.9% at atmospheric pressure. Also, the contribution of reaction (2) in the Dayma mechanism decreased by 7.5%, and in the new mechanism it is only by 2.7%. The reaction (3) in the Dayma mechanism has changed direction at atmospheric pressure, and its contribution is turned out to be quite insignificant. It is important to note that the contribution of reaction (3) according to the Dayma mechanism was quite noticeable and amounted to 14.3% under the low pressure conditions. According to the analysis of the new mechanism, the contribution of reaction (3), on the contrary, is increased by 5% and the direction of isomerization remain the same as at low pressure.

Thus, the use of the refined rate constants for the H-abstractions at positions *2* and *M* significantly influenced the contribution of these reactions to the complete consumption of EPe in comparison with the Dayma mechanism. It can be seen from the analysis that the pressure change has the greatest effect on the isomerization reactions (1) - (3). As it shown, the isomerizations play a significant role in the redistribution of the fuel consumption pathways and, as a consequence, affect the resulting pool of shorter intermediate compounds.



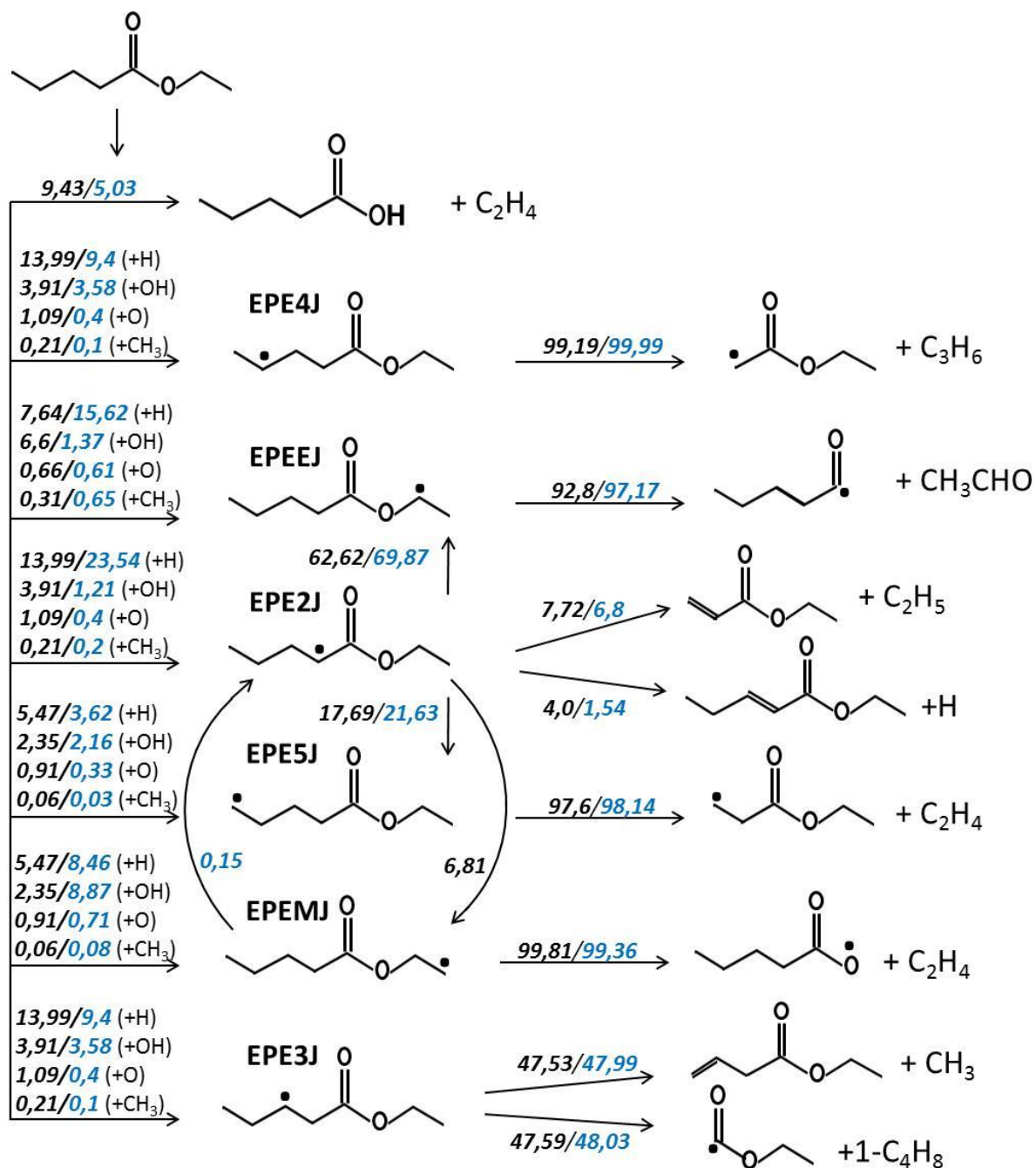


Figure 3.25. IROP analyses of the main oxidation pathways of EPE in stoichiometric flame at atmospheric pressure. Black values: percentage contribution to the total component consumption according to the mechanism of Dayma; blue values: according to the new model.

A more accurate description of the mole fraction profiles of light hydrocarbons by the new model, apparently, is associated with a more accurate

kinetics of C<sub>0</sub>-C<sub>4</sub> species, incorporated into the AramcoMech 1.3 mechanism. However, ethylene in ethyl ester flames forms much earlier and in larger quantities than most of short hydrocarbons. Thus, an insufficient accuracy of the ethylene mole fraction description by the new model was observed.

The insufficient accuracy of the fuel decomposition description is also indicated by the fact that both models have underestimated the maximum mole fraction of valeric acid (C<sub>4</sub>H<sub>9</sub>COOH) in each of the experiments. The analysis has shown a very low, less than 10%, contribution of the unimolecular decomposition. In the stoichiometric atmospheric flame of EB, which is shorter than ethyl pentanoate by only one carbon atom, the contribution of the unimolecular decomposition was about 20%. Also, an overestimation of EPE2J formation in the new model should be mentioned. All these shortcomings signal the need of more accurate calculations of the rate constants for the H-abstraction reactions with particular attention to the branching ratio between them and the six-centered unimolecular decomposition.

### 3.2.2. Calculation of the ethyl pentanoate laminar burning velocity

The propagation speed of a laminar flame is one of the most important global combustion parameters from a practical point of view. At the same time, the experimental measurement of the laminar burning velocities in a wide range of conditions is a rather complicated task. That cause a great interest to the exact numerical simulations of this parameter. In this regard, the question has arisen about the accuracy the new mechanism in description of the experimental data on the laminar burning velocities of EPe/air mixtures published in the work of Dayma et al. [79].

Figure 3.26 shows the results of the laminar flame velocity calculations based on the new kinetic mechanism (red lines) in comparison with experimental data (symbols) and calculations by the Dayma model (black lines). The experiments and corresponding calculations were carried out for pressures of 1,

3 and 5 atm, the initial temperature of the mixtures  $T_i$  was 423 K. The laminar burning velocity was measured as a function of the equivalence ratio  $\phi$ , which was varied from 0.7 to 1.4 at pressures of 1 and 3 atm, and from 0.8 to 1.0 at 5 atm. Experimental uncertainty declared by the authors [79] was about  $\pm 2$  cm/s.

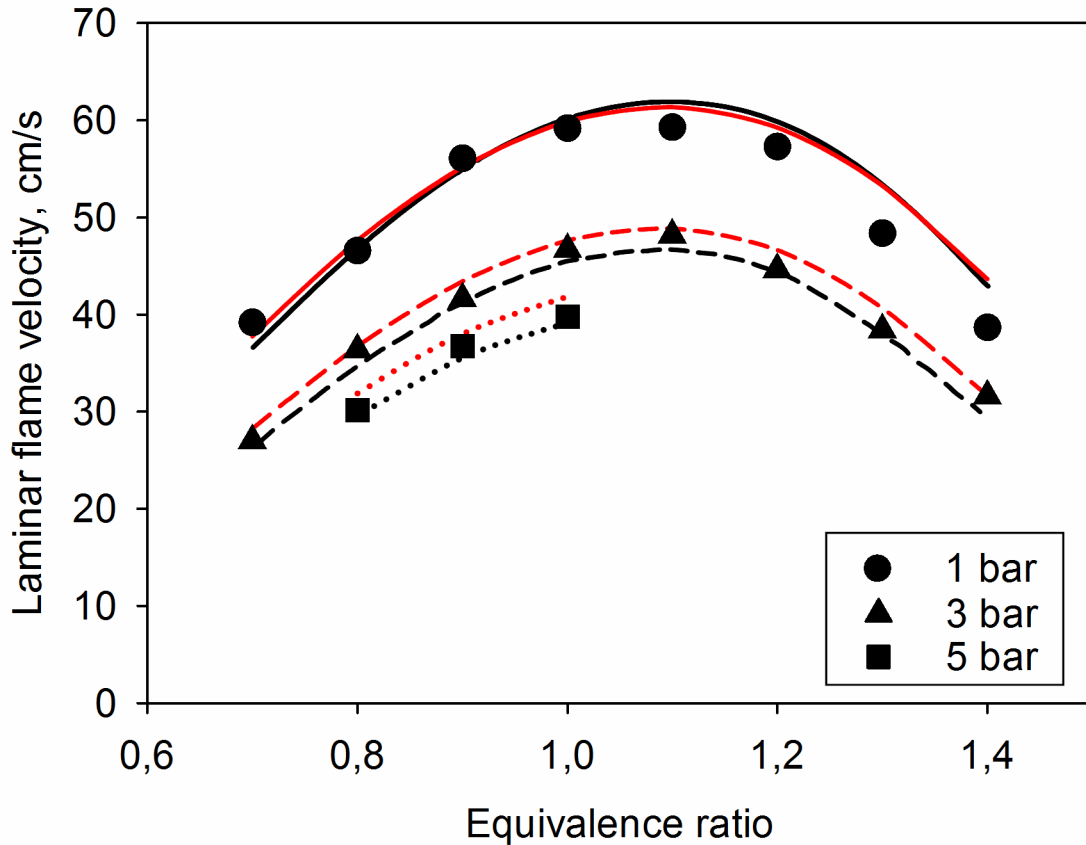


Figure 3.26. Laminar burning velocities of EPe/air mixtures at various equivalence ratios and pressures. Initial mixture temperature  $T_i = 423$  K. Symbols: experimental data from [79]; black lines: mechanism of Dayma; red lines: new mechanism.

The values of the laminar burning velocities at atmospheric pressure calculated using the new model almost completely match the predictions of the Dayma model. In this case, an excellent agreement with the experiment is observed in the lean and near-stoichiometric regions. With the equivalence ratio increase both models slightly overestimate the burning velocities. However, even

the greatest discrepancy between the model predictions and experimental values does not exceed 5 cm/s in the investigated range of  $\varphi$ .

Predictions of the new model at higher pressures differ slightly from those of the Dayma model. As can be seen from the figure, the shapes of the calculated curves at 3 atm completely coincide, but the new mechanism predicts about 2-3 cm/s higher EPe burning velocities than the mechanism of Dayma. Considering the measurement accuracy in the work [79], the red curve lays closer to the upper bound of the confidence interval, while the Dayma mechanism predicts values at the lower bound relative to the experimental points. A similar behaviour of the calculated curves relative to the experimental data is observed at 5 atm. Thus, the new model shows a good agreement with the experimental data within the declared accuracy. It is important to note that the new model's predictions for 3 atm coincide with the experiment over the entire  $\varphi$  range in contrast to the atmospheric flame. Unfortunately, experimental data at 5 atm were obtained for only three EPe/air mixtures, so there is no way to test the new model for a fuel-rich conditions. Nevertheless, the available data are also well described by the new mechanism within the experimental uncertainty.

Based on the above comparison, it can be argued that the new mechanism quite accurately describes the experimental data on the laminar burning velocities of EPe/air mixtures presented in the literature. The result obtained confirms the consistency of the proposed EPe combustion mechanism. Even so, for practical applications it is necessary to check the mechanism on a larger set of experimental data, especially at elevated pressures.

The new mechanism and the mechanism of Dayma have shown quite similar values of the laminar burning velocities of EPe/air mixtures in a wide range of conditions. However, these models differ significantly from each other since they are based on the different submechanisms describing the kinetics of light compounds transformations. In this regard, we were interested in a deeper understanding of the similarities and differences of the models in describing EPe burning speeds.

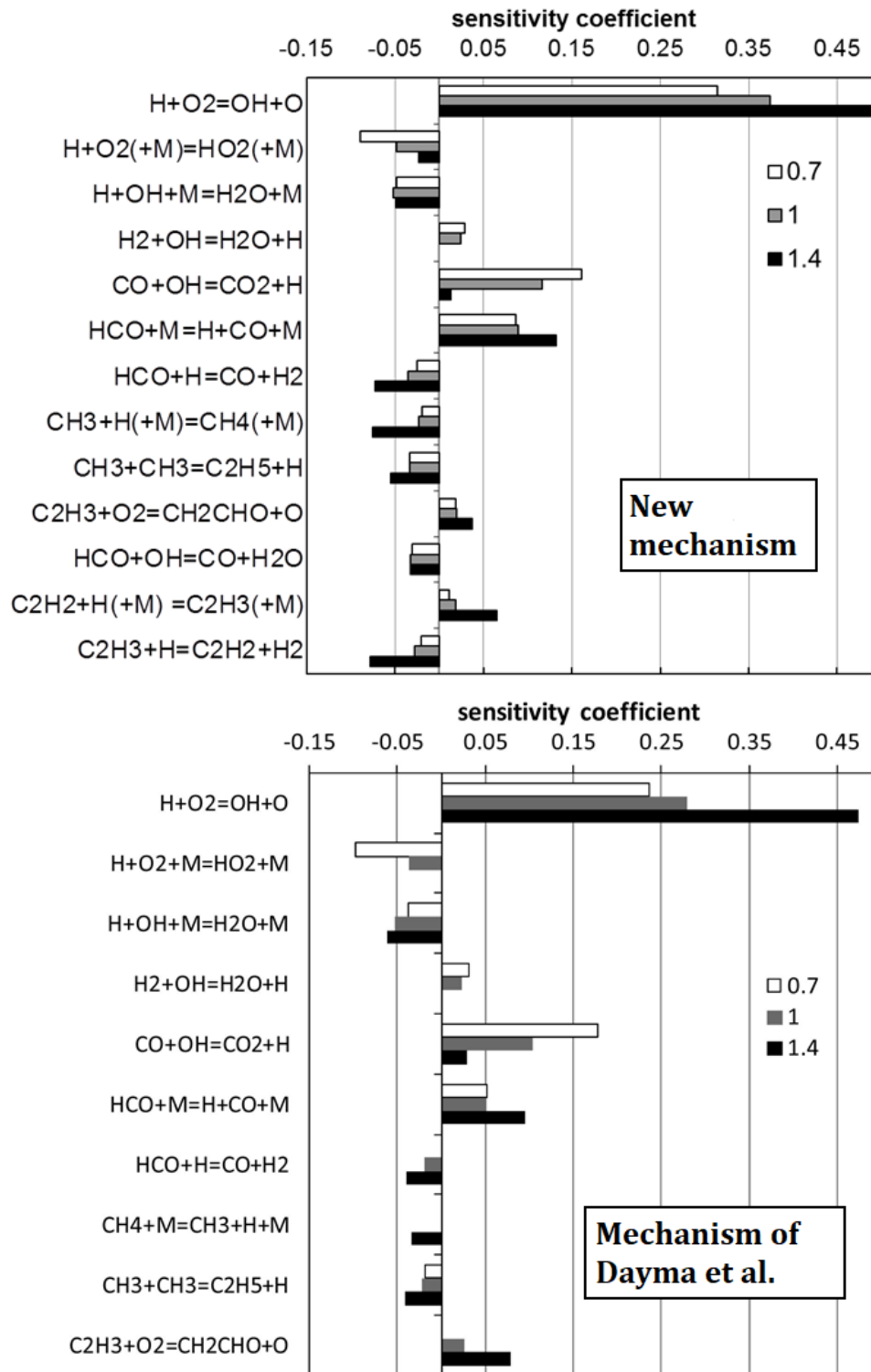
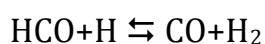
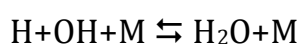
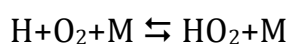


Figure 3.27. The highest sensitivity coefficients of EPe laminar burning velocity to the reaction rate constants in the new mechanism (above) and the model of Dayma et al. (bottom). Sensitivity analysis performed for EPe/air mixtures in lean ( $\varphi = 0.7$ ), stoichiometric ( $\varphi = 1.0$ ) and fuel rich ( $\varphi = 1.4$ ) ratios.

To solve this problem, it was necessary to identify the most important chemical reactions in the mechanisms that effect the velocity calculations. Therefore, an analysis of the sensitivity coefficients of burning velocity to the reaction rate constants in the new mechanism was carried out. For ease of comparison, the analysis was performed in the same way as it was done in the work of Dayma [79]: for lean ( $\varphi=0.7$ ), stoichiometric ( $\varphi=1.0$ ) and rich ( $\varphi=1.4$ ) flame at atmospheric pressure and  $T_i=423$  K. The coefficients obtained are presented in Figure 3.27 in comparison with the sensitivity analysis from the work of Dayma. The figure shows elementary chemical reactions, to the which rate constants the highest (in absolute value) sensitivity was found.

It is obvious that the burning velocity depends most strongly on the rate of the branching reaction  $\text{H}+\text{O}_2 \rightleftharpoons \text{OH}+\text{O}$ , that was demonstrated by the analysis of the mechanisms. However, the sensitivity to the rate constant of this reaction in the new mechanism is about 20-30% higher than in the Dayma mechanism. Moreover, the values of the constant itself are also different. Another most important reaction is the reaction  $\text{CO}+\text{OH} \leftrightarrow \text{CO}_2+\text{H}$  which was also expected. This reaction has the same rate constant in both mechanisms and the sensitivity to this reaction, as can be seen, seems to be the same. Apart from these two reactions, the most important reactions in the mechanisms are the radical recombination reactions:



Thus, as in the case of shorter esters [77], EPe laminar burning velocity is controlled by the basic  $\text{H}_2/\text{O}_2$  kinetics and the kinetics of light  $\text{C}_0\text{-C}_2$  hydrocarbons. Unfortunately, despite significant efforts focused on the studies of oxidation kinetics of light compounds, the scientific community still does not have an unified understanding of the processes taking place. As a result, there is currently not a generally accepted set of reaction rate constants for the basic chemistry of hydrogen and light hydrocarbons [140].

In the Dayma mechanism and the AramcoMech 1.3, which underlies the new mechanism, the sets of kinetic parameters of the basic chemistry differ markedly, especially in terms of pressure dependence. This is expressed in the accuracy of describing the mole fraction profiles of C<sub>2</sub>-C<sub>4</sub> hydrocarbons. The sensitivity analysis has shown that the kinetics of the conversion of acetylene to vinyl radical plays a more important role in the new mechanism than in the Dayma model, especially under fuel-rich flame conditions. The rate constant of the reaction  $C_2H_2 + H (+M) \leftrightarrow C_2H_3 (+M)$  has an explicit dependence on pressure. Considering the differences in the chemistry of acetylene formation and consumption might be responsible for discrepancies in the predictions of the combustion velocities by the models at elevated pressures. It should be noted that in all the flames studied, the new mechanism described most accurately the mole fraction profiles of acetylene. Hence, it can be assumed that, thanks to AramcoMech 1.3, kinetics of the  $C_2H_4 \rightarrow C_2H_3 \rightarrow C_2H_2$  transformation chain in the new mechanism is described better.

In general, the new mechanism has shown a good predictive ability at different pressures and in a wide range of  $\phi$ . Despite the differences in the kinetic parameters incorporated into the Dayma mechanism and the new mechanism, it is impossible to draw an unambiguous conclusion about the higher accuracy of one or the other mechanism from the available data. For this reason, additional experimental studies of the EPe laminar burning velocities at elevated pressures are of great practical and academic interest. It should also be noted that the study of the burning speeds of EPe mixtures with model components of gasoline and diesel is of particular interest.

## **MAIN RESULTS AND CONCLUSIONS**



1. Molecular-beam mass-spectrometry was used to measure the mole fraction profiles of reactants, main products and key intermediate species in the atmospheric flames of the model components of biofuels based on fatty acid ethyl esters: ethyl acetate, ethyl butanoate and ethyl pentanoate. The chemical flame structure of ethyl pentanoate at a pressure of 50 Torr was measured by gas chromatography.
2. Using the chemical kinetics mechanisms of high-temperature oxidation of light ethyl esters presented in the literature, a numerical simulation of the chemical flame structures was carried out. Comparison of the simulation results with experimental data has shown the unsatisfactory predictions of the mole fraction profiles of individual flame components, in particular, light hydrocarbons.
3. An updated detailed combustion mechanism of ethyl pentanoate was proposed on the basis of modern literature data on the kinetics of high-temperature oxidation of small ethyl esters. The mechanism developed includes oxidation stages of lighter ethyl esters and could be used for their simulations. A special attention has been paid to the reaction rate constants of H atom abstractions from a fuel molecule.
4. The new mechanism was verified against experimental data obtained and in comparison with the combustion mechanism of ethyl pentanoate presented in the literature. A more accurate mole fraction predictions of light hydrocarbons by the new model compared to the literature known model were observed. A slightly lower accuracy of the new mechanism in describing the concentrations of individual oxygenated species was also noted.
5. A numerical simulation of laminar burning velocities of ethyl pentanoate/air mixtures by the new mechanism has been carried out. The simulation results were compared with the experimental data presented in the literature. It was shown that the new mechanism describes experimental data very well in a wide range of equivalence ratios and pressures.

6. The main advantages and key disadvantages of the proposed combustion mechanism were analysed by the sensitivity analyses and the integral rate of production analysis. It was determined that the use of more recent rate constants for the H-abstraction reactions from the fuel molecule significantly effected the redistribution of the primary oxidation pathways of ethyl butanoate and ethyl pentanoate. At the same time, the use of AramcoMech 1.3 mechanism has helped to describe the mole fraction profiles of several light compounds. It is shown that it is necessary to revise the isomerization reactions of fuel radicals and the formation of acetic acid from them in the new mechanism for a more accurate description of the chemical structure of ethyl acetate flames. It is necessary to conduct additional experiments in a wide range of conditions, especially at elevated pressures to improve accuracy of the model predictions. Also, quantum-chemical calculations of the H-abstraction rate constants from ethyl pentanoate and ethyl butanoate are needed, as well as refinement of the rate constants of the six-centered unimolecular decomposition of ethyl esters.

# APPENDIX 1

Table of compounds measured in flames, their ionization potentials (IP) corresponding to the energy of ionizing electrons (EIE) in the experiment, calibration method and uncertainty of the mole fraction ( $X_i$ ) determination.

<i>M/Z</i> ( <i>m/z</i> *)	<i>Formula</i>	<i>Name</i>	<i>IP, эВ</i>	<i>EIE, eV</i>	<i>Calibration method</i>	<i>Uncertainty of <math>X_i</math></i>	<i>Flame</i>
1	H	atomic hydrogen	13,6	16,65	RICS on H <sub>2</sub>	±50 %	EA, EPe
2	H <sub>2</sub>	molecular hydrogen	15,43	20	direct	±30%	EB, EPe
15	CH <sub>3</sub>	methyl radical	9,84	13,2	RICS on CH <sub>4</sub>	±50 %	EA, EB, EPe
16	CH <sub>4</sub>	methane	14,25	15,4	direct	±30%	EA, EB, EPe
17	OH	hydroxyl radical	13,17	16,65	RICS on H <sub>2</sub> O	±50 %	EA, EB, EPe
18	H <sub>2</sub> O	water	12,62	15,4	direct	±15%	EA, EB, EPe
26	C <sub>2</sub> H <sub>2</sub>	acetylene	11,4	12,3	RICS on C <sub>2</sub> H <sub>4</sub>	±30%	EA, EB, EPe
28	C <sub>2</sub> H <sub>4</sub>	ethylene	10,51	12,3	direct	±30%	EA, EB, EPe
28	CO	carbon monoxide	14,01	15,4	direct	±15%	EA, EB, EPe
30	CH <sub>2</sub> O	formaldehyde	10,88	11,5	RICS on CO	±50 %	EA, EB, EPe
30	C <sub>2</sub> H <sub>6</sub>	ethane	11,52	12,3	direct	±30%	EA, EB, EPe
32	O <sub>2</sub>	oxygen	12,07	14,35	direct	±15%	EA, EB, EPe

40	Ar	argon	15,76	16,2	direct	±15%	EA, EB, EPe
40	C <sub>3</sub> H <sub>4</sub>	allene propyne	10,22 10,48	12,3	RICS on O <sub>2</sub> not separated	±50 %	EB, EPe
42	C <sub>3</sub> H <sub>6</sub> CH <sub>2</sub> CO	propene keten	9,73 9,62	12,3	RICS on CO <sub>2</sub> not separated	±50 %	EA, EB, EPe
44	CH <sub>3</sub> CHO	acetaldehyde	10,23	10,9	RICS on CO <sub>2</sub>	±50 %	EA, EB, EPe
44	C <sub>3</sub> H <sub>8</sub>	propane	10,94	12,3	direct	±30%	EA, EB, EPe
44	CO <sub>2</sub>	carbon dioxide	13,78	15,4	direct	±15%	EA, EB, EPe
54	C <sub>4</sub> H <sub>6</sub>	1,3-butadiene	9,07	12,3	direct	±30%	EB, EPe
56	C <sub>4</sub> H <sub>8</sub>	1-butene 2-butene	9,86 9,38	12,3	direct not separated	±30%	EB
60	CH <sub>3</sub> COOH	acetic acid	10,65	12,3	direct	±30%	EA
88(60)	C <sub>3</sub> H <sub>7</sub> COOH	butanoic acid	10,17	12,3	direct	±30%	EB
88(43)	CH <sub>3</sub> COOC <sub>2</sub> H <sub>5</sub>	ethyl acetate	10,01	12,3	direct	±15%	EA
102(60)	C <sub>4</sub> H <sub>9</sub> COOH	valeric acid	10,53	12,3	direct	±30%	EPe
116(71)	C <sub>3</sub> H <sub>7</sub> COOC <sub>2</sub> H <sub>5</sub>	ethyl butanoate	10,06	12,3	direct	±15%	EB
130(88)	C <sub>4</sub> H <sub>9</sub> COOC <sub>2</sub> H <sub>5</sub>	ethyl pentanoate	10,4 [141]	12,3	direct	±15%	EPe

\* mass peak used to determine the mole fraction of the compound

## APPENDIX 2

Operating conditions of methods during GC-analyses.

<i>GC analyzer</i>	<b>Agilent 7890 A</b>
<i>Sample loop</i>	V=2 ml T <sub>valve</sub> =200°C
<i>Injector</i>	Split 1 :1 T=250°C
<i>Switch valve event</i>	0 min : Off (carrier gas passes through two columns) 3,7 min: On (carrier gas doesn't pass through the column HP-Molesieve) (60-150) min: Off (carrier gas passes through two columns)
<i>Columns</i>	HP-Plot Q (capillary column: 30 m×0,32 mm×20 μm) Carrier gas : He HP-Molesieve (30 m×0,53 mm×50 μm) Carrier gas : He
<i>Flow in column</i>	6 ml/min->(65-155) min, 4 ml/min->12 ml/min until the end
<i>Oven program</i>	40°C->5,3 min, 10°C/min->150°C, 150°C->12 min, 10°C/min->190°C, 190°C->(5-120) min, 20°C/min->70°C, 70°C->5 min, 20°C/min->190°C, 190°C->10 min
<i>FID detector</i>	T=400°C Q <sub>v</sub> (H <sub>2</sub> )=45 ml/min Q <sub>v</sub> (Air)=425 ml/min Q <sub>v</sub> (He)=25 ml/min
<i>TCD detector</i>	T=250°C Q <sub>v</sub> (He)=16 ml/min (reference) Q <sub>v</sub> (He)=5 ml/min
<i>Methaniser</i>	T=375°C

<i>GC analyzer</i>	<b>HP 5890 Series II</b>
<i>Sample loop</i>	V= 0,35 ml T <sub>valve</sub> = 255°C
<i>Columns</i>	Carbosphere Carrier gas: Ar Q <sub>v</sub> (Ar)= 6,6 ml/min
<i>Oven program</i>	40°C->12 min, 20°C/min->250°C, 250°C->40 min.
<i>TCD detector</i>	T=250°C Q <sub>v</sub> (Ar)=22 ml/min (référence)

## APPENDIX 3

Table of species detected in the low-pressure experiments. Retention times and corresponding calibration coefficients are provided.

<i>Formula</i>	<i>Name</i>	<i>Retention time, min</i>	<i>Calibration coefficient</i>	<i>Detector</i>
<b>Agilent 7890 A</b>				
CO <sub>2</sub>	carbon dioxide	4,35	7916	FID
C <sub>2</sub> H <sub>4</sub>	ethylene	6,03	15356	FID
C <sub>2</sub> H <sub>2</sub>	acetylene	6,61	13906	FID
C <sub>2</sub> H <sub>6</sub>	ethane	7,24	15562	FID
H <sub>2</sub> O	water	11,88-12,24	282	TCD
C <sub>3</sub> H <sub>6</sub>	propene	12,53	23267	FID
C <sub>3</sub> H <sub>8</sub>	propane	12,93	22977	FID
a-C <sub>3</sub> H <sub>4</sub>	allene	13,19	20824	FID
CH <sub>2</sub> O	formaldehyde	13,47	7807	FID
p-C <sub>3</sub> H <sub>4</sub>	propyne	13,48	26664	FID
CH <sub>3</sub> CHO	acetaldehyde	15,30	15615	FID
iC <sub>4</sub> H <sub>10</sub>	iso-butane	16,31	30536	FID
1-C <sub>4</sub> H <sub>8</sub>	1-butene	16,68	31229	FID
1,3-C <sub>4</sub> H <sub>6</sub>	1,3-butadiene	16,84	32067	FID
nC <sub>4</sub> H <sub>10</sub>	n-butane	17,07	31229	FID
2-C <sub>4</sub> H <sub>8</sub>	2-butene	17,28	31229	FID
C <sub>2</sub> H <sub>5</sub> OH	ethanol	18,41	15615	FID
CH <sub>3</sub> COCH <sub>3</sub>	acetone	20,34	23422	FID
C <sub>4</sub> H <sub>8</sub> O <sub>2</sub>	ethyl acetate	30,79	31229	FID
CH <sub>3</sub> COOH	acetic acid	35,21	31229	FID
C <sub>7</sub> H <sub>14</sub> O <sub>2</sub>	ethyl pentanoate	76,33	54651	FID
C <sub>4</sub> H <sub>9</sub> COOH	pentanoic acid	107,60	39037	FID
Ar*	argon	120,57	684	TCD
CH <sub>4</sub> *	methane	122,47	7807	FID
CO*	carbon monooxide	124,35	7567	FID
<b>HP 5890 Series II</b>				
H <sub>2</sub>	hydrogen	8,35	3451	TCD
O <sub>2</sub>	oxygen	18,16	189	TCD

\*depends on the method time

# LIST OF REFERENCES

- [1] X. Yu, N. S. Sandhu, Z. Yang, and M. Zheng, 'Suitability of energy sources for automotive application – A review', *Applied Energy*, vol. 271, p. 115169, Aug. 2020, doi: 10.1016/j.apenergy.2020.115169.
- [2] H. L. MacLean and L. B. Lave, 'Evaluating automobile fuel/propulsion system technologies', *Progress in Energy and Combustion Science*, vol. 29, no. 1, pp. 1–69, Jan. 2003, doi: 10.1016/S0360-1285(02)00032-1.
- [3] R. D. Reitz *et al.*, 'IJER editorial: The future of the internal combustion engine', *International Journal of Engine Research*, vol. 21, no. 1, pp. 3–10, Jan. 2020, doi: 10.1177/1468087419877990.
- [4] J. M. Bergthorson and M. J. Thomson, 'A review of the combustion and emissions properties of advanced transportation biofuels and their impact on existing and future engines', *Renewable and Sustainable Energy Reviews*, vol. 42, pp. 1393–1417, 2015, doi: 10.1016/j.rser.2014.10.034.
- [5] A. K. Agarwal, 'Biofuels (alcohols and biodiesel) applications as fuels for internal combustion engines', *Progress in Energy and Combustion Science*, vol. 33, no. 3, pp. 233–271, 2007, doi: 10.1016/j.pecs.2006.08.003.
- [6] A. K. Hossain and P. A. Davies, 'Plant oils as fuels for compression ignition engines: A technical review and life-cycle analysis', *Renewable Energy*, vol. 35, no. 1, pp. 1–13, 2010, doi: 10.1016/j.renene.2009.05.009.
- [7] J.-P. Lange *et al.*, 'Valeric Biofuels: A Platform of Cellulosic Transportation Fuels', *Angewandte Chemie International Edition*, vol. 49, no. 26, pp. 4479–4483, 2010, doi: 10.1002/anie.201000655.
- [8] H. A. Dabbagh, F. Ghobadi, M. R. Ehsani, and M. Moradmand, 'The influence of ester additives on the properties of gasoline', *Fuel*, vol. 104, pp. 216–223, 2013, doi: 10.1016/j.fuel.2012.09.056.
- [9] F. Contino, F. Foucher, F. Halter, G. Dayma, P. Dagaut, and C. Mounaïm-Rousselle, 'Engine Performances and Emissions of Second-Generation Biofuels in Spark Ignition Engines: The Case of Methyl and Ethyl Valerates', *SAE Technical Paper*, vol. 2013-24-0098, 2013, doi: 10.4271/2013-24-0098.
- [10] A. E. Atabani, A. S. Silitonga, I. A. Badruddin, T. M. I. Mahlia, H. H. Masjuki, and S. Mekhilef, 'A comprehensive review on biodiesel as an alternative energy resource and its characteristics', *Renewable and Sustainable Energy Reviews*, vol. 16, no. 4, pp. 2070–2093, 2012, doi: 10.1016/j.rser.2012.01.003.
- [11] G. Knothe, 'Biodiesel fuels', *Progress in Energy and Combustion Science*, vol. 58, pp. 36–59, 2017, doi: 10.1016/j.pecs.2016.08.001.
- [12] A. K. Agarwal, J. G. Gupta, and A. Dhar, 'Potential and challenges for large-scale application of biodiesel in automotive sector', *Progress in Energy and Combustion Science*, vol. 61, pp. 113–149, Jul. 2017, doi: 10.1016/j.pecs.2017.03.002.

- [13] M. Mofijur, M. G. Rasul, N. M. S. Hassan, H. H. Masjuki, M. A. Kalam, and H. M. Mahmudul, 'Chapter Fourteen - Assessment of Physical, Chemical, and Tribological Properties of Different Biodiesel Fuels', in *Clean Energy for Sustainable Development*, M. G. Rasul, A. Kalam Azad, and S. C. Sharma, Eds. Academic Press, 2017, pp. 441–463.
- [14] B. S. Chauhan, R. K. Singh, H. M. Cho, and H. C. Lim, 'Practice of diesel fuel blends using alternative fuels: A review', *Renewable and Sustainable Energy Reviews*, vol. 59, pp. 1358–1368, 2016, doi: 10.1016/j.rser.2016.01.062.
- [15] European Standard EN 14214:2012+A2:2019, 'Liquid petroleum products – fatty acid methyl esters (FAME) for use in diesel engines and heating applications – requirements and test methods', 2019.
- [16] ASTM Standard D6751-02, 'Specification for Biodiesel Fuel Blend Stock (B100) for Middle Distillate Fuels', ASTM International. doi: 10.1520/D6751-02.
- [17] ASTM Standard D7467-20a, 'Specification for Diesel Fuel Oil, Biodiesel Blend (B6 to B20)', ASTM International. doi: 10.1520/D7467-20A.
- [18] SCC Standard CAN/CGSB-3.524-2017, 'Biodiesel (B100) for blending in middle distillate fuels', 2017.
- [19] K. Bozbas, 'Biodiesel as an alternative motor fuel: Production and policies in the European Union', *Renewable and Sustainable Energy Reviews*, vol. 12, no. 2, pp. 542–552, 2008, doi: 10.1016/j.rser.2005.06.001.
- [20] К. Кугучин and Е. Алеханова, 'Мировая индустрия биотоплива: общая характеристика, история и факторы развития отрасли', *Риск: Ресурсы, Информация, Снабжение, Конкуренция*, no. 1, pp. 199–204, 2012.
- [21] 'Biofuels Mandates Around the World: 2012: Biofuels Digest'. <http://www.biofuelsdigest.com/bdigest/2012/11/22/biofuels-mandates-around-the-world-2012/> (accessed Jun. 22, 2020).
- [22] H. Joo and A. Kumar, *World Biodiesel Policies and Production*. CRC Press, 2019.
- [23] M. F. M. Yusoff, X. Xu, and Z. Guo, 'Comparison of Fatty Acid Methyl and Ethyl Esters as Biodiesel Base Stock: a Review on Processing and Production Requirements', *Journal of the American Oil Chemists' Society*, vol. 91, no. 4, pp. 525–531, 2014, doi: 10.1007/s11746-014-2443-0.
- [24] L. F. Gutiérrez, Ó. J. Sánchez, and C. A. Cardona, 'Process integration possibilities for biodiesel production from palm oil using ethanol obtained from lignocellulosic residues of oil palm industry', *Bioresource Technology*, vol. 100, no. 3, pp. 1227–1237, 2009, doi: 10.1016/j.biortech.2008.09.001.
- [25] C. Brunschwig, W. Moussavou, and J. Blin, 'Use of bioethanol for biodiesel production', *Progress in Energy and Combustion Science*, vol. 38, no. 2, pp. 283–301, 2012, doi: 10.1016/j.pecs.2011.11.001.
- [26] P. Verma and M. P. Sharma, 'Review of process parameters for biodiesel production from different feedstocks', *Renewable and Sustainable Energy Reviews*, vol. 62, pp. 1063–1071, Sep. 2016, doi: 10.1016/j.rser.2016.04.054.
- [27] J. M. Encinar, J. F. González, and A. Rodríguez-Reinares, 'Ethanolysis of used frying oil. Biodiesel preparation and characterization', *Fuel Processing*



- Technology*, vol. 88, no. 5, pp. 513–522, May 2007, doi: 10.1016/j.fuproc.2007.01.002.
- [28] G. Mendow, N. S. Veizaga, and C. A. Querini, 'Ethyl ester production by homogeneous alkaline transesterification: Influence of the catalyst', *Bioresource Technology*, vol. 102, no. 11, pp. 6385–6391, Jun. 2011, doi: 10.1016/j.biortech.2011.01.072.
- [29] Q. Li, J. Xu, W. Du, Y. Li, and D. Liu, 'Ethanol as the acyl acceptor for biodiesel production', *Renewable and Sustainable Energy Reviews*, vol. 25, pp. 742–748, Sep. 2013, doi: 10.1016/j.rser.2013.05.043.
- [30] V. Makareviciene and P. Janulis, 'Environmental effect of rapeseed oil ethyl ester', *Renewable Energy*, vol. 28, no. 15, pp. 2395–2403, Dec. 2003, doi: 10.1016/S0960-1481(03)00142-3.
- [31] O. S. Stamenković, A. V. Veličković, and V. B. Veljković, 'The production of biodiesel from vegetable oils by ethanolysis: Current state and perspectives', *Fuel*, vol. 90, no. 11, pp. 3141–3155, Nov. 2011, doi: 10.1016/j.fuel.2011.06.049.
- [32] I. Reyero, G. Arzamendi, S. Zabala, and L. M. Gandía, 'Kinetics of the NaOH-catalyzed transesterification of sunflower oil with ethanol to produce biodiesel', *Fuel Processing Technology*, vol. 129, pp. 147–155, Jan. 2015, doi: 10.1016/j.fuproc.2014.09.008.
- [33] M. Kim, C. DiMaggio, S. Yan, S. O. Salley, and K. Y. S. Ng, 'The synergistic effect of alcohol mixtures on transesterification of soybean oil using homogeneous and heterogeneous catalysts', *Applied Catalysis A: General*, vol. 378, no. 2, pp. 134–143, Apr. 2010, doi: 10.1016/j.apcata.2010.02.009.
- [34] G. Santori, G. Di Nicola, M. Moglie, and F. Polonara, 'A review analyzing the industrial biodiesel production practice starting from vegetable oil refining', *Applied Energy*, vol. 92, pp. 109–132, Apr. 2012, doi: 10.1016/j.apenergy.2011.10.031.
- [35] Deutsche Akademie der Naturforscher Leopoldina, Ed., *The current status of biofuels in the European Union, their environmental impacts and future prospects*. Halle (Saale), 2012.
- [36] D. Singh, D. Sharma, S. L. Soni, S. Sharma, P. Kumar Sharma, and A. Jhalani, 'A review on feedstocks, production processes, and yield for different generations of biodiesel', *Fuel*, vol. 262, p. 116553, Feb. 2020, doi: 10.1016/j.fuel.2019.116553.
- [37] M. Hajjari, M. Tabatabaei, M. Aghbashlo, and H. Ghanavati, 'A review on the prospects of sustainable biodiesel production: A global scenario with an emphasis on waste-oil biodiesel utilization', *Renewable and Sustainable Energy Reviews*, vol. 72, pp. 445–464, May 2017, doi: 10.1016/j.rser.2017.01.034.
- [38] J. Hill, E. Nelson, D. Tilman, S. Polasky, and D. Tiffany, 'Environmental, economic, and energetic costs and benefits of biodiesel and ethanol biofuels', *Proceedings of the National Academy of Sciences*, vol. 103, no. 30, pp. 11206–11210, Jul. 2006, doi: 10.1073/pnas.0604600103.

- [39] B. P. Chapagain, Y. Yehoshua, and Z. Wiesman, 'Desert date (*Balanites aegyptiaca*) as an arid lands sustainable bioresource for biodiesel', *Bioresour. Technol.*, vol. 100, no. 3, pp. 1221–1226, Feb. 2009, doi: 10.1016/j.biortech.2008.09.005.
- [40] A. E. Atabani *et al.*, 'Non-edible vegetable oils: A critical evaluation of oil extraction, fatty acid compositions, biodiesel production, characteristics, engine performance and emissions production', *Renewable and Sustainable Energy Reviews*, vol. 18, pp. 211–245, Feb. 2013, doi: 10.1016/j.rser.2012.10.013.
- [41] C. Öner and Ş. Altun, 'Biodiesel production from inedible animal tallow and an experimental investigation of its use as alternative fuel in a direct injection diesel engine', *Applied Energy*, vol. 86, no. 10, pp. 2114–2120, Oct. 2009, doi: 10.1016/j.apenergy.2009.01.005.
- [42] M. J. Montefrio, T. Xinwen, and J. P. Obbard, 'Recovery and pre-treatment of fats, oil and grease from grease interceptors for biodiesel production', *Applied Energy*, vol. 87, no. 10, pp. 3155–3161, Oct. 2010, doi: 10.1016/j.apenergy.2010.04.011.
- [43] S. N. Gebremariam and J. M. Marchetti, 'Economics of biodiesel production: Review', *Energy Conversion and Management*, vol. 168, pp. 74–84, Jul. 2018, doi: 10.1016/j.enconman.2018.05.002.
- [44] B. Riazi, J. M. Mosby, B. Millet, and S. Spatari, 'Renewable diesel from oils and animal fat waste: implications of feedstock, technology, co-products and ILUC on life cycle GWP', *Resources, Conservation and Recycling*, vol. 161, p. 104944, Oct. 2020, doi: 10.1016/j.resconrec.2020.104944.
- [45] A. E.-F. Abomohra, M. Elsayed, S. Esakkimuthu, M. El-Sheekh, and D. Hanelt, 'Potential of fat, oil and grease (FOG) for biodiesel production: A critical review on the recent progress and future perspectives', *Progress in Energy and Combustion Science*, vol. 81, p. 100868, Nov. 2020, doi: 10.1016/j.pecs.2020.100868.
- [46] A. Talebian-Kiakalaieh, N. A. S. Amin, and H. Mazaheri, 'A review on novel processes of biodiesel production from waste cooking oil', *Applied Energy*, vol. 104, pp. 683–710, Apr. 2013, doi: 10.1016/j.apenergy.2012.11.061.
- [47] Y. Chisti, 'Chapter 1 - Introduction to algal fuels', in *Biofuels from Algae (Second Edition)*, A. Pandey, J.-S. Chang, C. R. Soccol, D.-J. Lee, and Y. Chisti, Eds. Elsevier, 2019, pp. 1–31.
- [48] T. M. Mata, A. A. Martins, and Nidia. S. Caetano, 'Microalgae for biodiesel production and other applications: A review', *Renewable and Sustainable Energy Reviews*, vol. 14, no. 1, pp. 217–232, Jan. 2010, doi: 10.1016/j.rser.2009.07.020.
- [49] J. Milano *et al.*, 'Microalgae biofuels as an alternative to fossil fuel for power generation', *Renewable and Sustainable Energy Reviews*, vol. 58, pp. 180–197, May 2016, doi: 10.1016/j.rser.2015.12.150.
- [50] T. Suganya, M. Varman, H. H. Masjuki, and S. Renganathan, 'Macroalgae and microalgae as a potential source for commercial applications along with biofuels production: A biorefinery approach', *Renewable and Sustainable*

- Energy Reviews*, vol. 55, pp. 909–941, Mar. 2016, doi: 10.1016/j.rser.2015.11.026.
- [51] Y. Chisti, 'Fuels from microalgae', *Biofuels*, vol. 1, no. 2, pp. 233–235, Mar. 2010, doi: 10.4155/bfs.10.9.
- [52] F. X. Malcata, 'Microalgae and biofuels: A promising partnership?', *Trends in Biotechnology*, vol. 29, no. 11, pp. 542–549, Nov. 2011, doi: 10.1016/j.tibtech.2011.05.005.
- [53] M. Mubarak, A. Shaija, and T. V. Suchithra, 'A review on the extraction of lipid from microalgae for biodiesel production', *Algal Research*, vol. 7, pp. 117–123, Jan. 2015, doi: 10.1016/j.algal.2014.10.008.
- [54] Y. Chisti, 'Constraints to commercialization of algal fuels', *Journal of Biotechnology*, vol. 167, no. 3, pp. 201–214, Sep. 2013, doi: 10.1016/j.jbiotec.2013.07.020.
- [55] I. Rawat, R. Ranjith Kumar, T. Mutanda, and F. Bux, 'Biodiesel from microalgae: A critical evaluation from laboratory to large scale production', *Applied Energy*, vol. 103, pp. 444–467, Mar. 2013, doi: 10.1016/j.apenergy.2012.10.004.
- [56] M. Kumar, Y. Sun, R. Rathour, A. Pandey, I. S. Thakur, and D. C. W. Tsang, 'Algae as potential feedstock for the production of biofuels and value-added products: Opportunities and challenges', *Science of The Total Environment*, vol. 716, p. 137116, May 2020, doi: 10.1016/j.scitotenv.2020.137116.
- [57] E. F. Aransiola, T. V. Ojumu, O. O. Oyekola, T. F. Madzimbamuto, and D. I. O. Ikhu-Omoregbe, 'A review of current technology for biodiesel production: State of the art', *Biomass and Bioenergy*, vol. 61, pp. 276–297, Feb. 2014, doi: 10.1016/j.biombioe.2013.11.014.
- [58] H. M. Mahmudul, F. Y. Hagos, R. Mamat, A. A. Adam, W. F. W. Ishak, and R. Alenezi, 'Production, characterization and performance of biodiesel as an alternative fuel in diesel engines – A review', *Renewable and Sustainable Energy Reviews*, vol. 72, pp. 497–509, May 2017, doi: 10.1016/j.rser.2017.01.001.
- [59] M. Tabatabaei *et al.*, 'Reactor technologies for biodiesel production and processing: A review', *Progress in Energy and Combustion Science*, vol. 74, pp. 239–303, Sep. 2019, doi: 10.1016/j.pecs.2019.06.001.
- [60] G. Knothe, 'Biodiesel and renewable diesel: A comparison', *Progress in Energy and Combustion Science*, vol. 36, no. 3, pp. 364–373, Jun. 2010, doi: 10.1016/j.pecs.2009.11.004.
- [61] L. Coniglio, H. Bennadji, P. A. Glaude, O. Herbinet, and F. Billaud, 'Combustion chemical kinetics of biodiesel and related compounds (methyl and ethyl esters): Experiments and modeling – Advances and future refinements', *Progress in Energy and Combustion Science*, vol. 39, no. 4, pp. 340–382, 2013, doi: 10.1016/j.pecs.2013.03.002.
- [62] F. Battin-Leclerc, 'Detailed chemical kinetic models for the low-temperature combustion of hydrocarbons with application to gasoline and diesel fuel surrogates', *Progress in Energy and Combustion Science*, vol. 34, no. 4, pp. 440–498, Aug. 2008, doi: 10.1016/j.pecs.2007.10.002.

- [63] W. J. Pitz and C. J. Mueller, 'Recent progress in the development of diesel surrogate fuels', *Progress in Energy and Combustion Science*, vol. 37, no. 3, pp. 330–350, Jun. 2011, doi: 10.1016/j.pecs.2010.06.004.
- [64] L. Lin, Z. Cunshan, S. Vittayapadung, S. Xiangqian, and D. Mingdong, 'Opportunities and challenges for biodiesel fuel', *Applied Energy*, vol. 88, no. 4, pp. 1020–1031, Apr. 2011, doi: 10.1016/j.apenergy.2010.09.029.
- [65] C. Cavallotti, M. Pelucchi, and A. Frassoldati, 'Analysis of acetic acid gas phase reactivity: Rate constant estimation and kinetic simulations', *Proceedings of the Combustion Institute*, vol. 37, no. 1, pp. 539–546, Jan. 2019, doi: 10.1016/j.proci.2018.06.137.
- [66] P. Dagaut, N. Smoucovit, and M. Cathonnet, 'Methyl Acetate Oxidation in a JSR: Experimental and Detailed Kinetic Modeling Study', *Combustion Science and Technology*, vol. 127, no. 1–6, pp. 275–291, Aug. 1997, doi: 10.1080/00102209708935697.
- [67] L. Gasnot, V. Decottignies, and J. F. Pauwels, 'Kinetics modelling of ethyl acetate oxidation in flame conditions', *Fuel*, vol. 84, no. 5, pp. 505–518, 2005, doi: 10.1016/j.fuel.2004.10.003.
- [68] P. Osswald *et al.*, 'Isomer-Specific Fuel Destruction Pathways in Rich Flames of Methyl Acetate and Ethyl Formate and Consequences for the Combustion Chemistry of Esters', *J. Phys. Chem. A*, vol. 111, no. 19, pp. 4093–4101, 2007, doi: 10.1021/jp068337w.
- [69] C. K. Westbrook *et al.*, 'A detailed chemical kinetic reaction mechanism for oxidation of four small alkyl esters in laminar premixed flames', *Proceedings of the Combustion Institute*, vol. 32, no. 1, pp. 221–228, 2009, doi: 10.1016/j.proci.2008.06.106.
- [70] Y. Zhang, Y. Yang, and A. L. Boehman, 'Premixed ignition behavior of C9 fatty acid esters: A motored engine study', *Combustion and Flame*, vol. 156, no. 6, pp. 1202–1213, Jun. 2009, doi: 10.1016/j.combustflame.2009.01.024.
- [71] W. K. Metcalfe, S. Dooley, H. J. Curran, J. M. Simmie, A. M. El-Nahas, and M. V. Navarro, 'Experimental and Modeling Study of C5H10O2 Ethyl and Methyl Esters', *J. Phys. Chem. A*, vol. 111, no. 19, pp. 4001–4014, mai 2007, doi: 10.1021/jp067582c.
- [72] W. K. Metcalfe, C. Togbé, P. Dagaut, H. J. Curran, and J. M. Simmie, 'A jet-stirred reactor and kinetic modeling study of ethyl propanoate oxidation', *Combustion and Flame*, vol. 156, no. 1, pp. 250–260, Jan. 2009, doi: 10.1016/j.combustflame.2008.09.007.
- [73] B. Akih-Kumgeh, 'Experimental and Modeling Study of Trends in the High-Temperature Ignition of Methyl and Ethyl Esters', *Energy Fuels*, vol. 25, no. 10, pp. 4345–4356, 2011, doi: 10.1021/ef200977p.
- [74] W. Ren, R. Mitchell Spearrin, D. F. Davidson, and R. K. Hanson, 'Experimental and Modeling Study of the Thermal Decomposition of C3–C5 Ethyl Esters Behind Reflected Shock Waves', *J. Phys. Chem. A*, vol. 118, no. 10, pp. 1785–1798, 2014, doi: 10.1021/jp411766b.
- [75] M. H. Hakka *et al.*, 'Oxidation of methyl and ethyl butanoates', *Int. J. Chem. Kinet.*, vol. 42, no. 4, pp. 226–252, 2010, doi: 10.1002/kin.20473.

- [76] H. Bennadji, P. A. Glaude, L. Coniglio, and F. Billaud, 'Experimental and kinetic modeling study of ethyl butanoate oxidation in a laminar tubular plug flow reactor', *Fuel*, vol. 90, no. 11, pp. 3237–3253, 2011, doi: 10.1016/j.fuel.2011.06.028.
- [77] Y. L. Wang, D. J. Lee, C. K. Westbrook, F. N. Egolfopoulos, and T. T. Tsotsis, 'Oxidation of small alkyl esters in flames', *Combustion and Flame*, vol. 161, no. 3, pp. 810–817, 2014, doi: 10.1016/j.combustflame.2013.09.013.
- [78] G. Dayma, F. Halter, F. Foucher, C. Mounaim-Rousselle, and P. Dagaut, 'Laminar Burning Velocities of C4–C7 Ethyl Esters in a Spherical Combustion Chamber: Experimental and Detailed Kinetic Modeling', *Energy Fuels*, vol. 26, no. 11, pp. 6669–6677, 2012, doi: 10.1021/ef301254q.
- [79] G. Dayma, F. Halter, F. Foucher, C. Togbé, C. Mounaim-Rousselle, and P. Dagaut, 'Experimental and Detailed Kinetic Modeling Study of Ethyl Pentanoate (Ethyl Valerate) Oxidation in a Jet Stirred Reactor and Laminar Burning Velocities in a Spherical Combustion Chamber', *Energy Fuels*, vol. 26, no. 8, pp. 4735–4748, 2012, doi: 10.1021/ef300581q.
- [80] L. Gasnot, V. Decottignies, and J. F. Pauwels, 'Ethyl acetate oxidation in flame condition: an experimental study', *Fuel*, vol. 83, no. 4–5, pp. 463–470, 2004, doi: 10.1016/j.fuel.2003.10.008.
- [81] W. R. Schwartz, C. S. McEnally, and L. D. Pfefferle, 'Decomposition and Hydrocarbon Growth Processes for Esters in Non-Premixed Flames', *J. Phys. Chem. A*, vol. 110, no. 21, pp. 6643–6648, 2006, doi: 10.1021/jp0549576.
- [82] B. Yang, C. K. Westbrook, T. A. Cool, N. Hansen, and K. Kohse-Höinghaus, 'Fuel-specific influences on the composition of reaction intermediates in premixed flames of three C<sub>5</sub>H<sub>10</sub>O<sub>2</sub> ester isomers', *Phys. Chem. Chem. Phys.*, vol. 13, no. 15, pp. 6901–6913, 2011, doi: 10.1039/C0CP02065F.
- [83] B. Yang, C. K. Westbrook, T. A. Cool, N. Hansen, and K. Kohse-Höinghaus, 'Photoionization mass spectrometry and modeling study of premixed flames of three unsaturated C<sub>5</sub>H<sub>8</sub>O<sub>2</sub> esters', *Proceedings of the Combustion Institute*, vol. 34, no. 1, pp. 443–451, 2013, doi: 10.1016/j.proci.2012.05.034.
- [84] W. Sun *et al.*, 'Experimental and modeling efforts towards a better understanding of the high-temperature combustion kinetics of C<sub>3</sub>C<sub>5</sub> ethyl esters', *Combustion and Flame*, vol. 185, pp. 173–187, 2017, doi: 10.1016/j.combustflame.2017.07.013.
- [85] D. A. Knyazkov, I. E. Gerasimov, N. Hansen, A. G. Shmakov, and O. P. Korobeinichev, 'Photoionization mass spectrometry and modeling study of a low-pressure premixed flame of ethyl pentanoate (ethyl valerate)', *Proceedings of the Combustion Institute*, vol. 36, no. 1, pp. 1185–1192, 2017, doi: 10.1016/j.proci.2016.07.038.
- [86] H. M. Katshiatshia, V. Dias, and H. Jeanmart, 'Experimental and Numerical Study of Ethyl Valerate Flat Flames at Low Pressure', *Combustion Science and Technology*, vol. 190, no. 4, pp. 632–662, 2018, doi: 10.1080/00102202.2017.1403910.

- [87] M. Boot, 'Biofuels from Lignocellulosic Biomass', in *Biofuels from Lignocellulosic Biomass*, John Wiley & Sons, Ltd, 2016, pp. 209–214.
- [88] J. Zhou, R. Zhu, J. Deng, and Y. Fu, 'Preparation of valeric acid and valerate esters from biomass-derived levulinic acid using metal triflates + Pd/C', *Green Chemistry*, vol. 20, no. 17, pp. 3974–3980, 2018, doi: 10.1039/c8gc01606b.
- [89] Y. Zhang and A. L. Boehman, 'Experimental study of the autoignition of C<sub>8</sub>H<sub>16</sub>O<sub>2</sub> ethyl and methyl esters in a motored engine', *Combustion and Flame*, vol. 157, no. 3, pp. 546–555, 2010, doi: 10.1016/j.combustflame.2009.09.003.
- [90] M. K. Ghosh *et al.*, 'The combustion kinetics of the lignocellulosic biofuel, ethyl levulinate', *Combustion and Flame*, vol. 193, pp. 157–169, 2018, doi: 10.1016/j.combustflame.2018.02.028.
- [91] M. K. Ghosh, M. S. Howard, and S. Dooley, 'Accurate and standard thermochemistry for oxygenated hydrocarbons: A case study of ethyl levulinate', *Proceedings of the Combustion Institute*, vol. 37, no. 1, pp. 337–346, Jan. 2019, doi: 10.1016/j.proci.2018.07.028.
- [92] T. Lei, Z. Wang, Y. Li, Z. Li, X. He, and J. Zhu, 'Performance of a Diesel Engine with Ethyl Levulinate-Diesel Blends: A Study using Grey Relational Analysis', *BioResources*, vol. 8, no. 2, Art. no. 2, Apr. 2013.
- [93] O. Herbinet, W. J. Pitz, and C. K. Westbrook, 'Detailed chemical kinetic oxidation mechanism for a biodiesel surrogate', *Combustion and Flame*, vol. 154, no. 3, pp. 507–528, Aug. 2008, doi: 10.1016/j.combustflame.2008.03.003.
- [94] C. K. Westbrook *et al.*, 'Detailed chemical kinetic reaction mechanisms for soy and rapeseed biodiesel fuels', *Combustion and Flame*, vol. 158, no. 4, pp. 742–755, Apr. 2011, doi: 10.1016/j.combustflame.2010.10.020.
- [95] O. Herbinet *et al.*, 'Modeling study of the low-temperature oxidation of large methyl esters from C<sub>11</sub> to C<sub>19</sub>', *Proceedings of the Combustion Institute*, vol. 33, no. 1, pp. 391–398, 2011, doi: 10.1016/j.proci.2010.07.060.
- [96] 'Russian Federation', *Sigma-Aldrich*. <https://www.sigmaaldrich.com/russian-federation.html> (accessed Jan. 30, 2020).
- [97] Botha J. P., Spalding Dudley Brian, and Egerton Alfred Charles, 'The laminar flame speed of propane/air mixtures with heat extraction from the flame', *Proceedings of the Royal Society of London. Series A. Mathematical and Physical Sciences*, vol. 225, no. 1160, pp. 71–96, Aug. 1954, doi: 10.1098/rspa.1954.0188.
- [98] O. P. Korobeinichev, S. B. Ilyin, V. M. Shvartsberg, and A. A. Chernov, 'The destruction chemistry of organophosphorus compounds in flames—I: quantitative determination of final phosphorus-containing species in hydrogen-oxygen flames', *Combustion and Flame*, vol. 118, no. 4, pp. 718–726, 1999, doi: 10.1016/S0010-2180(99)00030-9.
- [99] D. A. Knyazkov, A. G. Shmakov, and O. P. Korobeinichev, 'Application of molecular beam mass spectrometry in studying the structure of a diffusive

- counterflow flame of CH<sub>4</sub>/N<sub>2</sub> and O<sub>2</sub>/N<sub>2</sub> doped with trimethylphosphate', *Combustion and Flame*, vol. 151, no. 1, pp. 37–45, 2007, doi: 10.1016/j.combustflame.2007.06.011.
- [100] I. E. Gerasimov, D. A. Knyazkov, S. A. Yakimov, T. A. Bolshova, A. G. Shmakov, and O. P. Korobeinichev, 'Structure of atmospheric-pressure fuel-rich premixed ethylene flame with and without ethanol', *Combustion and Flame*, vol. 159, no. 5, pp. 1840–1850, 2012, doi: 10.1016/j.combustflame.2011.12.022.
- [101] A. M. Dmitriev *et al.*, 'Structure of CH<sub>4</sub>/O<sub>2</sub>/Ar flames at elevated pressures studied by flame sampling molecular beam mass spectrometry and numerical simulation', *Combustion and Flame*, vol. 162, no. 10, pp. 3946–3959, 2015, doi: 10.1016/j.combustflame.2015.07.032.
- [102] A. M. Dmitriev, D. A. Knyazkov, T. A. Bolshova, A. G. Shmakov, and O. P. Korobeinichev, 'The effect of methyl pentanoate addition on the structure of premixed fuel-rich n-heptane/toluene flame at atmospheric pressure', *Combustion and Flame*, vol. 162, no. 5, pp. 1964–1975, 2015, doi: 10.1016/j.combustflame.2014.12.015.
- [103] D. A. Knyazkov, T. A. Bolshova, A. M. Dmitriev, A. G. Shmakov, and O. P. Korobeinichev, 'The effect of methyl pentanoate addition on the structure of a non-premixed counterflow n-heptane/O<sub>2</sub> flame', *Energy Fuels*, 2018, doi: 10.1021/acs.energyfuels.7b03185.
- [104] O. P. Korobeinichev *et al.*, 'Substantiation of the probe mass-spectrometric method for studying the structure of flames with narrow combustion zones', *Combust Explos Shock Waves*, vol. 21, no. 5, pp. 524–530, 1985, doi: 10.1007/BF01463575.
- [105] O. P. Korobeinichev, 'Dynamic flame probe mass spectrometry and condensed-system decomposition', *Combust Explos Shock Waves*, vol. 23, no. 5, pp. 565–576, 1987, doi: 10.1007/BF00756538.
- [106] Е. В. Апарин, А. А. Балакай, А. Ф. Додонов, Н. В. Кирьяков, and М. И. Маркин, 'Ионный источник', SU 1122106А.
- [107] N. O. of D. and Informatics, 'NIST Chemistry WebBook'. <https://webbook.nist.gov/chemistry/> (accessed Dec. 03, 2019).
- [108] T. A. Cool *et al.*, 'Studies of a fuel-rich propane flame with photoionization mass spectrometry', *Proceedings of the Combustion Institute*, vol. 30, no. 1, pp. 1681–1688, Jan. 2005, doi: 10.1016/j.proci.2004.08.103.
- [109] G. Springer, Ed., *Engine Emissions: Pollutant Formation and Measurement*. Springer US, 1973.
- [110] Y.-K. Kim, K.K. Irikura, M.E. Rudd, M.A. Ali, P.M. Stone, 'Electron-Impact Cross Sections for Ionization and Excitation Database', NIST, 2009. <https://www.nist.gov/pml/electron-impact-cross-sections-ionization-and-excitation-database> (accessed Oct. 26, 2016).
- [111] H. A. Gueniche, P. A. Glaude, G. Dayma, R. Fournet, and F. Battin-Leclerc, 'Rich methane premixed laminar flames doped with light unsaturated hydrocarbons: I. Allene and propyne', *Combustion and Flame*, vol. 146, no. 4, pp. 620–634, Sep. 2006, doi: 10.1016/j.combustflame.2006.07.004.

- [112] E. Pousse, P. A. Glaude, R. Fournet, and F. Battin-Leclerc, 'A lean methane premixed laminar flame doped with components of diesel fuel: I. n-Butylbenzene', *Combustion and Flame*, vol. 156, no. 5, pp. 954–974, mai 2009, doi: 10.1016/j.combustflame.2008.09.012.
- [113] L.-S. Tran *et al.*, 'An experimental and modeling study of the combustion of tetrahydrofuran', *Combustion and Flame*, vol. 162, no. 5, pp. 1899–1918, May 2015, doi: 10.1016/j.combustflame.2014.12.010.
- [114] W. E. Kaskan, 'The dependence of flame temperature on mass burning velocity', *Proceedings of the Combustion Institute*, vol. 6, no. 1, pp. 134–143, 1957, doi: 10.1016/S0082-0784(57)80021-6.
- [115] A. G. Tereshchenko, D. A. Knyazkov, P. A. Skovorodko, A. A. Paletsky, and O. P. Korobeinichev, 'Perturbations of the flame structure due to a thermocouple. I. Experiment', *Combust Explos Shock Waves*, vol. 47, no. 4, pp. 403–413, 2011, doi: 10.1134/S0010508211040034.
- [116] J. H. Kint, 'A noncatalytic coating for platinum-rhodium thermocouples', *Combustion and Flame*, vol. 14, no. 2, pp. 279–281, Apr. 1970, doi: 10.1016/S0010-2180(70)80040-2.
- [117] U. Bonne, Th. Grewer, and H. G. Wagner, 'Messungen in der Reaktionszone von Wasserstoff—Sauerstoff- und Methan—Sauerstoff-Flammen', *Zeitschrift für Physikalische Chemie*, vol. 26, no. 1\_2, pp. 93–110, 1960, doi: 10.1524/zpch.1960.26.1\_2.093.
- [118] R. J. Kee, F. M. Rupley, and J. A. Miller, 'Chemkin-II: A Fortran Chemical Kinetics Package for the Analysis of Gas-Phase Chemical Kinetics', Sandia National Labs., Livermore, CA (USA), SAND-89-8009, Sep. 1989. Accessed: Dec. 27, 2016. [Online]. Available: <https://www.osti.gov/scitech/biblio/5681118-chemkin-ii-fortran-chemical-kinetics-package-analysis-gas-phase-chemical-kinetics>.
- [119] 'Ansys Chemkin-Pro: Combustion Simulation Software'. <https://www.ansys.com/products/fluids/ansys-chemkin-pro> (accessed Mar. 13, 2020).
- [120] 'Cantera: An Object-oriented Software Toolkit for Chemical Kinetics, Thermodynamics, and Transport Processes | Zenodo'. <https://zenodo.org/record/1174508#.XmtYeKP7SUK> (accessed Mar. 13, 2020).
- [121] A. Cuoci, A. Frassoldati, T. Faravelli, and E. Ranzi, 'Formation of soot and nitrogen oxides in unsteady counterflow diffusion flames', *Combustion and Flame*, vol. 156, no. 10, pp. 2010–2022, Oct. 2009, doi: 10.1016/j.combustflame.2009.06.023.
- [122] A. Cuoci, A. Frassoldati, T. Faravelli, and E. Ranzi, 'A computational tool for the detailed kinetic modeling of laminar flames: Application to C<sub>2</sub>H<sub>4</sub>/CH<sub>4</sub> coflow flames', *Combustion and Flame*, vol. 160, no. 5, pp. 870–886, May 2013, doi: 10.1016/j.combustflame.2013.01.011.
- [123] E. Ranzi, A. Frassoldati, A. Stagni, M. Pelucchi, A. Cuoci, and T. Faravelli, 'Reduced Kinetic Schemes of Complex Reaction Systems: Fossil and



- Biomass-Derived Transportation Fuels', *International Journal of Chemical Kinetics*, vol. 46, no. 9, pp. 512–542, 2014, doi: 10.1002/kin.20867.
- [124] 'Chemical Workbench – integrated software tool for kinetic mechanism development, reactor modeling and conceptual design'. <http://www.kintechlab.com/products/chemical-workbench/> (accessed Mar. 13, 2020).
- [125] 'ITV -FlameMaster'. <https://www.itv.rwth-aachen.de/en/downloads/flamemaster/> (accessed Mar. 13, 2020).
- [126] 'Cosilab Home'. <https://www.rotexo.com/index.php/en/> (accessed Mar. 13, 2020).
- [127] P. Dagaut and C. Togbé, 'Experimental and Modeling Study of the Kinetics of Oxidation of Ethanol–Gasoline Surrogate Mixtures (E85 Surrogate) in a Jet-Stirred Reactor', *Energy Fuels*, vol. 22, no. 5, pp. 3499–3505, Sep. 2008, doi: 10.1021/ef800214a.
- [128] S. M. Sarathy, M. J. Thomson, C. Togbé, P. Dagaut, F. Halter, and C. Mounaim-Rousselle, 'An experimental and kinetic modeling study of n-butanol combustion', *Combustion and Flame*, vol. 156, no. 4, pp. 852–864, Apr. 2009, doi: 10.1016/j.combustflame.2008.11.019.
- [129] G. Dayma, C. Togbé, and P. Dagaut, 'Experimental and Detailed Kinetic Modeling Study of Isoamyl Alcohol (Isopentanol) Oxidation in a Jet-Stirred Reactor at Elevated Pressure', *Energy Fuels*, vol. 25, no. 11, pp. 4986–4998, Nov. 2011, doi: 10.1021/ef2012112.
- [130] W. K. Metcalfe, S. M. Burke, S. S. Ahmed, and H. J. Curran, 'A Hierarchical and Comparative Kinetic Modeling Study of C1 – C2 Hydrocarbon and Oxygenated Fuels', *International Journal of Chemical Kinetics*, vol. 45, no. 10, pp. 638–675, Oct. 2013, doi: 10.1002/kin.20802.
- [131] Q.-D. Wang, X.-J. Wang, Z.-W. Liu, and G.-J. Kang, 'Theoretical and kinetic study of the hydrogen atom abstraction reactions of ethyl esters with hydrogen radicals', *Chemical Physics Letters*, vol. 616–617, pp. 109–114, 2014, doi: 10.1016/j.cplett.2014.10.032.
- [132] J. Mendes, C.-W. Zhou, and H. J. Curran, 'Theoretical Study of the Rate Constants for the Hydrogen Atom Abstraction Reactions of Esters with •OH Radicals', *J. Phys. Chem. A*, vol. 118, no. 27, pp. 4889–4899, 2014, doi: 10.1021/jp5029596.
- [133] N. M. Marinov, 'A detailed chemical kinetic model for high temperature ethanol oxidation', *International Journal of Chemical Kinetics*, vol. 31, no. 3, pp. 183–220, 1999, doi: 10.1002/(SICI)1097-4601(1999)31:3<183::AID-KIN3>3.0.CO;2-X.
- [134] A. Ahmed *et al.*, 'Small ester combustion chemistry: Computational kinetics and experimental study of methyl acetate and ethyl acetate', *Proceedings of the Combustion Institute*, 2018, doi: 10.1016/j.proci.2018.06.178.
- [135] T. Tan, X. Yang, Y. Ju, and E. A. Carter, 'Ab initio kinetics studies of hydrogen atom abstraction from methyl propanoate', *Phys. Chem. Chem. Phys.*, vol. 18, no. 6, pp. 4594–4607, 2016, doi: 10.1039/C5CP07282D.

- [136] T. Bolshova, V. Shvartsberg, A. Dmitriev, and D. Knyazkov, 'Flame structure and a compact reaction mechanism for combustion of dimethyl ether at atmospheric pressure', *Fuel*, vol. 255, p. 115752, 2019, doi: 10.1016/j.fuel.2019.115752.
- [137] V. Dias, H. M. Katshiatshia, and H. Jeanmart, 'The influence of ethanol addition on a rich premixed benzene flame at low pressure', *Combustion and Flame*, vol. 161, no. 9, pp. 2297–2304, Sep. 2014, doi: 10.1016/j.combustflame.2014.03.005.
- [138] S. M. Sarathy, M. J. Thomson, W. J. Pitz, and T. Lu, 'An experimental and kinetic modeling study of methyl decanoate combustion', *Proceedings of the Combustion Institute*, vol. 33, no. 1, pp. 399–405, Jan. 2011, doi: 10.1016/j.proci.2010.06.058.
- [139] Z. Tian *et al.*, 'An experimental and kinetic investigation of premixed furan/oxygen/argon flames', *Combustion and Flame*, vol. 158, no. 4, pp. 756–773, Apr. 2011, doi: 10.1016/j.combustflame.2010.12.022.
- [140] H. J. Curran, 'Developing detailed chemical kinetic mechanisms for fuel combustion', *Proceedings of the Combustion Institute*, vol. 37, no. 1, pp. 57–81, 2019, doi: 10.1016/j.proci.2018.06.054.
- [141] J. A. Dean and N. A. Lange, Eds., *Lange's handbook of chemistry*, 15. ed. New York, NY: McGraw-Hill, 1999.

## Introduction

La demande toujours croissante de ressources énergétiques et la lutte pour le respect de l'environnement obligent les chercheurs du monde entier à développer des carburants alternatifs aux combustibles fossiles. Une attention particulière est accordée aux carburants alternatifs pour les transports terrestres, car ces carburants doivent répondre à de nombreuses contraintes physiques, chimiques et économiques. L'une des solutions les plus efficaces est l'utilisation de biodiesel à base d'esters d'acides gras. De tels carburants ont une densité d'énergie suffisamment élevée, ne forment pratiquement pas de suie et de composés polyaromatiques lors de la combustion, et présentent des caractéristiques physiques proches du diesel classique, ce qui leur permet d'être utilisés sans modification significative des moteurs.

Le biodiesel est produit à partir d'huiles végétales dans une réaction de transestérification avec du méthanol ou de l'éthanol pour produire des esters méthyliques d'acide gras (EMAG) ou des esters éthyliques d'acide gras (EEAG). Le méthanol est moins cher, car la majeure partie est produite à partir de gaz naturel, donc la plus grande partie du biodiesel est produite en ce moment à base d'EMAG. Cependant, l'éthanol est moins toxique et volatil que le méthanol et l'éthanol est moins corrosif, ce qui rend la production d'éthanol plus sûre. De plus, cet alcool rend le carburant à base d'EEAG complètement renouvelable, puisque l'éthanol peut être obtenu à partir de la biomasse. De nouvelles approches de la production de bioéthanol à partir de la biomasse, par exemple des déchets agricoles, rendent le biodiesel à base d'EEAG économiquement viable.

En raison de sa prévalence dans les carburants actuellement utilisés, la combustion du biodiesel à base d'EMAG a été étudiée beaucoup plus intensivement que les carburants à base d'EEAG. Cependant, d'un point de vue pratique et académique, la pyrolyse et la combustion d'EEAG sont également très intéressantes. Contrairement à des EMAG, la chimie des esters éthyliques est caractérisée par une réaction de la décomposition monomoléculaire en formant un état de transition cyclique à six centres avec la production finale d'éthylène et de l'acide carboxylique correspondant (Fig.1). Cette décomposition se produit à des températures plus basses que l'initiation

radicalaire ; par conséquent, les EEAG subissent une décomposition plus rapide que les EMAG isomères.

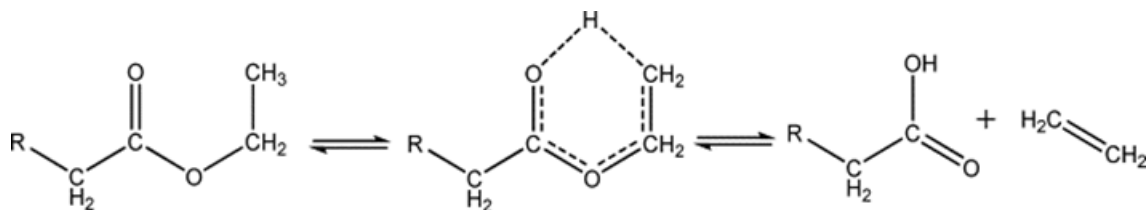


Figure : 1. Décomposition monomoléculaire à six centres du propionate d'éthyle.

Le biodiesel est composé de grosses molécules avec de longues chaînes alkyle en  $C_{16}$ - $C_{22}$ . Ces composés lourds sont très difficiles à mettre en œuvre pour des études cinétiques détaillées. Pour résoudre ce problème, une approche hiérarchique "du petit au grand" est appliquée dans la littérature. Par conséquent, dans le cas des esters éthyliques, les plus petits représentants de la série homologue ont été les plus étudiés : le formiate d'éthyle ( $C_3H_6O_2$ ), l'acétate d'éthyle ( $C_4H_8O_2$ ) et le propanoate d'éthyle ( $C_5H_{10}O_2$ ). Par contre, beaucoup moins d'études cinétiques ont été publiées sur des esters éthyliques plus lourds.

Les esters d'acide pentanoïque (ou valérique) sont particulièrement intéressants, car ils peuvent être obtenus à partir de la lignocellulose. Les valérates se sont avérés efficaces comme carburant pur et comme un additif pour carburant. De plus, ils ont un indice d'octane élevé par rapport aux carburants traditionnels.

Ainsi donc des études cinétiques complémentaires des esters éthyliques sont nécessaires. En conséquence, la thèse est consacrée à l'étude de la cinétique de combustion de divers esters éthyliques d'acides gras de l'acétate d'éthyle au pentanoate d'éthyle. Les flammes des esters éthyliques lourds étant du plus grand intérêt scientifique, l'accent principal dans le travail est fait sur l'étude cinétique de l'oxydation de valérate d'éthyle.

Les tâches principales de la thèse ont été formulées comme suit :

1. Mesurer la structure chimique des flammes laminaires prémélangées stabilisées sur un brûleur plat à basse pression et pression atmosphérique alimenté par de l'acétate d'éthyle, du butanoate d'éthyle et du pentanoate d'éthyle. Clarifier les données ambiguës sur la structure des flammes de pentanoate d'éthyle à basse pression présentées dans la littérature.

2. Analyser les modèles cinétiques existant d'oxydation des esters éthyliques et développer un nouveau mécanisme détaillé de combustion des esters étudiés en se basant sur les travaux les plus modernes sur la cinétique d'oxydation des petits EEAG.

3. Effectuer une simulation numérique de la structure chimique des flammes étudiées en utilisant un nouveau mécanisme et les mécanismes présentés dans la littérature, et déterminer les avantages et les inconvénients du modèle proposé. Effectuer une analyse comparative de la capacité de différents mécanismes à décrire qualitativement et quantitativement la structure chimique des flammes des esters étudiés.

4. Effectuer une analyse numérique des mécanismes cinétiques afin de déterminer les raisons des écarts entre les simulations et les résultats expérimentaux. Suggérer des façons possibles d'améliorer le mécanisme.

## **L'approche méthodique**

Deux dispositifs expérimentaux sont été utilisés pendant cette thèse. Les flammes laminaires de pré-mélange stabilisées sur un brûleur plat à basse pression (50 Torr) ont été étudiées par la chromatographie en phase gazeuse (GC) au Laboratoire Réactions et Génie des Procédés (LRGP), Nancy, France. La flamme a été stabilisée sur un brûleur McKenna (60 mm de diamètre) dans une chambre de combustion métallique sous 50 Torr. Le brûleur a été maintenu à une température de 333 K par refroidissement à eau. Des régulateurs de débit massique étalonnés ont été utilisés pour fournir les gaz et le carburant liquide qui sont mélangés dans un évaporateur en amont du brûleur. L'échantillonnage de la flamme a été réalisé à l'aide d'une sonde de quartz mince avec un orifice de 100  $\mu\text{m}$  de diamètre et un angle interne d'environ 10°. La sonde était connectée à une ligne pompée à chaud connectée au GC. Deux GC ont été utilisés pour analyser l'échantillon :

- Agilent 7890 A équipé de colonnes HP-Plot Q et HP-Molesieve pour la séparation des hydrocarbures, des oxygénés et de l'argon. L'hélium était utilisé comme gaz vecteur. Un détecteur à ionisation de flamme (FID) avec un méthaniseur et un détecteur de conductivité thermique a permis d'identifier et de quantifier les composés.

• HP 5890 Série II avec colonne Carbosphère et détecteur de conductivité thermique utilisé pour déterminer les fractions molaires de H<sub>2</sub> et O<sub>2</sub>. L'argon a été utilisé comme gaz vecteur.

<i>Ester</i>	$X(\text{ester})$	$X(\text{O}_2)$	$X(\text{Ar})$	$Q_v, \text{cm}^3/\text{s}$	$Q_m, \text{g}/(\text{s}\cdot\text{cm}^2)$	$\varphi$
EA	0,042	0,208	0,75	91,7	0,00584	1,0
EPe	0,024	0,226	0,75	100,1	0,00577	1,0

Tableau 1. Composition et débits de mélanges gazeux d'esters éthyliques étudiés à basse pression.

L'étude des flammes à la pression atmosphérique a été réalisée à l'aide d'une installation de spectrométrie de masse à faisceau moléculaire à l'Institut de cinétique chimique et de combustion, Novossibirsk, Russie. La flamme a été stabilisée sur un brûleur Botha-Spalding (diamètre 16 mm) qui été maintenu à une température constante de 368 K grâce à une chemise d'eau de refroidissement. La consommation d'oxygène et d'argon a été contrôlée par les régulateurs de débit massique étalonnés. L'ester liquide a été introduit par une seringue à un évaporateur en utilisant un moteur pas à pas. Le système de prélèvement par faisceau moléculaire a fourni un échantillonnage direct du gaz de la flamme. Le faisceau moléculaire était formé par une sonde conique en quartz avec un orifice de 80  $\mu\text{m}$  ; l'angle du cône intérieur était de 40°. Le faisceau a été focalisé par un écorceur ou skimmer puis modulé avec un modulateur à disque pour faire la distinction entre les signaux utiles et de fond. La détection des composants de la flamme à partir d'un échantillon de gaz a été réalisée par un spectromètre de masse quadripolaire EZAN MS-7302 avec un système d'ionisation par impact d'électrons doux, c'est-à-dire de basse énergie (la dispersion des énergies électroniques était d'environ  $\pm 0,25$  eV). L'énergie d'ionisation des électrons a été sélectionnée individuellement pour chaque composant afin d'obtenir le meilleur rapport signal sur bruit et de minimiser les problèmes de fragmentation.

<i>Ester</i>	$X(\text{ester})$	$X(O_2)$	$X(\text{Ar})$	$Q_v, \text{cm}^3/\text{s}$	$Q_m, \text{g}/(\text{s}\cdot\text{cm}^2)$	$\varphi$
EA	0,037	0,163	0,8	25	0,0245	1,1
EA	0,077	0,223	0,7	15,24	0,0155	1,7
EB	0,022	0,178	0,8	24,98	0,0244	1,0
EB	0,047	0,253	0,7	15,24	0,0154	1,5
EPe	0,019	0,181	0,8	25	0,0203	1,0

Tableau 2. Composition et débits de mélanges gazeux d'esters éthyliques étudiés à pression atmosphérique.

Les profils de température des flammes ont été déterminés comme le changement de température de la flamme en fonction de la hauteur au-dessus du brûleur. Dans les expériences à basse pression, le profil de température a été mesuré à l'aide d'un thermocouple PtRh (6%) - PtRh (30%) (diamètre de fil 100  $\mu\text{m}$ ). Le fil a été recouvert d'un revêtement céramique  $\text{BeO-Y}_2\text{O}_3$  pour éviter les réactions catalytiques sur la surface du thermocouple. Pour prendre en compte les pertes de chaleur par rayonnement, la méthode de compensation électrique a été utilisée. L'erreur de mesure de température était d'environ  $\pm 100$  K. Des mesures de température à pression atmosphérique ont également été réalisées par la méthode du thermocouple. Un thermocouple Pt - PtRh (10%) avec une épaisseur de fil de 50  $\mu\text{m}$  a été utilisé. Pour éviter les réactions catalytiques, un revêtement de  $\text{SiO}_2$  a été appliqué sur la surface. Pour prendre en compte les pertes au rayonnement, la correction de température a été calculée par la méthode analytique.

Les structures chimiques des flammes étudiées ont été simulées numériquement en utilisant le code PREMIX du package CHEMKIN-PRO. Les profils de température mesurés ont été utilisés comme paramètres d'entrée pour prendre en compte les perturbations par la sonde et les pertes de chaleur vers le brûleur. Pour les simulations des structures des flammes d'esters éthyliques, le mécanisme de Dayma et al. 2012 été utilisé. Ce mécanisme est le premier mécanisme cinétique détaillé de l'oxydation de pentanoate d'éthyle (EPe) proposé dans la littérature. Puisque seules les flammes sont étudiées dans la thèse, la chimie à basse température a été supprimée du mécanisme. La

version réduite qui a été utilisée dans le travail comprend 232 espèces et 1845 réactions.

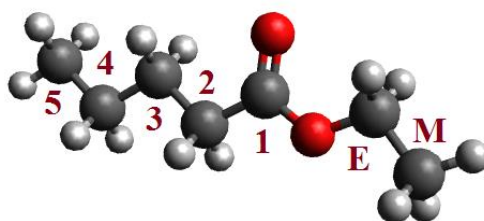


Figure. 2. Structure pentanoate d'éthyle avec marquages d'atomes de carbone.

Les résultats des calculs par ce mécanisme ont montré une concordance insatisfaisante avec certains profils expérimentaux des fractions molaires des hydrocarbures intermédiaires en C<sub>2</sub>-C<sub>3</sub>. Ce fait nous a incité à créer une nouvelle version du mécanisme de combustion de l'EPE basée sur des études plus récentes de la cinétique de combustion des éthers éthyliques. Le mécanisme récent d'oxydation des petits EEAG de Sun et al. (2017) a été pris comme base. Ce mécanisme a été étendu par les réactions de combustion de butanoate d'éthyle (EB) et de pentanoate d'éthyle. Les constantes de vitesse des réactions d'abstraction de l'atome H des molécules EB et EPE par les radicaux (H, O, OH et CH<sub>3</sub>) aux positions M, E et 2 (Fig. 2) ont été prises de manière similaire à celles utilisées dans le mécanisme de Sun et al. pour les esters éthyliques plus légers. Pour décrire correctement les résultats des expériences avec l'EPE à basse pression, la réaction principale de formation d'éthanol C<sub>2</sub>H<sub>5</sub>OH (+M) ⇌ C<sub>2</sub>H<sub>5</sub> + OH (+M) a été prise avec la constante de vitesse du mécanisme bien connu de Marinov et al. Le mécanisme final qui en résulte contient 320 espèces participant à 2027 réactions. Les données thermochimiques et de transport ont été extraites du mécanisme de Sun et al. et ont été complétées par les données du mécanisme de Dayma et al.

## Discussion des résultats

Les structures chimiques de flamme des esters ont été mesurées dans les expériences à pression atmosphérique et basse pression. Les données expérimentales sont présentées avec les résultats des simulations numériques. La discussion est s'appuie sur la confrontation des simulations issues des modèles aux données



expérimentales. Pour simuler les flammes d'acétate d'éthyle, un mécanisme récent additionnel (Ahmed et al., 2018) été utilisé. Une analyse numérique des modèles est fournie avec une attention particulière au mécanisme nouveau.

Les trois mécanismes prédisent différents profils de fraction molaire des hydrocarbures dans la flamme d'EA à basse pression. La précision des prédictions diffère également beaucoup. Comparé aux données expérimentales, le mécanisme de Dayma a fourni la meilleure prédiction du profil de la fraction molaire du méthane, lors que les mécanismes d'Ahmed et de Sun ont sous-estimé la fraction molaire maximale de  $\text{CH}_4$  d'un facteur deux. Cependant, comme dans la flamme atmosphérique, les mécanismes de Sun et d'Ahmed prédisaient très bien le pic de fraction molaire d'acétylène, et le mécanisme de Dayma l'a sous-estimé. Le profil expérimental de la fraction molaire de l'éthylène semble être plusieurs fois plus élevé que dans la flamme atmosphérique. La position du pic est nettement décalée vers le brûleur, ce qui indique une formation de  $\text{C}_2\text{H}_4$  plus rapide que par simulation. Comme dans le cas de la pression atmosphérique, les mécanismes de Sun et Ahmed ont prédit le pic de fraction molaire d'éthylène deux fois plus élevé que celui par le mécanisme de Dayma. Il est intéressant de noter que le mécanisme du Sun semble être le moins précis dans la prédiction de la fraction molaire de  $\text{C}_2\text{H}_6$  à 50 Torr, considérant que ce mécanisme a été le plus efficace à la pression atmosphérique. Vice versa, les deux autres mécanismes démontrent une excellente concordance avec la fraction molaire du pic expérimentale de l'éthane.

Pour les flammes de butanoate d'éthyle on peut conclure que le nouveau modèle décrit la structure chimique des flammes d'EB nettement mieux que le mécanisme de Dayma. Cependant, pour les espèces individuelles, dont l'éthane et le butène, des écarts significatifs ont été observés. D'une manière générale, compte tenu de l'erreur expérimentale dans la mesure des composés oxygénés, on peut supposer une concordance satisfaisante entre les calculs issus des modèles et l'expérience.

Comme dans la flamme riche d'EA, les profils de fraction molaire calculés d'acétylène dans la flamme riche d'EB n'atteignent pas zéro dans la zone finale de la flamme. Mais l'expérience donne une concentration quasi nulle d'acétylène dans cette zone avec une bonne précision. On peut voir que le nouveau modèle prédit la moitié moins de fraction molaire d'acétylène que le modèle de Dayma dans la zone finale de la flamme. Il faut noter que le mécanisme de Dayma décrit le profil de fraction molaire de

l'éthylène ( $C_2H_4$ ) un peu plus précisément dans la flamme stœchiométrique. La même tendance dans la flamme d'EA a également été observée.

En regardant la comparaison des profils de fractions molaires expérimentaux et calculés des composés oxygénés, en général, on peut noter la précision satisfaisante des modèles utilisées. Le plus grand écart entre l'expérience et la modélisation est observé dans le cas du formaldéhyde ( $CH_2O$ ). Les fractions molaires mesurées expérimentalement d'acide butanoïque ( $C_3H_7COOH$ ) ont été décrites avec une précision acceptable par les deux modèles. Mais une meilleure concordance du modèle de Dayma avec l'expérience dans des conditions stœchiométriques peut être observée. Dans le même temps, dans la flamme riche, les deux modèles ont surestimé la fraction molaire maximale d'acide.

Dans le cas de la flamme atmosphérique du pentanoate d'éthyle, les deux modèles ont montré une description généralement satisfaisante des données expérimentales. Pour cette flamme, le nouveau modèle semble être plus précis dans la description des profils de fraction molaire d'acétylène, d'éthane et de propane, et il est un peu moins précis avec la fraction molaire d'acide valérique. Au contraire, le modèle de Dayma prédit un peu plus précisément la fraction molaire d'acide maximale, mais l'a également sous-estimé de plus d'une fois et demie. La même sous-estimation de la fraction molaire acide a été observée dans le cas de la flamme d'EB qui a un poids moléculaire proche de l'EPe.

Dans le cas de la flamme d'EPe à basse pression le nouveau mécanisme a très bien décrit les profils de fraction molaire de l'acétylène, de l'allène et du propyne, lors que le mécanisme de Dayma a sous-estimé les fractions molaires maximales de ces composés de 3 à 5 fois. Les fractions molaires maximales de méthane et d'éthane, au contraire, ont été calculées un peu mieux par le modèle Dayma, alors que dans le nouveau mécanisme, les fractions molaires maximales de ces espèces ont été sous-estimées de 1,5 à 2 fois. Pour les autres espèces intermédiaires détectées, les positions et les formes des profils des fractions molaires maximales ont été bien reproduites dans les simulations, mais il existe des écarts notables dans les valeurs absolues entre les prédictions du modèle et l'expérience.

Pour la flamme d'EPe, le calcul et la comparaison avec les données expérimentales de la vitesse de flamme laminaire ont été effectués. Les simulations ont montré d'excellentes prédictions du nouveau modèle avec des expériences dans

l'intervalle large de pressions et de richesse, ce qui confirme une fois de plus l'efficacité du nouveau modèle.

Une analyse numérique détaillée des mécanismes utilisés a été réalisée pour tous les esters. Une analyse intégrale des voies de consommations et une analyse de sensibilité ont été effectuées pour analyser les inexactitudes du nouveau modèle. En générale, une certaine inexactitude systématique dans la description des voies de destruction primaires peut être mentionnée. De plus, le problème pourrait être dans la relation entre la décomposition unimoléculaire et les réactions de destruction radicalaires. Il est également montré qu'il est nécessaire de réviser les réactions d'isomérisation des radicaux combustibles et la formation d'acide acétique à partir de ceux-ci dans le nouveau mécanisme pour une description plus précise de la structure chimique des flammes d'acétate d'éthyle.

Pour le futur, pour améliorer la précision des prévisions du modèle il est nécessaire de mener des expériences supplémentaires dans une large gamme de conditions, en particulier à pressions élevées. En outre, des calculs de chimie quantique des constantes de vitesse d'arrachage d'un atome H du pentanoate d'éthyle et du butanoate d'éthyle sont nécessaires, ainsi que le raffinement des constantes de vitesse de la décomposition unimoléculaire à six centres des esters éthyliques.

## Étude cinétique de la combustion en flammes laminaires de biocarburants de type ester

Le progrès partout dans le monde nécessite une variété de sources d'énergie propre. Les biocarburants liquides de type ester semblent être très efficaces dans ce contexte, car ils sont faciles à utiliser dans les véhicules modernes, ils peuvent être produits à partir de diverses ressources renouvelables et ils offrent des caractéristiques de combustion respectueuses de l'environnement. À cet égard, les esters éthyliques d'acides gras (EEAG) sont considérés comme une classe prometteuse de biocarburants.

L'objectif principal de cette thèse était de développer un mécanisme cinétique chimique actualisé de la combustion des EEAG légers jusqu'au pentanoate d'éthyle et de le valider par rapport aux nouvelles données expérimentales sur la structure de flammes laminaires prémélangées à basse pression et pression atmosphérique. Les flammes alimentées par trois EEAG, l'acétate d'éthyle, le butanoate d'éthyle et le pentanoate d'éthyle, ont été étudiées au moyen de la spectrométrie de masse avec faisceau moléculaire et de la chromatographie en phase gazeuse. Plus de 40 espèces stables et intermédiaires comprenant des radicaux ont été détectées et quantifiées dans les flammes. Une analyse complète du mécanisme développé a été réalisée.

La thèse se compose de 3 chapitres. Le premier chapitre présente une revue bibliographique. Les études expérimentales et théoriques les plus importantes sur la combustion des EEAG sont discutées. Le deuxième chapitre présente un aperçu des méthodes expérimentales et de simulation utilisées dans la thèse. Des détails sur le développement du mécanisme sont également fournis dans cette partie. Le dernier chapitre présente des résultats expérimentaux et de modélisation sur les esters étudiés en comparaison avec les mécanismes cinétiques de la littérature.

*Mots clés: Combustion, Biocarburant, Chromatographie en phase gazeuse, Spectrométrie de masse à faisceau moléculaire, Flamme prémélangée, Modélisation cinétique chimique, Mécanisme cinétique chimique détaillé*

### Kinetic study of ester biofuels in flames

Global progress all over the world requires a variety of clean energy sources. Liquid ester-based biofuels seem to be very effective in this context since they are easy to use in modern vehicles, they can be produced from a variety of renewable resources, and they provide environmentally friendly combustion characteristics. In this regard, fatty acid ethyl esters (FAEEs) are considered as a promising class of biofuels.

The main goal of this thesis was to develop an updated chemical kinetic mechanism of combustion of light FAEEs up to ethyl pentanoate and validate it against the new experimental data on chemical speciation in low and atmospheric pressure premixed laminar flames. The flames fueled by three FAEEs, ethyl acetate, ethyl butanoate and ethyl pentanoate, were investigated by means of molecular-beam mass-spectrometry and gas-chromatography. More than 40 stable and intermediate species including radicals were detected and quantified in the flames. A comprehensive analysis of the developed mechanism was performed.

The thesis consists of 3 chapters. In the first chapter a review of literature is presented. The most important experimental and theoretic studies on FAEEs are discussed. The second chapter presents an overview of experimental and simulation methods used in the work. Details on the mechanism development are also provided in this part. The last chapter present experimental and modeling results on the esters studied in comparison with the literature kinetic mechanisms.

*Keywords: Combustion, Biofuel, Gas chromatography, Molecular beam mass spectrometry, Premixed flame, Chemical kinetic modeling, Detailed chemical kinetic mechanism*